Dissertation

Submitted to the
Combined Faculty of Natural Sciences and Mathematics
of the Ruperto Carola University of Heidelberg, Germany
for the degree of
Doctor of Natural Sciences

Presented by

Areej Albariri, M.Sc.

born in Amman, Jordan

Oral examination: 08 October 2019

Golgi apparatus and Golgi outposts in neurons studied by correlative microscopy

Referees:

Prof. Dr. Thomas Kuner

Prof. Dr. Thomas Holstein

Acknowledgements

First of all, I would like to thank Prof. Dr. Thomas Kuner for giving me the opportunity to work in his lab and for the financial resources for this research project. I am especially thankful for his supervision and scientific discussions.

Especially, I would like to thank Dr. Markus Grabenbauer for providing the project topic, supervising my research and helping me improve my scientific writing and presenting skills, and many more.

I am very grateful to Heinz Horstmann, who introduced me to many insights related to electron microscopy. I would like to express my deepest gratitude to all members in the electron microscopy core Facility, especially to Dr. Stefan Hillmer, Dr. Charlotta Funaya, Steffi Gold, Uta Has and Sebastian Wurzbacher.

Special thanks to Michaela Keiser, Claudia Kocksch, Marion Schmitt, Gabie Krämer, Inge Frommer, Andrea Schlicksupp and Rita Rosner for the excellent technical support that makes life in the lab possible. Thanks to Dr. Hongwei Zheng who helped me with the 3D analysis.

Many thanks to all members of the Kuner lab for creating a nice working atmosphere. Especially, I would like to thank my friends, Dr. Maja Klevanski and Helia Saber for helpful discussions and technical support in all kinds of problems that I encountered in the lab.

I would like to thank my friends Mira, Adrian, Nade and Yomn and my family in Jordan and in Argentina for their love and support.

And finally, special thanks to my beloved husband Santiago and my beloved children Francesca, Mila and Alexander for the continuous love, patience, support and for always believing in me.

Abstract

The Golgi apparatus is a highly dynamic organelle, which has many vital functions in cellular mechanisms like lipid metabolism, protein secretion, intracellular signaling, and regulation of cell division. First described in neurons, the ultrastructure and function of this complex network is still not well delineated. Recent studies have shown this secretory organelle also in dendrites of neurons, named Golgi outposts (GOs). To date, these GOs have been analyzed mainly by light microscopy while their ultrastructural appearance remained only poorly defined.

To study the morphology of GOs in dendrites and to examine if GOs show a different ultrastructure to that of somatic Golgi apparatus, I established new applications of correlative light and electron microscopy in cultured neurons and brain slices, which combine fluorescence microscopy with the superior resolution of electron microscopy. Photo-oxidation-based approaches allow for the direct ultra-structural visualization of fluorescent markers in 3D, like genetically encoded green fluorescent proteins (GFPs). However, this challenging methodology had to be adapted to detect Golgi enzymes in neuronal cell cultures and brain tissue. Therefore, I first optimized the chemical fixation conditions for cultured hippocampal neurons to approximate the morphologic quality of high-pressure freeze fixation. Secondly, I enhanced sensitivity, reliability, and precision of photo-oxidation procedures on neurons, which allowed to analyse the 3D ultrastructure of GOs in dendrites of cultured neurons and mammalian brain slices.

Correlative 3D microscopy showed that GOs are smaller in volume and have lower number of cisternae per stack compared to somatic Golgi apparatus of the same cell. Further, the number of peri-Golgi vesicles around GOs appears to be less. Additionally, while the stack polarity of somatic Golgi apparatus might switch along the ribbon, GOs have strictly unidirectional polarity.

The technical achievements and enhanced sensitivity regarding correlative microscopy of GFPs in cultured neurons and brain slices allow for further ultrastructural investigations of GOs at different metabolic states to better understand their vital functions.

Zusammenfassung

Der Golgi-Apparat ist eine hochdynamische Organelle, die viele lebenswichtige Funktionen in zellulären Mechanismen wie dem Lipidstoffwechsel, der Proteinsekretion, der intrazellulären Signalübertragung und der Regulation der Zellteilung hat. Erstmals in Neuronen beschrieben, ist die Ultrastruktur und Funktion dieses komplexen Netzwerks noch nicht genau beschrieben. Neuere Studien haben gezeigt, dass diese sekretorische Organelle auch in Dendriten vorkommt, genannt Golgi-Außenposten (engl. „Golgi outposts“: GOs). Bisher wurden diese GOs hauptsächlich lichtmikroskopisch analysiert, während ihre Ultrastruktur nur unzureichend definiert blieb.

Um die Morphologie von GOs in Dendriten zu untersuchen, habe ich neue Methoden der korrelativen Licht- und Elektronenmikroskopie in kultivierten Neuronen und Hirnschnitten etabliert, wobei Fluoreszenzmikroskopie mit der überlegenen Auflösung der Elektronenmikroskopie kombiniert wird. Photo-Oxidationsbasierte Ansätze ermöglichen die direkte ultra-strukturelle Analyse von fluoreszenten Markern in 3D, zum Beispiel von genetisch kodierten grün fluoreszierenden Proteinen (GFPs). Diese anspruchvolle Methodik musste jedoch stark angepasst werden, um Golgi-Enzyme in neuronalen Zellkulturen und Gehirngewebe spezifisch nachzuweisen. Daher optimierte ich zuerst die chemischen Fixierungsbedingungen für die kultivierten hippocampalen Neuronen, um sie der morphologischen Qualität der Hochdruck-Gefrierfixierung anzunähern. Zweitens verbesserte ich die Empfindlichkeit, Zuverlässigkeit und Präzision von Photo-Oxidationsverfahren, um die 3D-Ultrastruktur von GOs in Dendriten von kultivierten Neuronen sowie Hirnschnitten von Säugetieren analysieren zu können.

Die korrelative 3D-Mikroskopie zeigte, dass GOs ein geringeres Volumen und eine geringere Anzahl von Zisternen pro Stapel aufweisen als somatische Golgi-Apparate derselben Zelle. Zusätzlich scheint die Anzahl der Peri-Golgi-Vesikel bei GOs geringer zu sein. Während die Polarität des somatischen Golgi-Apparates entlang des Organells wechseln kann, haben GOs eine streng unidirektionale Polarität.

Diese technischen Fortschritte und die erhöhte Sensitivität der korrelativen Mikroskopie von GFPs in kultivierten Neuronen und Hirnschnitten ermöglichen weitere

ultrastrukturelle Untersuchungen von GOs in verschiedenen Stoffwechselzuständen, um deren grundsätzlichen Funktionen besser zu verstehen.

I hereby declare, that the presented dissertation is my own original work and has not been previously submitted to any other institution of higher education. I further declare that no sources and supporting materials have been used other than those indicated and referenced.

Heidelberg, 24th of July

Areej Albariri

Contents

1. Introduction

1.1 Somatic versus dendritic Golgi apparatus

The Golgi apparatus is a key organelle for lipid metabolism, protein secretion, intracellular signaling, and regulation of cell division, which was described by its discoverer, the Italian physician and histologist Camillo Golgi, in 1898 as an "internal reticular apparatus" in neurons (Bentivoglio and Mazzarello, 1998; Golgi, 1898). Studies have revealed dendritic mRNAs and ribosomes, suggesting that local translation can happen even in distal dendrites (Schuman et al., 2006; Hanus and Ehlers, 2008). Distal dendritic translation makes it mandatory to provide Golgi functionality in order to process locally translated proteins. Surprisingly, decades of electron microscopic studies of the nervous system have not revealed typical Golgi stacks in dendrites of neurons, raising the possibility that the ultrastructural appearance of the Golgi apparatus may differ between the somatic and dendritic compartments. Ultrastructural evidence for Golgi outposts as of now has been reported in only two studies (Pierce, 2001; Horton et al., 2005), leaving many questions open.

1.2 Structure of the somatic Golgi apparatus

The structure of the Golgi apparatus is mainly defined as a stack of disk-like membranes, called the cisternae. The number of cisternae varies from 4 to 11 in mammalian cells (Rambourg and Clermont, 1997) with their thickness varying from 0.7 to 1.1 μm with a space of 10 to 20 nm between the membranes (Rabouille et al., 1995). Golgi apparatus has a polar structure, i.e. it has an entry site, the cis-Golgi network (CGN) and an exit site, the trans-Golgi network (TGN). In between is a stack of cisterns, which is categorized in a cis-, medial- and trans-side, depending on their orientation and enzymes they contain (Glick and Luini, 2011) (Figure 1.1)

Secretory proteins enter the Golgi at the CGN and are transported through it until they leave via the TGN (Rothman and Wieland, 1996). As they pass through the various cisterns, the proteins are modified in a strict order. These include O-glycosylation

(Jentoft, 1990), and modification of N-glycosidically linked oligosaccharides (Kornfeld and Kornfeld, 1985). The enzymes that catalyze these reactions are therefore also used as markers for the various Golgi subcompartments.

Protein glycosylation is an important posttranslational modification. In this process, (oligo-) saccharides are linked to amino acid residues by means of N- or O-glycosidic bonds (Müller and Graeve, 2014). Typical monosaccharides involved are hexoses such as D-glucose or hexosamines such as N-acetyl-D-glucosamine (GlcNAc) or N-acetylgalactosamine (GalNAc) (Varki and Sharon, 2017). Glycoproteins pass through the Golgi apparatus after folding and quality control, before they subsequently get distributed from the trans-Golgi network to their destinations (Henrissat et al., 2017).

Polypeptide N-acetylgalactosaminyltransferase 2 (GalNAc-T2) catalyzes the transfer of GalNAc from the nucleotide sugar UDP-GalNAc to the hydroxyl group of serine and threonine residues (ten Hagen et al., 2003). All its isoforms are type II trans-membrane proteins with different substrate preferences (Tian et al., 2009). Initiation of the glycosylation process is controlled by the GalNAc-Ts. Additionally, the location and density of O-glycans in the protein are determined by the GalNAc-Ts (ten Hagen et al., 2003). GalNAc-T2 is primarily located in the medial and trans-Golgi compartment (Lowe and Marth, 2003) and has been used as a molecular marker for these compartments.

Both cis-Golgi and trans-Golgi are described as cargo protein sorting stations (Farquhar, 1985; Hsu et al., 1991). In the cis-Golgi, proteins can either be trafficked back into the endoplasmic reticulum (ER) due to an ER feedback signal, or they are transported further forward through the Golgi complex (Jackson et al., 1990; Nilsson et al., 1989). In the TGN it is decided whether the proteins should be transported to the lysosomes, the endosomes or the plasma membrane (Griffiths and Simons, 1986; Lemmon and Traub, 2000).

Transport within the secretory pathway occurs in all eukaryotic organisms via protein-enveloped vesicles. So far, three vesicle types, COPI, COPII and clathrin vesicles (COP, coat protein), have been characterized (Kirchhausen, 2000). COPI-coated vesicles are tangled in many steps of early secretory transport (Orci et al., 1986; Wieland and Harter, 1999). They mediate bidirectional transport between Golgi apparatus and intermediate compartment (IC); secretory proteins are synthesized at the ER and

transported via IC and the Golgi apparatus to their destination (Saraste and Marie, 2018; Lowe and Kreis, 1998). They are also responsible for the anterograde and retrograde transport inside the Golgi and for the retrograde transport from Golgi to the ER (Harter and Reinhard, 2000; Nickel and Wieland, 1998). COPII-coated vesicles mediate transport from the ER to the IC (Barlowe, 1998). Clathrin-coated vesicles facilitate transport to the early endosomes at the plasma membrane and to the late endosomes and lysosomes at TGN (Pearse and Robinson, 1990; Hirst and Robinson, 1998).

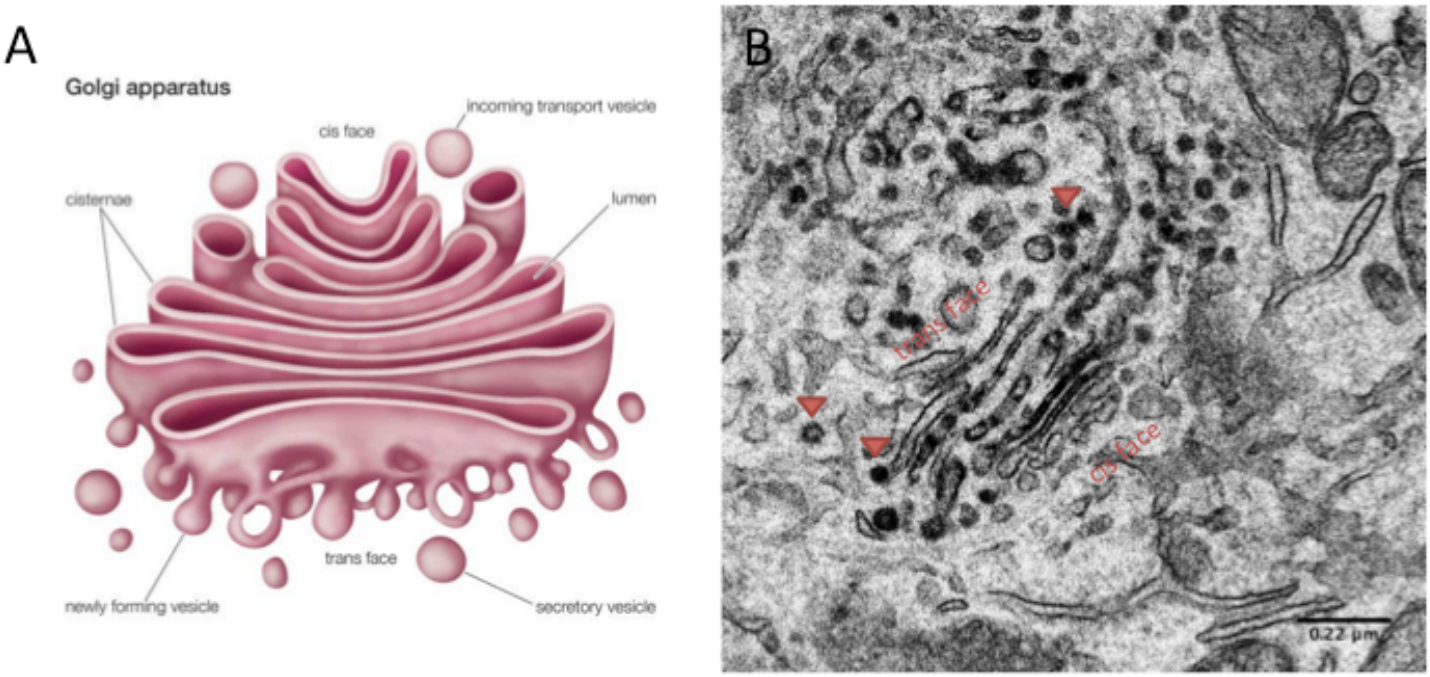

Figure 1.1 Golgi apparatus. **(A)** Schematic overview of the Golgi apparatus. Figure Adopted from Encyclopaedia Britannica/UIG/Getty Images/golgi. **(B)** A transmission electron microscopy image of a Golgi apparatus in a neuron stained through photo-oxidation (unpublished personal data). Red arrowheads designate **v**esicles. Scale bar: 0.2 µm (B).

Using a technique based on silver-staining, Camillo Golgi was able to visualize for the first time the Golgi complex (*Grant, 2007*). Eventually, studies have been focused to understand its functionality. Electron microscopy (EM) for the first time has revealed the ultrastructure of the Golgi apparatus in the 1950s (Dalton and Felix, 1954). To be able to study the 3D structure of the Golgi complex, slices need to be thicker than 100 nm to contain the whole structure. Therefore, high voltage transmission electron microscopy (TEM) came into use to be able to visualize Golgi stacks in 1 μm sections (Rambourg et al., 1974). After that, the ultra-high voltage TEM was used to thoroughly study the Golgi and visualize its full structure (Lindsey and Ellisman, 1985). High voltage dual-axis tilt TEM tomography has significantly improved the 3D EM analysis using thicker samples and displaying better resolution in the x and y resolution (Marsh, 2005). Enzyme-activity-based cytochemical staining as well as antibody staining allowed to locate and study proteins and their functions within the Golgi apparatus (Farquhar and Palade, 1981). The merge between electron and light microscopy then allowed to get time-resolved data as well as ultrastructural details from the same biological sample (van Rijnsoever et al., 2008). This led to novel insights of Golgi apparatus, its structure and function (Quinn, Griffiths et al., 1983; Griffiths, 2000).

1.3 Dendritic outposts of the Golgi apparatus

As in many animal cells, the neuronal Golgi apparatus localizes in the perinuclear region. Recent studies have shown small Golgi-like structures in dendrites named Golgi outposts (GOs) (Pierce et al., 2001; Hanus and Ehlers, 2008; Valenzuela and Perez, 2015) (Figure 1.2). Thus, mini-Golgi apparatus may influence dendrite morphology and function as platforms for the local delivery of synaptic receptors (Ye et al., 2007; Quassollo et al., 2015). Golgi outposts can also contribute to dendritic growth and branch dynamics (Zheng et al., 2008).

Golgi outposts in dendrites can be found in around 18% of mature neurons (Horton et al., 2005). In the case of mature hippocampal neurons, Golgi outposts are found in 70-80% of them. They are usually located in the apical dendrite in the cortex or in the corresponding main dendrite (Horton and Ehlers, 2003; Horton et al., 2005). Golgi outposts are discrete structures; some of them have been described to be composed of

stacked cisternae, and separated of somatic Golgi (Pierce et al., 2001; Horton et al., 2005).

Additionally, glycosylation, which is a post-translational ER- and Golgi-dependent protein modification, can occur in single dendrites (Torre and Steward, 1996). Moreover, recent studies have shown single-compartment Golgi outposts in dendritic shafts of *Drosophila* neurons *in vivo* where the cisterns (*trans, medial, and cis* cisternae) of the outposts are detached from one another. This contrast to multi-compartment Golgi outposts localized in the dendritic shafts and branch points that are ordered as stacks in an GM130-dependent way (Zhou et al., 2014; Valenzuela and Perez, 2015).

The only ultrastructural images of Golgi outposts by electron microscopy were demonstrated in adult rat brain through immunogold labeling for GM130 (Pierce et al., 2001; Horton et al., 2005). In all other further functionality studies, the detection of Golgi outposts was mainly by fluorescence (Bourke et al., 2018; Cajigas et al., 2012; Chung et al., 2017; Cui-Wang et al., 2012, Evans et al., 2017; Hanus and Ehlers et al.; 2016, Hanus and Schuman; 2013, Kelliher et al., 2018; Merianda et al., 2009; Mikhailova et al., 2016; Nguyen et al., 2014; Ori-McKenney et al., 2012; Ye et al., 2007; Zhou et al., 2014). The contribution of Golgi outposts in distal dendrites and apical dendrites were observed using several Golgi antibodies by FM or by transfected cells using live-cell imaging, but their ultrastructural correlate remains are still unknown.

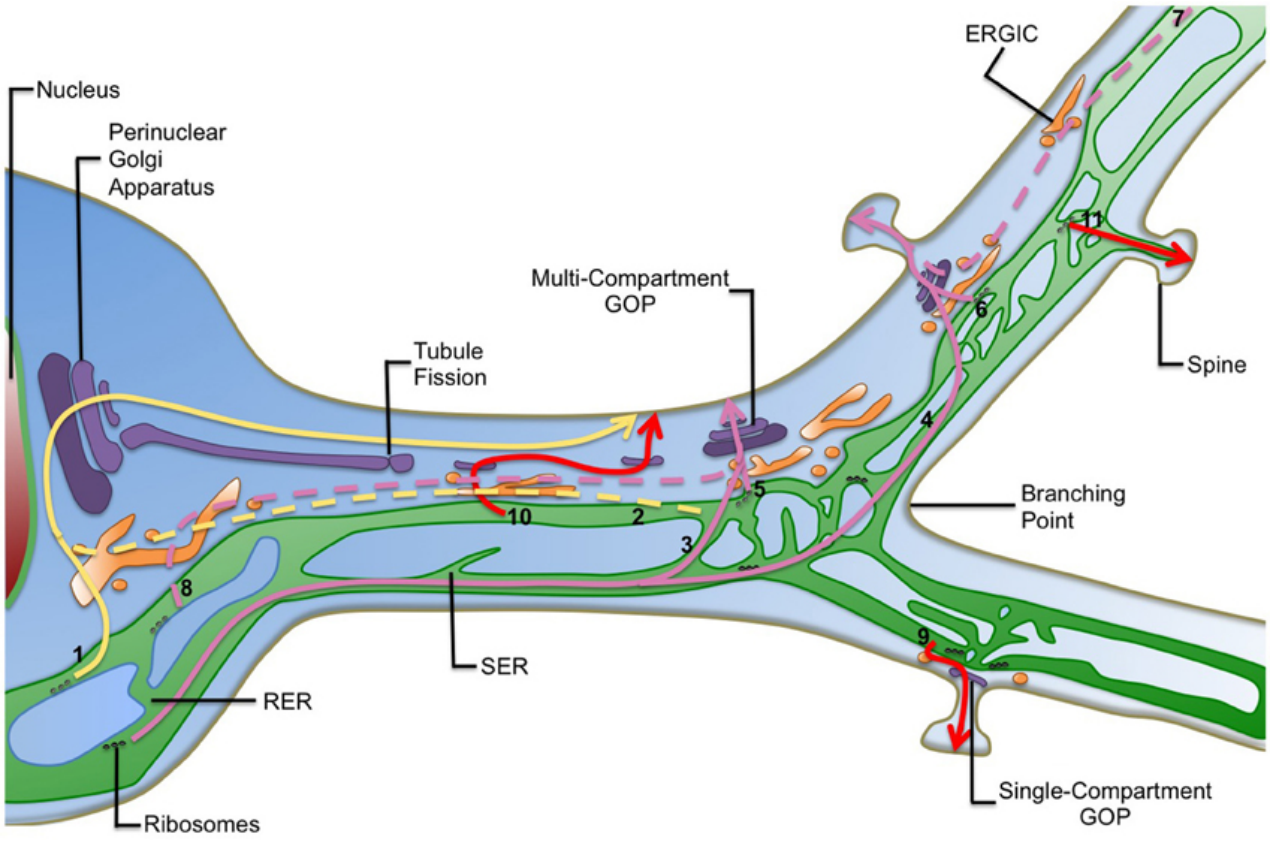

Figure 1.2 Schematic overview of Golgi outposts in neurons. Distribution of Golgi outposts in neurons and their role in the secretory pathways in dendrites. Figure adopted from Valenzuela and Perez (2015).

To understand the generation and regulation of dendritic Golgi outposts and to answer the question if Golgi outposts are produced by a fragmentation of somatic Golgi or generated locally from dendritic ER, the ultrastructure of Golgi outposts must be studied more systematically (Hanus and Ehlers, 2008).

The aim of this study is to analyze the ultrastructure of Golgi outposts in mammalian neurons and to examine their morphological differences from Golgi apparatus in soma. To localize these relatively rare organelles in neurons, I established and applied correlative light and electron microscopy methods in neuronal cell cultures and neuronal tissue.

1.4 Correlative Light and Electron Microscopy (CLEM)

Correlative light and electron microscopy (CLEM) is a technique that links the use of light and electron microscopes in order to analyze different characteristics of samples. This is a powerful technique as it involves the use of light microscopy (LM) low magnification range, which is essential for spotting regions of interest for consecutive high-resolution transmission electron microscopy (van Driel et al., 2008). To find specific and rare regions of interest using solely TEM is very challenging because of the fact that TEM functions best at higher magnification range (Koster and Klumperman, 2003). This is the case with electron tomography, because of using thick specimens, which may conceal important features in 2D mode. In contrast, live-cell imaging is a common use of LM, which helps to acquire valuable data about biological processes in living cells, along with the data acquired from the TEM (Svitkina and Borisy, 1998).

Despite the fact that CLEM techniques have been utilized in scientific research for decades (Figure 1.3), they are often not the preferred tools for carrying out experiments. One reason might be the limited availability of protocols for performing wide variety of experiments, in addition to the complex methodology that is not quite simple to follow (Kukulski et al., 2012; Bumbarger et al., 2013; Durdu et al., 2014). Moreover, the sample preparation methods for LM are different to TEM preparation, and combining both techniques makes one to choose between a good staining of cells for LM or preserving their ultrastructure for EM (Giepmans et al., 2005; Valentijn et al., 2010).

Therefore, an important target of my thesis work is improving the chemical fixation conditions for neuronal cell cultures and increasing the generation of DAB (3,3'-diaminobenzidine) precipitate by establishing a unique workflow for neuronal cell culture and neuronal tissue.

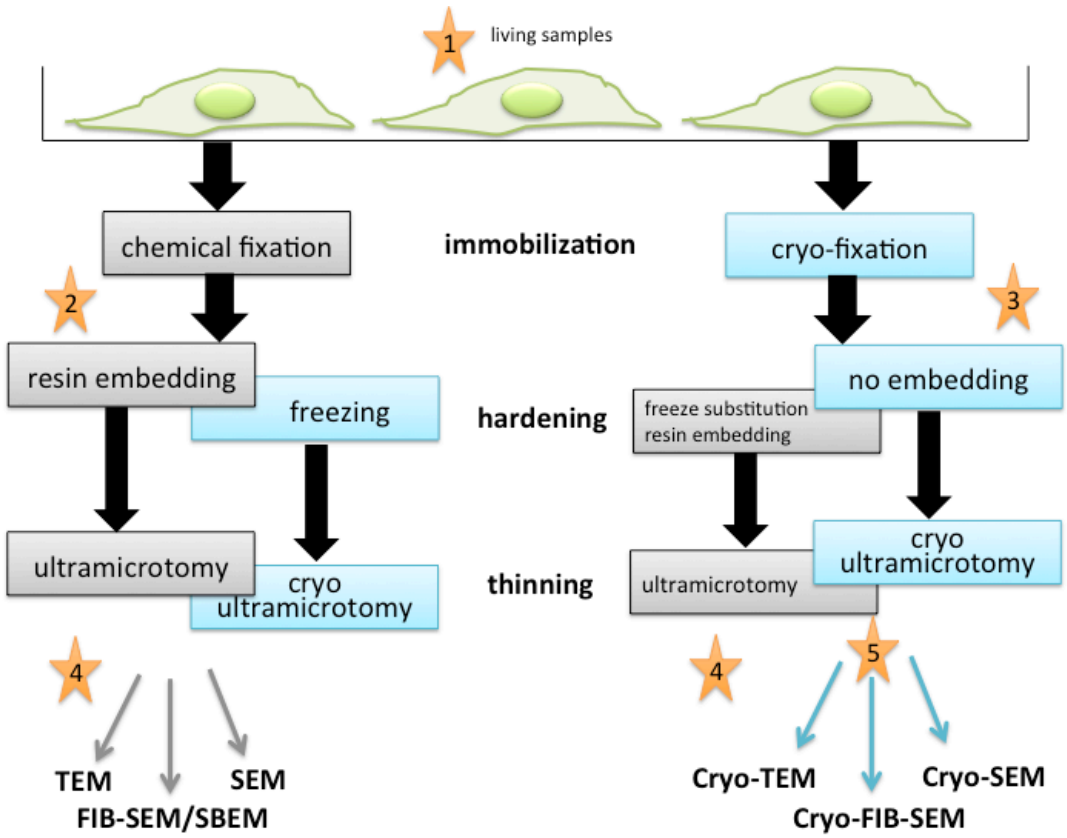

Figure 1.3 Schematic representations of correlative light and electron microscopy (CLEM) techniques. The present figure indicates the way for preparing samples for electron microscopy with various CLEM techniques. Orange stars marks the steps where LM could be utilized. (1) LM is applied on living samples. (2) LM is applied after chemical fixation. (3) On-section CLEM where correlation occurs, either by immunofluorescence and immunogold, or by correlating the conserved signal from fluorescent probes with EM. (4) Fluorescence is inspected on embedded samples. (5) LM imaging is executed on vitrified samples or sections. On the left are the different means of chemical fixation and on the right the different means of cryo-fixation. Figure based on Spiegelhalter et al., 2014.

1.4.1 Correlative light and electron microscopy through photo-oxidation

Photo-oxidation is a powerful technique for correlative light and electron microscopy. It is directly correlating fluorescent signals as detected by light microscopy, to electron densities embedded in their ultrastructural environment as detected by EM and electron tomography. The DAB is precipitated as a product of free oxygen radicals production (Grabenbauer, 2012; Maranto, 1982). The majority of the organic fluorophores used today, when excited, are able to create reactive oxygen species. These then react readily with DAB molecules producing radical intermediates (Figure 1.4). An electron-dense DAB polymer forms as a result of oxidative polymerization and cyclization. This

insoluble product can then be used to locate the structures of interest with great detail using EM (Grabenbauer, 2012).

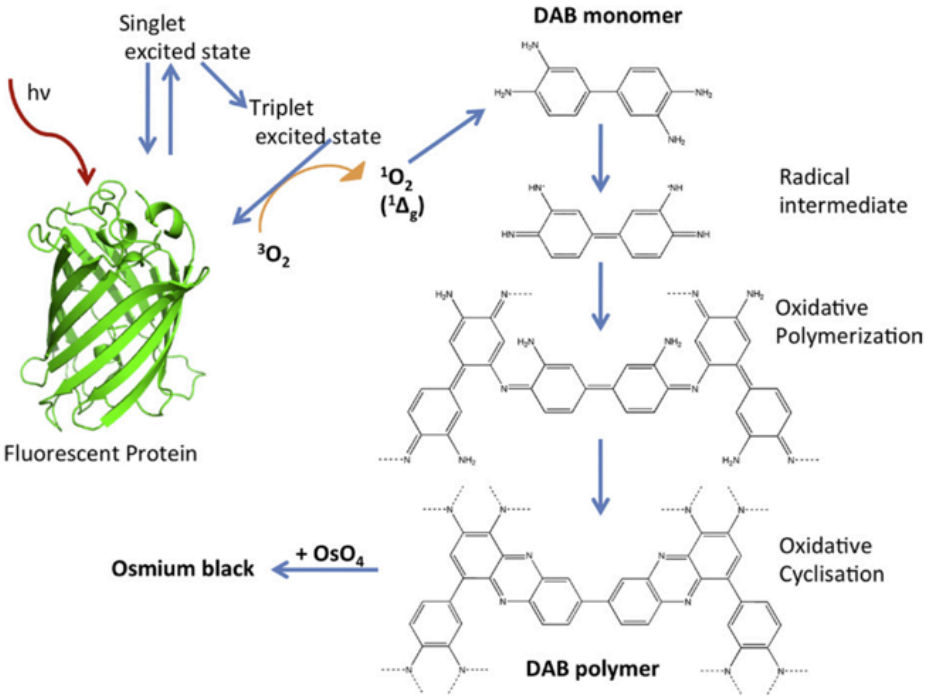

Figure 1.4 Reaction scheme of the DAB photo-oxidation through GFP. Excitation of GFP electrons generates singlet oxygen radicals which then interact with DAB monomers. This interaction triggers oxidative polymerization followed by oxidative cyclisation producing a DAB polymer that can then be stained by osmium tetroxide and visualized in electron microscopes. Figure adopted from Grabenbauer (2012).

Originally, the photo-oxidation technique was performed for neuronal mapping using micro-injected Lucifer yellow as fluorescent marker (Maranto, 1982). Meanwhile, several organic fluorophores have been described to photo-oxidize DAB in correlative microscopy studies (von Bartheld et al., 1990; Pagano et al., 1991; Deerinck et al., 1994). Styryl dyes such as FM 1-43 were used for staining synaptic vesicles (Harata et al., 2001; Denker et al., 2011; Hoopmann et al., 2012, Borst and Hoeve, 2012). Moreover, to better target correlative tagging in specific intracellular membranes, BODIPY was used as a ceramide analogue (Pagano et al., 1991). Recently, DNA-binding fluorophores have been used to determine 3D chromatin structure and compaction in cells (Ou et al., 2017).

1.4.2 Photo-oxidation mediated by green fluorescent protein

The Green Fluorescent Protein (GFP) was first isolated from the hydrozoa *Aequorea victoria* (Shimomura et al., 1962). The body of the animals contains a Ca^{2+} activating photoprotein (aequorin), which transfers energy (blue light) to GFP. In this process, GFP absorbs energy and emits green light. The gene for the GFP was cloned and subsequently characterized (Prasher et al., 1992; Inouye and Tsuji, 1994). The general structure of GFP is an "11-strand β-tube" surrounded by an α-helix. This structure protects the chromophore from solvents and oxygen (Yang et al., 1996).

Since Prasher has succeeded in using GFP as a marker for proteins, this technique has become a standard method and revolutionized cell biology research (Prasher et al., 1992). One of the most important applications is the genetic fusion of GFP with proteins in order to explore their expression, localization and intracellular transport. In this way, GFP mutants could already be introduced into many cellular structures such as different cell organelles. GFP can be readily fused either N- or C-terminally with any protein of interest (Romoser et al., 1997; Royston and Sorkin, 1998; Deo and Daunert, 2000), in most cases preserving the native localization and function of the protein.

GFP has been successfully used for photo-oxidation, the generation of oxygen radicals during the GFP bleaching process photo-oxidizes DAB into a precipitate with high electron density. The DAB precipitate can be visualized both by EM of thin sections and by electron tomography for 3D analysis (Grabenbauer et al., 2005; Meisslitzer-Ruppitsch et al., 2008; Grabenbauer, 2012; Horstmann et al., 2013). For correlative microscopy of GFPs can generally be used with certain spectral variants of GFP. The mTurquoise2 fluorescent protein has a higher quantum yield compared to GFP, EGFP or ECFP (K. van Eickels, MPI Dortmund, unpublished results) and therefore promises better performance.

1.4.3 Correlative light and electron Microscopy (CLEM) using high-pressure freeze fixation and freeze substitution

By the high pressure cryofixation, the sample is frozen as quickly as possible. This process takes a few milliseconds in practice. It has been demonstrated that cryofixed

samples better describe in vivo conditions of cells and tissue specimens than other preparation procedures, since it overcomes the problem of slow fixation rates (Shimoni and Müller, 1998). However, the problem of cryofixation is the tendency of water to form ice crystals upon freezing, which has a negative effect on structure conservation (Studer et al., 1995). The slower a sample is cooled, the more time the ice crystals grow and the bigger they become. To avoid this problem, the sample has to be frozen very fast at a pressure of 2100 bar (Moor and Riehle, 1968).

In order to embed the frozen sample in the hydrophobic polymer, the frozen water must be removed and replaced with organic solvent. This is achieved by the freeze substitution process, in which the frozen samples are heated in an organic solvent over an exponentially increasing temperature gradient from -90° C to 0° C or to -20° C for a period of 18 hours. During this warming, the water/ice is replaced by the organic solvent. The low initial temperature of -90° C prevents secondary ice crystal formation and also prevents extraction of biological fine structure. Acetone has been proven as good solvent, because it has a favorable polarity. Osmium tetroxide and uranyl acetate, which have been previously added to the solvent, are used as contrasting agents and fixatives (Steinbrecht and Müller, 1987). Osmium tetroxide binds nucleophilically or electrophilically to double bonds of unsaturated carbon atoms, e.g. in membrane lipids (Plattner and Zingsheim, 1987). The uranyl acetate interacts with negatively charged groups, such as phosphate residues or carboxyl groups, which contributes to contrasting and additional fixation of fine structures such as proteins or fibrils (Plattner and Zingsheim, 1987). The substitution solution might also contain a small amount of water (5%), which contributes to better preservation of fine morphological structures by stabilizing cellular membranes before fixation by osmium tetroxide and uranyl acetate (Plattner and Zingsheim, 1987; Walther and Ziegler, 2002). At the end of the freeze substitution process, the organic solvent in the sample is replaced again with an embedding resin that polymerizes to a hard block that can be cut by ultra-microtomy (Walther and Ziegler, 2002).

1.5 Protein Tags for Electron Microscopy

Pea ascorbate peroxidase (APEX) is a 28 kDa peroxidase that was developed as genetically encoded protein tag for electron microscopy analysis. APEX can endure the

processes of fixation needed for imaging samples utilized in electron microscopy. To emit it's signal, it does not need an external light source. Different than horse-radish peroxidase, which is not active in the cytosol, it is also active in any of the cell compartments (Hopkins et al., 2000; Martell et al., 2012).

The monomer APEX is derived from APX. The APX, a dimeric molecule ascorbate peroxidase, is a class I cytosolic plant peroxidase which has no disulfide bonds or calcium ions (Patterson WR and Poulos TL, 1995). To give EM contrast, after treatment with OsO_4, the APEX is utilized to catalyze the H_2O_2-dependent polymerization of DAB into a localized precipitate (Martell et al., 2012). The DAB polymer made by APEX at 4°C stays very localized at the site of production and without crossing any membranes (Ariotti et al., 2015), allowing very high spatial resolution.

The size of GFP (27 kDa) is very similar to APEX, which is a monomeric heme enzyme. Usually, APEX fusion constructs expressed by cells use aldehydes for the fixation process and are afterwards stained with H_2O_2 and DAB. These small molecules disperse easily into the non-permeabilized cells. APEX then oxidizes them to an insoluble DAB polymer. Then, to become visible in EM, the treatment with osmium tetroxide (OsO_4) is performed. After the cell fixation with glutaraldehyde, APEX stays active and that yields excellent preservation of ultrastructure (Martell et al., 2017).

The original APEX tag allowed EM imaging of many proteins. However, in some cases, APEX failed to produce DAB precipitate visible in EM, especially for fusion constructs expressed at low levels. APEX2, which is a single mutant of APEX (A134P), was developed (Martell et al., 2017). While having the benefits of APEX, APEX2 produces the DAB polymer with faster kinetics and integrates better the heme cofactor in the cells (Lam et al., 2015). In all cases tested, a better EM contrast was generated by APEX2 than with APEX (Martell et al., 2017).

1.6 Aim of the study

The aim of this study is to examine the morphology of Golgi apparatus in neurons, in particular to address possible differences between Golgi structures in neuronal soma compared to Golgi outposts in dendrites. Therefore, the establishment of correlative microscopy methods in neuronal cell cultures and neuronal tissues with emphasis on high precision correlation using photo-oxidation was required. This labeling method allows the detection of rare neuronal organelles like Golgi outposts by fluorescence microscopy and subsequently examine their ultrastructure using high resolution electron microscopy. For this purpose, I first aim to improve the chemical fixation conditions for hippocampal neuronal cell cultures. Further, increasing the generation of GFP-specific DAB precipitation by establishing a unique workflow for neuronal cell cultures and neuronal tissue. To enable specific labelling of Golgi apparatus, two constructs were cloned, GalNAcT2 and GalNAcT2-APEX, and utilized for the creation of recombinant adeno- associated viruses (rAAVs) to genetically induce the expression of mTuorquoise2 in neurons.

Finally, electron tomography and three dimensional analysis methods would be applied on somatic Golgi apparatus and Golgi outposts to identify whether Golgi outposts in dendrites differ from Golgi complex in soma.

Demonstrating several high-resolution images of Golgi outposts in this study will allow us to better understand the organization and the morphology of this crucial organelle, which was discussed in recent studies by showing it mainly using fluorescence microscopy.

2. Materials and Methods

2.1 Molecular biology

2.1.1 Plasmid cloning

pAM-CAG-mTurquoise2

The mTurquoise2 coding sequence was generated by multiple mutagenesis reactions on template DNA Cerulean3 at three different positions (Table 2.1) by the QuikChange II XL Site-Directed Mutagenesis Kit (Cat.No 200521, Agilent) according to manufacturer's instructions. Subsequently, it was subcloned *via* EcoRI and HindIII into the pAM vector (Klugmann et al., 2005). Expression is controled by the CAG-promoter.

pAM-CAG GalNAcT2 (Pos1-348)-Turquoise2

The plasmid carrying the coding sequence of GalNAcT2 (Pos1-348-encoding the cytoplasmic, transmembrane and stalk region) was amplified by reverse transcription polymerase chain reaction (RT-PCR) from mouse brain using the primers listed in Figure 2.1 and subcloned into pAM_CAGProm mTurquoise2 plasmid *via* BamHI.

pAM-CAG GalNAcT2 (Pos1-348)-Apex2-mTurquoise2

To generate the plasmid pAM_CAGProm GalNAcT2 (Pos1-348)-Apex2-mTurquoise2, the APEX2 coding sequence was amplified by PCR from template DNA APEX2-GBP (Addgene plasmid #67651) and subcloned between GalNAcT2 and mTurquoise2 using BglII.

All restriction enzymes were sourced from New England Biolabs (Ipswich, MA) and used according to manufacturers recommendations. All plasmid constructs were validated by restriction analysis and DNA sequencing.

Mut-Turquoise-F1	5'end-ACAAGCTGGAGTACAACTACTTTAGCGACAACGTCTATATCA3'end
Mut-Turquoise-R1	5'end- TGATATAGACGTTGTCGCTAAAGTAGTTGTACTCCAGCTTGT-3'end
Mut-Turquoise-F2	5'end- AACATCGAGGACGGCGGCGTGCAGCTCGCCG-3'end
Mut-Turquoise-R2	5'end- CGGCGAGCTGCACGCCGCCGTCCTCGATGTT-3'end
Mut-Turquoise-F3	5'end- CTCGTGACCACCCTGTCCTGGGGCGTGCAGT-3'end
Mut-Turquoise-R3	5'end- CTCGTGACCACCCTGTCCTGGGGCGTGCAGT-3'end
m-Galnt2-B-F	5'end-tttggatCCGCCATGCGGCGGCGCTCGCGGATGCT-3'end
m-galnt2-B-R	5'end-ttttggatccACGAAGCTTATCACTCTCCACCTGGTTGAACTTG-3'end
Apex(Galnt2)-BglII-F	5'end-ttaagatctctcgagATGGGAAAATCTTACCCAACTGTTAGTCCCG-3'end
Apex(Galnt2)-BglII-R	5'end-attagatctgagctcGGCTTCAGCAAATCCAAGCTCAGAGA-3'end

Table 2.1 List of PCR-primers used for subcloning and mutagenesis of GalNAcT2, APEX2 and mTurquoise2 plasmids.

2.1.2 Production of recombinant Adeno-associated virus (rAAV)

Adeno-associated virus (AAV) particles were created in HEK293 cells (293AAV, Agilent Technologies, Santa Clara, California (CA), USA). 4×10^6 HEK cells were seeded in DMEM medium (PAN-Biotech, Aidenbach, Germany), supplemented with 10 % FCS, 0.2 mM non-essential amino acids, 2 mM sodiumpyruvate, and 1 % penicillin/ streptomycin per 14.5 cm cell culture dish. The targeted rAAV expressed the AAV capsids of serotype 1 and 2 as a mosaic provided by the plasmids pDP1 and pDP2 (Grimm et al., 2003), respectively.

The HEK cells were transfected 24 h after plating with equimolar quantities of pAM plasmid (plasmid containing the ITRs with the gene of interest), pDP1rs and pDP2rs applying calcium phosphate as the method of precipitation. The transfection mixture for a single 14.5 cm dish was composed of 125 mM $CaCl_2$ and 37.5 µg DNA in 2 ml HBS buffer (140 mM NaCl, 25 mM HEPES, 0.7 mM Na_2HPO_4, pH 7.05). This mixture

incubated then for 3 min before the dropwise addition to each dish. After 24 h the medium was replaced.

Three days after transfection, cells were gathered from which viral particles were purified. For this, the cells were scraped from the dish, pelleted at 200 g for 10 min, then re-suspended in a lysis buffer (150 mM NaCl, 50 mM Tris-HCl, pH 8.5), and subsequently lysed *via* three cycles of freeze and thaw. Unpacked genomic DNA was digested for 2 h at 37 °C with 50 Units of benzonase nuclease (Sigma-Aldrich, St. Louis, MO, USA) per 14.5 cm culture dish. To remove the cell debris, centrifugation was performed at 3640 g for 15 min and the supernatant was passed through a 0.45 μm pore-size filter to yield the crude lysate. From the lysate, the rAAV particles were purified by affinity chromatography in a heparin-agarose Type I packed Econo-Pac chromatogaphy column (Biorad, Hercules, CA, USA). For the packing of the column, first the column was prewashed with 10 ml equilibration buffer (1 mM $MgCl_2$, 2.5 mM KCl in PBS, pH 7.2), then the resin was prepared: 5 ml of heparin-agarose (Sigma-Aldrich, Munich, Germany) were mixed with 10 ml of equilibration buffer and applied to the column. After the settling of the heparin-agarose, the excess fluid above the heparin agarose bed was drained. To the column the crude lysate was applied, and then incubated on a shaker for 2 h at 4 °C. Then again the excess fluid was drained and the column washed with 20 ml of equilibration buffer. The viral particles were eluted with 15 ml elution buffer (500 mM NaCl, 50 mM Tris-HCl, pH 7.2) and gathered in an AmiconUltra15 centrifugal filter unit (Merck Millipore, Darmstadt, Germany). The eluate was concentrated by centrifugation (3645 g) until less than 1 ml remained (typically <3 h) and the rAAV sample was washed 3 × with 15 ml of PBS and concentrated until less than 200 μl volume remained. This virus was finally filtered through a 0.22 micron pore size filter and stored at 4 °C.

2.2 Cell culture

2.2.1 HeLa cell culture

HeLa cells (No. CCL 185; Rockville, MD, USA) were grown in Dulbecco's modified Eagle's medium supplemented with 10 % fetal calf serum (FCS) and 2 mM L-glutamine (GIBCO BRL, Life Technologies) at 37 °C and 5 % CO_2 on uncoated glass bottom (No. 1.5) petri dishes (MatTek, Ashland, MA, USA). The cells were stably transfected to express an established Golgi marker, human Golgi-resident enzyme N-acetylgalactosaminyltransferase 2 (GalNAcT2), which was fused to enhanced green or cyan GFP-mutants, EGFP (GalNAcT2 ^{GFP}) and ECFP (GalNAcT2 ^{CFP}) as described in (Storrie, B. et al., 1998).

2.2.2 Primary hippocampal neuronal culture

Primary cultures of rat hippocampal neurons were produced according to a standard protocol described in the following chapters (Banker and Goslin, 1998). The primary hippocampal cells were also produced as described in (Dresbach T. et al., 2003).

2.2.2.1 Preparation of coverslips for light microscopy

Sterilized glass-bottom petri dishes were used. Glass slides were covered with poly-L-lysine (20 µg/ml, Sigma-Aldrich, Munich) and incubated at 37 °C for at least 1 h. The poly-L-lysine solution was removed and the coverslips washed 3 × with PBS before storing in HBSS at 37 °C.

2.2.2.2 Harvesting neuronal cells from rat fetuses

Pregnant Wistar rats were acquired from Charles River (Sulzfeld, Germany) and fetuses were surgically removed when they reached the developmental stage E19. The rats were anesthetized using Narcoren (Merial GmbH, Germany). All fetuses were extracted from the mother without damaging the amniotic sac. Afterwards, the fetuses heads were

removed close to the skull and placed on an ice cooled petri dish. Under a binocular microscope, the heads were then fixed with a forceps close to the eyes. The blade of a fine scissor was then pushed through the medulla towards the rostrum to perform a horizontal cut through half of the brain. On the other side of the head, the step was repeated. Using another forceps, the skullcap was lifted from the medulla towards the rostrum. The separated dorsal brain part including the hippocampus was relocated on an ice-cooled petri dish. The meninges were removed before the cortical hemispheres were bent to the side to reveal the hippocampus. With two forceps, the hippocampal tissue was dissected from the attached brain regions and put into ice cold Hank's Buffered Salt Solution (HBSS, Gibco, Thermo Scientific, Darmstadt, Germany). The hippocampal tissues from all fetuses were pooled as described below.

2.2.2.3 Isolation and plating of hippocampal cells from tissue

The hippocampal tissue was then transferred with 2 ml of HBSS into a 15 ml conical tube and by addition of 200 µl trypsin solution digested for 20 min at 37 °C. The excess trypsin solution was removed and the tissue was then washed 2 × with 12 ml plating medium (Serum containing DMEM (Invitrogen 41966-029) with 10% FCS (PAN), 1% Penicillin/Streptomycin (Invitrogen 15140-122) without glutamine. The hippocampi then were transferred to a 2 ml tube and re-suspended 3 × with a syringe and injection needle and 3 × with a smaller needle (BD, 300400). A cell filter (BD, 352360) was placed on a 50 ml conical tube and wetted with 2 ml plating medium without glutamine. A filtration of the tissue suspension was carried out into the conical tube and filled to 10 ml plating medium. The cells were then counted and the cell density was adjusted with plating medium to between 50,000 – 60,000 cells per petri dish (500 µl). Before the cells were seeded, HBSS was aspirated from the coverslips. The next day or after at least 3 h, the plating medium was replaced with growth medium (Neurobasal (Invitrogen 21103-49) supplemented with Neuropan 27 Supplement 50x (PAN P07-07210), 1% Penicillin/Streptomycin, 0.5 mM Glutamin and 5µg/ml HoloT) and kept at 37 °C for 6 days.

2.3 Preparation of neuronal tissue

2.3.1 Animal housing

Male C57Bl/6 (22g) mice were ordered from Charles River. The animals were kept alone in Makrolon type IV cages (40 x 18 x 12 cm) and kept in humid room Bioscape system with Venti racks, daily humidity control 55% relative humidity and temperature 22 °C with conditions on a 12h day-12h night cycle. The mice had access to food and water ad libitum.

All animal experiments were done in accordance with the German welfare guidelines and were approved by the Regierungspräsidium Karlsruhe.

2.3.2 Stereotaxic injection of recombinant adeno-associated viral particles

All injections were executed operating a stereotaxic alignment system (basic model: 1900, David Kopf Instruments, Tujunga, CA, USA). Mice (22g) were anesthetized by an intraperitoneal injection of a mixture of 40 µl Fentanyl (1 mg/ml, Janssen-Cilag, Neuss, Germany), 160 µl Midazolam (5 mg/ml, Hameln Pharma Plus, Hameln, Germany) and 60 µl Medetomidin (1mg/ml, Sedan Alvetra-Werfft, Neumünster, Germany) at a dosage of 3.1 µl/g body weight. The mice were observed for up to one hour after injection and the hind limb reflexes were checked before, when reflexes disappeared, initiating the surgery. The mice received at the end of the surgery a subcutaneous mixture of 3 substances to counter anesthesia, containing 120 µl Naloxon (0.4 mg/ml, Inresa, Freiburg im Breisgau, Germany), 800 µl Flumazenil (0.1 mg/mL, Fresenius Kabi, Bad Homburg vor der Höhe, Germany) and 60 µl Antipamezole (5 mg/ml, Antisedan, Pfizer, Karlsruhe, Germany) at a dosage of 6.2 µl/g body weight. The mice body temperature was maintained at 38 °C during the entire surgical procedure. Once the surgery ended, the mice received as an analgesic a subcutaneous

injection of Carprofen (Rimadyl, Pfizer, Karlsruhe, Germany) dosed 10 µg/g body weight.

The mice heads were shaved and their skin disinfected in order to conduct the surgical procedure. Once the mouse no longer showed reflexes, it was fixed into the head-holder with ear bars attached to the os petrosum and the tongue pulled out of the mouth. Thereafter, as a local anesthetic, ~100 µl Xylocain solution (1 %, Astra Zeneca, Wedel, Germany) was applied subcutaneously. An incision along the midline of the skull was done and the skin retracted laterally. As reference, two marker points of the skull were used: bregma – the point of connection between the frontal bone and the parietal bones, and lambda – between the occipital bone and the parietal bones. The head was then leveled in the sagittal and coronal plane using an electronic leveling device (eLeVeLeR) (Wimmer et al., 2004) (Sigmann Elektronik). Afterwards, small holes were drilled by operating a hand-held dental drill (Osada EXL-40, Los Angeles CA, USA) in the skull at coordinates AP –2.18 mm, Lat ± 1.5 mm relative to bregma to target the hippocampus or at AP –1.26 mm, Lat ± 2.8 mm relative to bregma to target the visual cortex. Virus was injected at depths of (CA1) 1300 µm, (DG) 1600 µm and (visual cortex) 850 µm delivering ~1 µl each *via* glass micropipettes (Blaubrand IntraMARK 5 µl, #708707, Wertheim, Germany) pulled with a P97 horizontal puller (Sutter Instruments, Novato CA, USA) to an inner diameter of 10 – 20 µm at the tips. The injections were conducted at a rate of about ~3 µl/h with manually controlled pressure applied with a 10 ml syringe. Crucially, the viral solution needed to remain in the brain tissue and not leak again at the injection site. Consequently, after placing the injection micropipette in the required depth, 2 min were allowed to pass before starting the injection to allow the tissue to tighten around the injection site. Additionally, to prevent the drying out of the brain surface, sterile PBS was applied at all times to keep it moist. At the end, the skin was sutured and the wound disinfected.

2.3.3 Perfusion fixation

Mice were perfused after 1-3 months of stereotaxic injection. To conduct this, the mouse was anesthetized with isoflurane and their abdominal cavity and their thorax opened. In the left ventricle, a 22G injection needle (BD Microlance TM3) was inserted, an opening in the right atrium was made and successively the solutions were infused.

First, mice were perfused trans-cardially with 40 ml of PBS, respectively, followed by approx. 40 ml fixative perfusion supplemented with 4 % paraformaldehyde (PFA) and 0.2 % glutaraldehyde (GA) in 0.1 M PHEM buffer (0.4 M PHEM buffer stock solution contains 240 mM Pipes, 100 mM Hepes, 8 mM $MaCl_2$, 40 mM EGTA, pH to 6.9 with KOH), respectively. After the perfusion brains were immediately extracted and postfixed in PFA/GA/PHEM buffer over night at 4 °C.

2.4 Correlative Light & Electron Microscopy

2.4.1 Fluorescence microscopy of HeLa cells

HeLa cells were grown in glass- bottom petri dishes (1.5; MatTek) 24 h to 48 h before use and observed at filter settings for CFP or GFP, respectively, using a fluorescence lamp on a Zeiss AxioVert.A1 inverted light microscope furnished with a 63x oil immersion objective. Live or fixed cells were imaged using Zeiss Axiocam camera operated by the Open Lab software (AxioVision Rel. 4.5).

2.4.2 Fluorescence microscopy of hippocampal neurons

Hippocampal neurons were infected with rAAV by adding 0.5 – 1 µl of virus stock solution in 2 ml growth medium per petri dishes for 9 days. For correlative light/electron microscopy the cells of interest were observed as described in 2.4.1.

2.4.3 Immunofluorescence microscopy

Cells were washed with prewarmed (37 °C) PBS buffer for 1 min and fixed with prewarmed fixative containing 4 % PFA and 4 % sucrose in PBS buffer for 20 min at RT. After 3 × 10 min washing steps in PBS at RT, samples were incubated in blocking solution (0.1 % Triton X-100 (Tx-100) (Sigma) and 2 % FCS (Anprotec) in PBS) for 10 min at RT. Primary antibodies (1:500) were diluted in blocking solution and applied to the sample ON at 4 ºC. Samples were again washed 3 × with PBS for a total of 15 min. Subsequently, the secondary antibodies (1:500) were applied for 1 h at RT, followed by

a final washing step (3 × for a total of 15 min). A detail of the primary and secondary antibodies that were used in this study can be found below, Table 2.2.

Primary Antibodies

Antigen	Species	Source (Cat. No.)
MAP2	rabbit	Merck #AB5622
MAP2	chicken	SySy #188 006
Lamp2	mouse	SCBT# 18822
TGN38	rabbit	NBPT#03495

Secondary Antibodies

Against	Species	Fluophore	Source (Cat. No.)
rabbit	goat	Alexa-647	ThermoFisher#A21245
chicken	goat	Alexa-647	ThermoFisher #A21449
mouse	goat	Alexa-647	ThermoFisher #A21235
rabbit	goat	Alexa-488	ThermoFisher #A11008

Table 2.2 Primary and secondary antibodies used in this study.

2.4.4 Photo-oxidation of HeLa cells

Photo-oxidation through GFPs was performed as described previously (M. Grabenbauer et al., 2005, Grabenbauer 2012). All the steps for the incubation including bleaching, dehydration and resin polymerization were conducted in glass-bottom tissue culture dishes. The cells were briefly washed with pre-warmed calcium- and magnesium-free phosphate-buffered saline (PBS) (500 ml PBS, Gibco, with 1 mM/l $MgCl_2$, 2.5 mM/l KCl, pH 7.2; Thermo Scientific, Darmstadt) and fixed for 30 minutes with pre-warmed fixative containing 2 % glutaraldehyde (25 % stock solution; EM grade, Merck Millipore, Darmstadt, Germany) and 2 % sucrose (Sigma -Aldrich, Steinheim, Germany) in PBS. After the cells were washed 3 × with PBS, endogenous enzyme activity and endogenous autofluorescence were blocked with 100 mM glycine (Sigma -Aldrich, Steinheim, Germany) and 50–100 mM potassium cyanide (Sigma -Aldrich, Steinheim, Germany) in PBS for 1.5 h followed by 40 min incubation with 100 mM ammonium chloride (Sigma -Aldrich, Steinheim, Germany) and 10 mg/ml sodium borohydrate (Sigma -Aldrich, Steinheim, Germany in PBS).

For photo-oxidation, samples were washed in Tris-buffered saline (TBS, Sigma -Aldrich, Steinheim, Germany) and then incubated in an oxygen-saturated newly prepared solution that contained 1-2 mg/ml diaminobenzidine (DAB) (Dako North America, Inc. 6392 Via Real Carpinteria, CA, USA) in TBS. For bleaching, the samples were illuminated with maximize intensity using the suitable filter settings for EGFP (38 HE excitation filter BP 470/40) or ECFP (47 HE excitation filter BP 436/20) (AttoArc; Zeiss, Heidelberg, Germany) at 4 °C by using a cooling unit (LKB Bromma 2219 / 2219-001 Multitemp II Digital Thermostatic Circulator, Germany); the low temperature maintains a high oxygen content and supports effective and specific DAB polymerization (Grabenbauer et al., 2005). The development of the DAB reaction was monitored and photo-oxidation was stopped when cytosolic background staining occurred, typically after 3 min in samples expressing GFP or 2 min for CFP.

After photo-oxidation, the samples were washed 3 x with distilled water and post-fixed for 30 min on ice in 1 % osmium tetroxide (OsO_4) reduced by 1.5 % potassium ferrocyanide (Serva, Heidelberg, Germany). Thereafter, samples were washed with distilled water for 10 min and then they were dehydrated by incubation in graded ethanol series of 75 %, 95 %, 3 × 100 % ethanol, 5 min each. During this procedure, the

cells should not dry out. After the dehydration step, Epon 812 (Serva, Heidelberg, Germany) was applied on the cells for at least 1 h at RT. Afterwards, Epon was removed carefully by dripping off without drying or damaging the samples. Next, fresh Epon was applied on the samples. A small Eppendorf tube without lid was filled with Epon placed on top of the cells. Finally, samples were incubated in an oven to polymerize Epon at 60 °C ON.

2.4.5 Photo-oxidation of hippocampal neurons

After several chemical fixatives were tested in neuronal cells (Table 2.3), different to the photo-oxidation preparation of HeLa cells (see above 2.4.4), the hippocampal neuronal cells were fixed with prewarmed (37 °C) fixative containing 2 % glutaraldehyde and 2 % sucrose in sodium cacodylate (CAC) buffer (CAC buffer; 0.15 M sodium cacodylate, pH 7.4 with 3 mM $CaCl_2$) for 30 min at room temperature (RT). Before the cells were washed with PBS (3 × 5 min at RT), samples were washed with CAC buffer for 3 × 5 min at RT. As described in chapter 2.2.4, the endogenous enzyme activity was blocked with 50–100 mM potassium cyanide and 100 mM glycine in PBS for 1 h and 30 min on ice. After the samples were shortly washed with PBS, also endogenous autofluorescence was blocked in two steps as in chapter 2.2.4. First by 100 mM ammonium chloride in PBS for 40 min on ice, then by 10 mg/ml sodium borohydrate freshly dissolved in PBS also for 40 min on ice. Between the two steps, samples were shortly washed with PBS. Thereafter, samples were washed with TBS for 3 × 5 min on ice.

For the photo-oxidation reaction – as described for HeLa cells (2.4.4) – the DAB solution was freshly prepared and kept in the dark. Directly before the application of DAB to the samples, the DAB solution (1-2 mg/ml) was enriched by letting pure oxygen gas bubbling through and the pH-value was checked in advance, and adjusted to pH 7.4. To bleach GFPs and generate reactive oxygen species for DAB photo-oxidation, the samples were illuminated with the suitable filter setting for CFP using a fluorescence lamp on an inverted microscope (Zeiss Axiovert-100 TV) and a high-numerical-aperture objective (63x oil immersion objective). The progress of the DAB

reaction was observed very carefully and immediately halted, if cytosolic background staining occurred, usually after 2 min when using mTurquoise2. After the photo-oxidation reaction was done, samples were washed shortly in TBS and subsequently for 3 × 5 min in distilled water. Afterwards, samples were post-fixed in 2 % OsO_4 reduced by 1.5 % potassium ferrocyanide for 30 min on ice.

After osmium post-fixation step – different to the HeLa-cells workflow – the next steps must not be continued at the same day. The samples were kept in distilled water ON at 4 °C after they were washed for 10 min in distilled water.

At the next day, samples were dehydrated as described in chapter 2.4.4 by incubation in graded ethanol series of 75 %, 95 %, 3 × 100 % ethanol, 5 min each. During this procedure, the samples should not be allowed to dry out. After the dehydration step, Epon was applied on the cells for 1 h at RT. Thereafter, Epon was removed carefully and fresh Epon was applied on the samples and a small Eppendorf tube without lid was filled with Epon and placed on top of the cells. Finally, samples were incubated in an oven to polymerize at 60 °C ON.

Fixative Solution	Time and Temperature of Fixation
4% PFA and 2% Sucrose in PBS	30 min, RT
4% PFA, 2% GA and 2% Sucrose in PBS	30 min, RT
2% GA and 2% sucrose in PBS	30 min, RT
2% GA and 2% Sucrose in CAC buffer with $CaCl_2$	30 min, RT

Table 2.3: Different chemical fixative solutions for neuronal cell culture.

2.4.6 Photo-oxidation of neuronal tissue

After post-fixation, using a vibratome slicer (Leica VT1000 S, Germany), 90 μm-thick coronal sections were cut containing the injected regions. Viruses were injected into the

visual cortex or into the hippocampus (C1 and DG) either using AAV1/2-GalNAcT2-mTurquoise2 or AAV1/2-GalNAcT2-APEX-mTurquoise2.

The coronal sections containing mTurquoise2 in the visual cortex or in the hippocampus were washed in CAC buffer and subsequently in PBS for 1 h each at 4 °C. As described in 2.2.4, the endogenous enzyme activity was blocked with 50–100 mM potassium cyanide and 100 mM glycine in PBS for 2 h on ice and the endogenous autofluorescence was blocked in two steps, first by 100 mM ammonium chloride in PBS for 1 h on ice, then by10 mg/ml sodium borohydrate freshly dissolved in PBS also for 1 h on ice. Between the steps, sections were shortly washed with PBS. Afterwards, sections were washed 3 × for 15 min in TBS on ice or ON at 4 °C

For the photo-oxidation reaction, sections were bubbled with O_2 for 60 min in 0.15 M TBS at pH 7.4. The DAB solution was newly prepared and kept in the dark. Directly before applying to the samples, the DAB solution (1-2 mg/ml) was enriched by letting pure oxygen gas bubbling through and the pH-value was checked in advance and adjusted to pH 7.4. To bleach GFPs for photo-oxidation, samples were illuminated with the suitable filter setting for CFP using a bright fluorescence lamp on a Zeiss AxioVert.A1-Inverted light microscope equipped with a 40x oil immersion objective. To generate an effective DAB precipitation, the climate chamber of the microscope was set at a low temperature (4 °C). The progress of the DAB reaction was observed carefully and halted once cytosolic background staining occurred, usually after 4 min. After stopping the photo-oxidation reaction, sections were washed shortly in TBS and subsequently for 3 × 15 min in distilled water. Afterwards, sections were postfixed in 1 % osmium tetroxide reduced by 1.5 % potassium ferrocyanide for 1h on ice. The sections were washed for 30 min in distilled water and kept in distilled water ON at 4 °C. At the next day, the bleached region containing the cells of interest were cut carefully with a scalpel, then the samples were dehydrated by incubation in graded ethanol series of 75 %, 95 %, 3 × 100 % ethanol, 15 min each. After the dehydration step, sections were shortly washed with propylenoxide then stored ON in a mixture consisting of propylenoxide and epon (1:1). The tissue was then transferred into fresh resin and polymerized at 60 °C for 36 h. Once the resin was polymerized and solidified, the block was trimmed using a Diatome ultra 45° 2,0 mm diamond knife (Science Services GmbH, Munich, Germany) and cut to a thickness of approximately 70 nm.

2.4.7 Correlative microscopy of hippocampal neurons using APEX

The cells were washed with prewarmed (37 °C) PBS for 30 s. Next, the cells were fixed with prewarmed fixative containing 2 % glutaraldehyde and 2 % sucrose in CAC for 30 min at RT. Thereafter, samples were washed 3 × 10 min with CAC buffer at RT and then incubated in freshly prepared buffered solution of 10 mg DAB in 40 ml of CAC buffer for 1 h at RT. For the DAB reaction, samples were incubated for 2 h at RT in 10 mg DAB in 40 ml CAC buffer supplemented with 0.03 % (w/v) H_2O_2. Then, samples were washed with CAC buffer for 3 × 15 min at RT. Next, as described in (Joesch M et al. 2016) samples were incubated in reduction buffer containing 0.8 % (w/v) sodium hydrosulfite and 60 % (v/v) 0.1 M sodium bicarbonate in 0.1 M sodium carbonate buffer with 3 mM $CaCl_2$ for 20 min at RT. Then, samples were washed with CAC buffer for 3 × 10 min at RT. Afterwards, samples were post-fixed and further treated as described in chapter 2.4.5.

2.4.8 Correlative microscopy preparation of neuronal tissue using APEX

The coronal sections (90 μm-thick) containing APEX2-mTurquoise2 in visual cortex or in hippocampus were washed in CAC buffer for 1 h at 4 °C. Thereafter, sections were bubbled for 2 h with pure O_2 in CAC buffer at RT, before they were incubated in freshly prepared solution of 10 mg DAB in 40 ml buffered by CAC buffer for 1 h at RT. For the DAB reaction, sections were incubated for 2 h at RT in 40 ml CAC buffer supplemented with 10 mg DAB and 0.03 % (w/v) H_2O_2. Then, they were washed with CAC buffer for 3 × 20 min at RT. Next, as described in (Joesch M et al. 2016) sections were incubated in reduction buffer containing 0.8 % (w/v) sodium hydrosulfite in 60 % (v/v) 0.1 M sodium bicarbonate 40 % (v/v) 0.1 M sodium carbonate buffer with 3 mM $CaCl_2$ for 30 min at RT. Then, they were washed with CAC buffer for 3 × 20 min at RT. Afterwards, sections were post-fixed in 1 % osmium tetroxide reduced by 1.5 % potassium ferrocyanide for 1 h at RT. The samples were kept in distilled water ON at 4 °C after they were washed for 30 min in distilled water. Further treatment of the samples was applied as described in chapter 2.4.6.

2.5 Correlative microscopy using high-pressure freeze fixation

2.5.1 Preparing sapphire discs for hippocampal cell culture

Sapphire discs (Engineering Office M. Wohlwend GmbH, Sennwald, Switzerland) were rinsed in ethanol and water blotted on filter paper prior to further use. Then, the sapphire discs were covered with coating buffer containing poly-DL-ornithine hydrobromide (100 mg Sigma P3655, Germany) in 200 ml H_3BO_3 (150 mM, pH 8.3) and incubated at 37 °C for at least 2 h. The coating solution was removed and sapphire discs were washed 3 × with prewarmed (37 °C) HBSS. A finder-grid (Plano, Wetzlar, Germany) was placed on the top of the sapphire discs followed by carbon coating with about 15 nm carbon (Carbon coater, Leica EM ACE600, Vienna, Austria) and then baked at 120 °C ON. Next, sapphire discs were sterilized under UV in the cell culture bench for 30 min. Thereafter, sapphire discs were again covered and incubated with coating buffer for another 2 h at 37 °C. After removal of the coating solution the sapphires were washed 3 × with prewarmed HBSS before they were stored in HBSS at 37 °C ON. It has to be enough media on top of the sapphire discs to make sure they stay at the bottom of the dish. Forceps were used to check that the sapphire discs are really at the bottom.

Finally, cells were added and dishes were moved south-north and east-west to make sure the cells spread evenly. There should be no air bubbles around the sapphire discs which could cause them to float. Hippocampal cell cultures were 6 DIV before they were infected with AAV1/2-GalNAcT2-mTurquoise2 by addition of 0.5 µl virus stock solution to 2 ml for 9 days at 37 °C.

2.5.2 High-pressure freezing and freeze substitution

The sapphire discs were sandwiched between two carriers: B-carriers and A-carriers. Both carriers were covered with a thin layer of 1-hexadecene. The 0.1 mm deep aluminum carriers (B-carriers) were placed on top of the cell layer and the flat surface of the 0.3 mm carriers (A-carriers) were placed below the sapphire discs. Thereafter, this sample was immediately placed into the sample holder of the Baltec HPM010 High Pressure Freezer (Hawes, Netherton, Mueller, Wileman, & Monaghan).

After the high-pressure freeze fixation was done, the frozen samples were transferred to liquid nitrogen as quickly as possible in order to prevent warming and crystallization of the frozen water inside the samples.

2.5.2.1 Freeze substitution solution

Final freeze substitution solution was 0.2 % Osmium + 0.1 % UA + 5 % water in dry acetone. A 4 % osmium solution in water was used as stock solution to obtain a final water content of 5 %. The stock solution for uranyl acetate (UA) contained 20 % UA in dry methanol. Cold dry acetone (-20˚C) was used as solvent. The mixture was kept cold, on ice. The solution was aliquoted in cryo tubes and deep frozen in liquid nitrogen before the sapphire discs together with carriers were transferred to the tubes under liquid nitrogen. The lids of the tubes were not completely closed.

2.5.2.2 Freeze substitution procedure

The freezing substitution started with a slowly increasing temperature gradient of -90 °C for 1 h, then it was increased from -90 °C to 20 °C (5˚C/h) for a period of 22 h and stayed for 1h at 20˚C. Thereafter, samples were rinsed 3 times shortly with acetone at RT, then Spurr's resin was infiltrated stepwise in acetone:Spurr's ratios of 2:1, 1:1, and 1:2 for 1 h each. Later, samples were infiltrated in 100 % Spurr's at RT ON and placed in fresh Spurr's in automatic freeze substitution (AFS) flow-through rings (Leica). The sapphires were placed at the bottom of the mold with cells facing up. At this step, air bubbles at the bottom of the wheel should be avoided. Next, the sapphire discs were placed inside the wheels. After the sapphire discs sunk into position, wheels were filled up with Spurr's and polymerized at 60˚C for 48h.

2.6 Electron microscopy and electron tomography

2.6.1 Transmission electron microscopy (TEM)

Different types of electron microscopes were used in this study. Electron microscopic imaging was mainly performed on a transmission electron microscope (TEM) (JEOL JEM-1400, JEOL Ltd., Tokyo, Japan) and a scanning electron microscopy (SEM) (LEO Gemini 1530, Carl Zeiss, Oberkochen, Germany). Specimens were imaged with a bottom mount 4k by 4k pixel digital camera (TemCam F416; TVIPS, Gauting, Germany). The microscope has a high contrast lens system optimal for viewing resin embedded specimen and can be operated up to 120 kV.

2.6.2 Correlation of specific regions of interest for EM analysis

After overnight (ON) polymerization, the glass bottom of tissue culture dishes was removed by hydrofluoric acid (30 % HF) for 2 h at RT. Thereafter, the samples were washed with water 3 x 15 min. To recognize the correctly bleached spots containing the cells of interest, the adjacent areas were purposely over-bleached. After recognizing the exact region of interest, the resin blocks were further processed with an EM trimmer (Diatome, Switzerland) set to an angle of 30 ° to obtain a truncated pyramid containing the bleached cells or areas.

2.6.3 Ultrathin Sectioning

Ultrathin sections were cut on an UC6 ultramicrotome (Leica Microsystems, Vienna, Austria) parallel to the surface of the former coverslip. The diamond knife-edge was oriented as parallel as possible to the sample to get already the first sections from the complete block. Ultrathin sections of 40–70 nm thickness were collected on the surface of the diamond knife water bath, and mounted on Formvar-coated EM grids (Plano, Wetzlar, Germany). After a 1h drying, the grids could be used for electron microscopic analysis. No post-staining procedures were applied.

2.6.4 Scanning electron microscopy (SEM)

A LEO Gemini 1530 scanning electron microscope (Carl Zeiss, Oberkochen, Germany) was also used in this study. Specimens were imaged with an in-lens detector with a low accelerating voltage of 3 kV and short working distances of 1.8-2 mm, in general following the procedures established by Horstmann et al., 2012.

2.6.5 Data acquisition for electron tomography and 3D analysis

Sectioning was done on a Leica UC6 microtome (Leica Microsystems, Vienna, Austria) and 250 nm thick serial sections were collected on Formvar-coated, copper slot grids. For tomography, 15 nm gold particles (Protein A conjugate, CMC University medical center Utrecht, Netherlands) were applied at both sides of the grid as fiducial markers. The grids were placed in a high-tilt holder (Model 2040; Fischione Instruments; Corporate Circle, PA) and parts of neurons containing Golgi apparatus or Golgi outposts were recorded on a Tecnai F20 EM (FEI, Eindhoven, Netherlands) operating at 200 kV using the SerialEM software package (Mastronarde, 2005). Images were taken every degree over a ±60 ° range on an FEI Eagle 4K x 4K CCD camera at a magnification of 19,000x and a binning factor of 2 (pixel size 1.13 nm). The tilted images were aligned using the positions of the fiducal gold particles. The tomograms were generated based on the R-weighted back-projection algorithm using the IMOD software package (Kremer et al., 1996).

After acquiring raw tilt series from the transmission electron microscope and calculation of the tomograms, the 3D reconstruction from series of tomographic sections is expressed by the acquisition and reassembly of images from diverse profiles of the same Golgi structures in consecutive sections. The 3D structure of Golgi apparatus comprised of regions of variable density is crossed by radiation (X-rays or electrons) angled differently. In this way, it is possible to measure at these comparative angles the intensity before and after hitting the sample. Differences of radiation absorption on the samples produce the differences between the intensities.

Next, the entire Golgi apparatus structures need to be identified and accurately segmented from electron tomograms. Therefore, I first applied manual labelling information based on identifying the boundaries of Golgi apparatus structures in key

frames of the acquired tomograms. Then, the algorithms of the reconstruction program designed and developed by Hongwei can propagate the boundary label information into the entire segmented 3D tomogram (Figure 2.1B and Figure 2.1C). Figure 2.1D shows the 3D visualization result of one somatic Golgi apparatus structure. Figure 2.1E and Figure 2.1F show the connected components of Golgi structure in green color and the individual components inside or around the Golgi structure in red color.

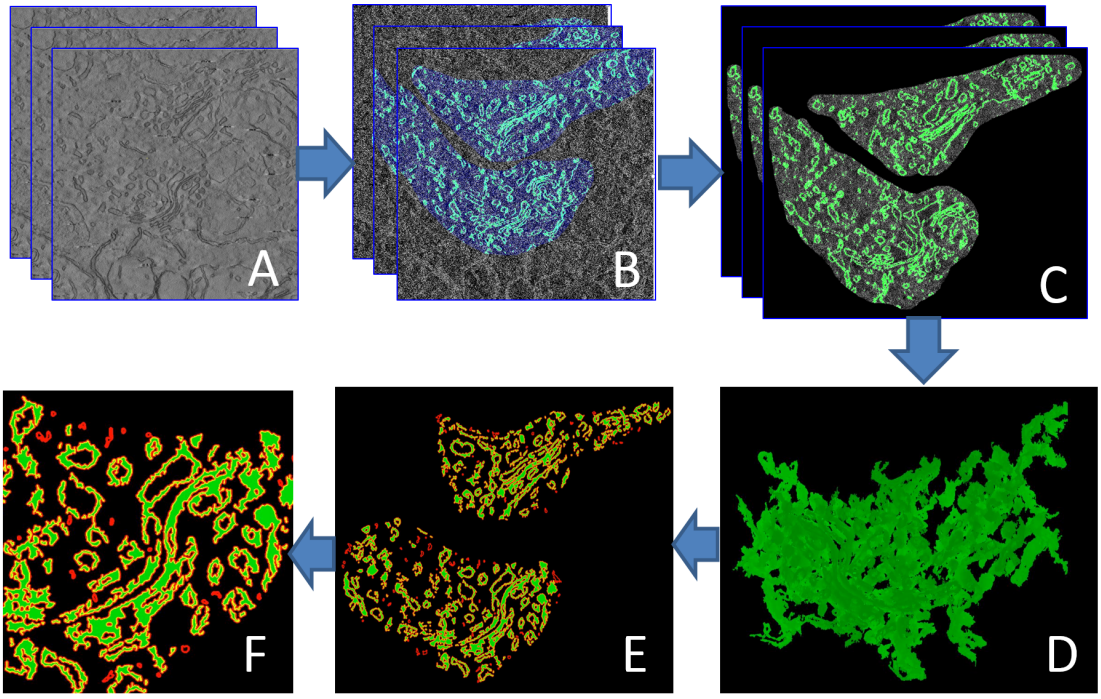

Figure 2.1 Computation workflow of 3D segmentation of TEM 3D stacks raw data. **(A-C)** Electron tomographic 2D images aligned in 3D stacks containing Golgi structures. **(D-F)** Identified and segmented 3D Golgi structures in 3D space. **(A)** Calibrated tomography datasets visualized as serial section 3D stacks. **(B)** Human-supervised labeling of Golgi structure boundaries as information seeds for detecting all Golgi structure boundaries in the entire 3D stack. **(C)** The segmented 3D stack of Golgi structure. **(D)** 3D visualization result of one Golgi structure. **(E)** Connected components of Golgi structure in green color and the individual components inside or around the Golgi structure in red color. **(F)** Zoom in results from E.

3. Results

3.1 Specific DAB staining of the Golgi-resident enzyme N-acetylgalactosaminyltransferase 2-GFP Fusion protein (GalNAcT2-ECFP) in HeLa cells.

Originally, the correlative light and electron microscopy of GFP-tagged proteins was established using stably transfected HeLa cells expressing EGFP or ECFP fusion proteins (Maranto, 1982, Grabenbauer, 2005). Therefore, I established the method of correlative light and electron microscopy of GFP-tagged proteins using these HeLa cell strains expressing the ECFP fusion proteins (Figure 3.1A). After photo-oxidation and Epon embedding, specific DAB staining can be identified both, by transmission electron microscopy (TEM) (Figure 3.1B and Figure 3.1C) and by scanning electron microscopy (SEM) (Figure 3.2A and Figure 3.2B), resembling the ECFP localization in specific stacks of the juxtanuclear Golgi apparatus (micrographs in both Figures taken from the same sample). At higher magnification, the DAB polymers at respective sites can be precisely localized to the cisternal lumina with a gradient-like distribution throughout the Golgi stack. In control experiments, I detected no DAB precipitate in Golgi-like structures in the absence of illumination or ECFP expression (Figure 3.1D). Thus, these results confirm that photo-oxidation of GalNAcT2-ECFP specifically labels the Golgi apparatus and extend this observation to another imaging modality, SEM.

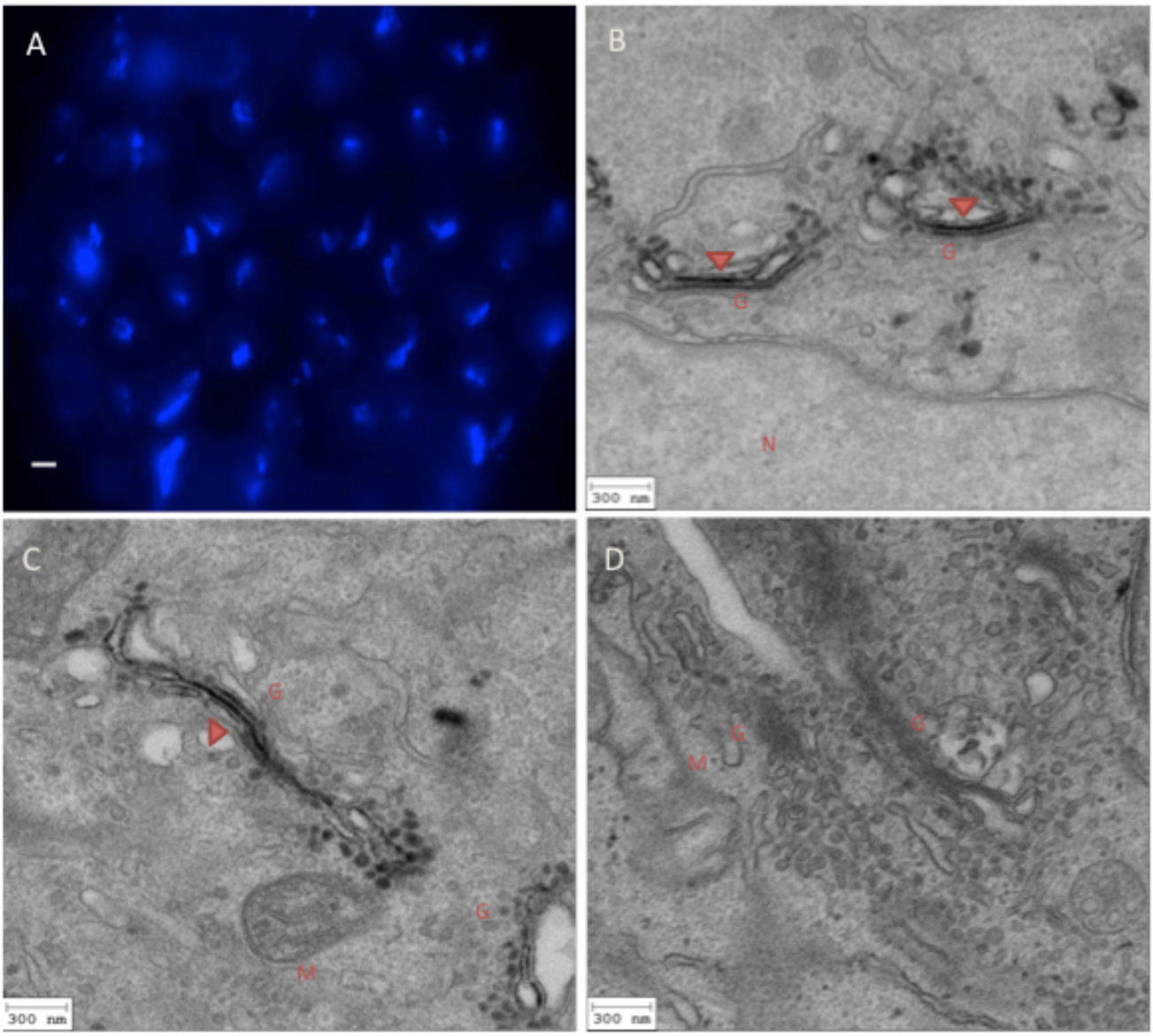

Figure 3.1 Photo-oxidation through ECFP polymerizes DAB to an electron-dense precipitate. (A) Wide-field fluorescence microscopy of a single image shows the Golgi resident protein GalNAcT2-ECFP expressed in HeLa cells. **(B)** and **(C)** TEM micrograph showing specific DAB staining in cisternal lumina of Golgi apparatus **(red arrowheads).** Golgi cisternae contain specific DAB precipitation. **G** = Golgi apparatus, **M =** Mitochondria, **N =** Nucleus. **N**=12 samples. **(D)** Control cell without illumination **N =** 8 samples. Scale bars: 25 µm (A), 300 nm (B-D).

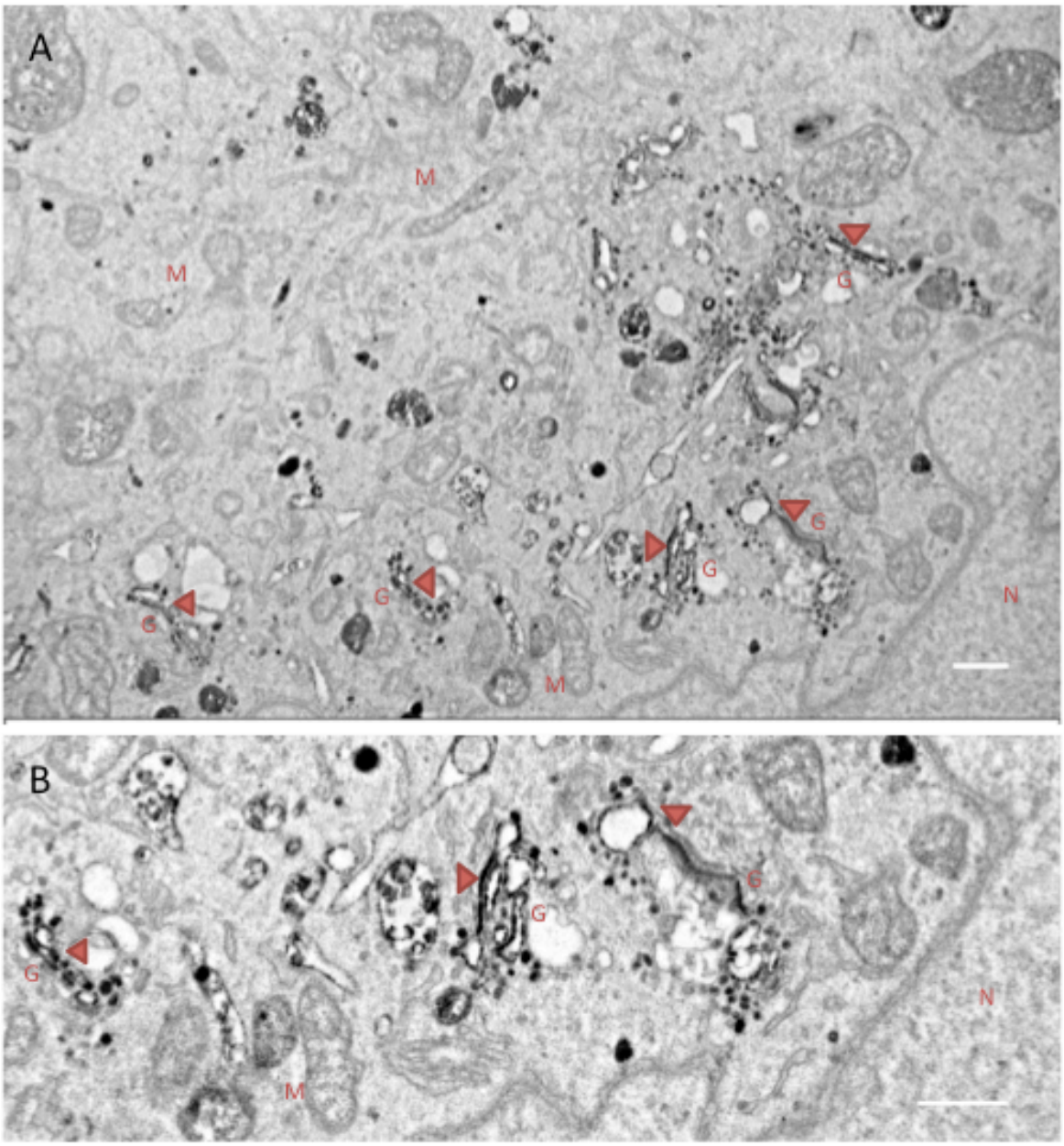

Figure 3.2 Scanning Electron Microscopy (SEM) image of specific DAB staining in cisternal lumina of Golgi stacks in HeLa cells. (A) After photo-oxidation through ECFP DAB polymerizes to an electron-dense precipitate **(red arrowheads)** Golgi cisternae contain specific DAB precipitate. **(B)** Higher magnification from A. **G =** Golgi apparatus, **M =** Mitochondria, **N =** Nucleus. **N**=8 samples. Scale bars: (A)1 µm, (B) 800 nm.

3.2 Morphology of Golgi apparatus in neuronal cell cultures studied by Correlative Light and Electron Microscopy

To investigate the ultrastructure of dendritic Golgi apparatus outposts in neurons – the main goal of my project - photo-chemical methods for correlative light and electron microscopy of fluorescent probes had to be applied, adapted and optimized for cultured hippocampal neurons.

3.2.1 Optimizing fixation conditions for photo-oxidation reactions in neuronal cell cultures

At first, several attempts to conduct chemical fixation were not successful, not preserving the general cell structure. Then, by optimizing the chemical fixation conditions for cultured hippocampal neurons, I achieved an essential improvement using photo-oxidation for correlative light and electron microscopy. My goal was to approach an ultra-structural preservation especially of secretory organelles comparable to samples that had been fixed by high-pressure freezing. Therefore, I tested different fixatives in different concentrations using also different buffers. For example, PFA fixative with sucrose, dissolved in PBS caused a vast damage of neuronal cell structures: Already the morphological identification of the plasma membrane or secretory organelles was difficult at the ultrastructural level (Figure 3.3A). Further, I tested the combination of the fixatives PFA and GA with sucrose, dissolved in PBS. Again, the general structure of hippocampal cells was severely damaged (Figure 3.3B). Similarly, fixative consisting simply of GA and sucrose dissolved in PBS, the fixation originally used for photo-oxidation experiments in HeLa cells, did not show satisfactory results in neuronal cell cultures (Figure 3.3C) see Materials and Methods Table 2.3. While the general morphology of neurons was improved as compared to PFA fixation, the ultrastructural preservation of secretory organelles was not satisfactory. Finally, a fixative containing GA and sucrose, dissolved in Sodium Cacodylate (CAC) buffer supplemented with $CaCl_2$ yielded superior results for subsequent photo-oxidation experiments (Figure 3.3D). The general morphology of neurons as well as the ultrastructural preservation of mitochondria and secretory organelles was well preserved.

In summary, the chemical fixation using GA and sucrose in CAC buffer supplemented with $CaCl_2$ yielded superior cell structure of cultured hippocampal neurons as well as an excellent preservation of their secretory pathway membrane systems.

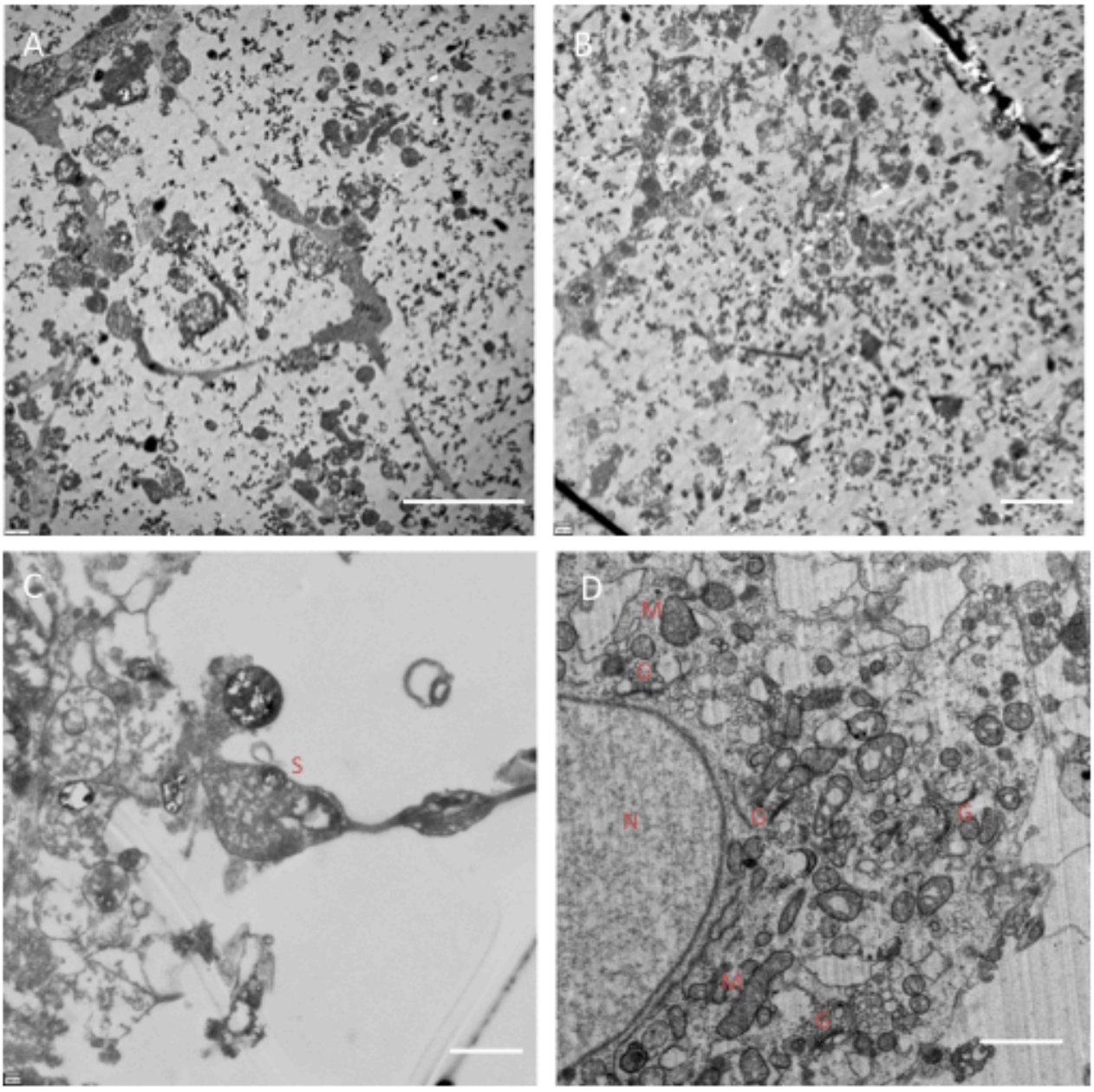

Figure 3.3 Optimizing conditions for chemical fixation of cultured hippocampal neurons by testing different fixatives. (A) TEM of hippocampal neurons fixed by 4% PFA and 2% Sucrose in PBS. Note severe membrane ruptures and extraction of cytosol. **(B)** TEM of hippocampal neurons fixed by 4% PFA, 2% GA and 2% Sucrose in PBS. Similarly to (A), note the poor ultrastructure preservation and damage of general cell structures. **(C)** TEM of hippocampal neurons fixed by 2% GA and 2% sucrose in PBS. Despite severe alterations to the overall cellular structures, the morphological preservation of the synapse is surprisingly well. **(D)** TEM of hippocampal neurons fixed by 2% GA and 2% Sucrose in CAC buffer with $CaCl_2$. The general cell structure is well preserved and the ultrastructure preservation of secretory pathway membrane systems is superior. **S =** Synapse, **G =** Golgi apparatus, **N =** Nucleus, **M =** Mitochondria. Scale bars: 4 μm (A), 2000 nm (B), 800 nm (C), 1 μm (D).

3.2.2 Optimizied workflow for photo-oxidation reactions in neuronal cell cultures

An important aspect regarding the application of correlative light and electron microscopy using photo-oxidation for cultured neurons was the development of a functional unified workflow (Figure 3.4). (See Materials and Methods for a detailed protocol).

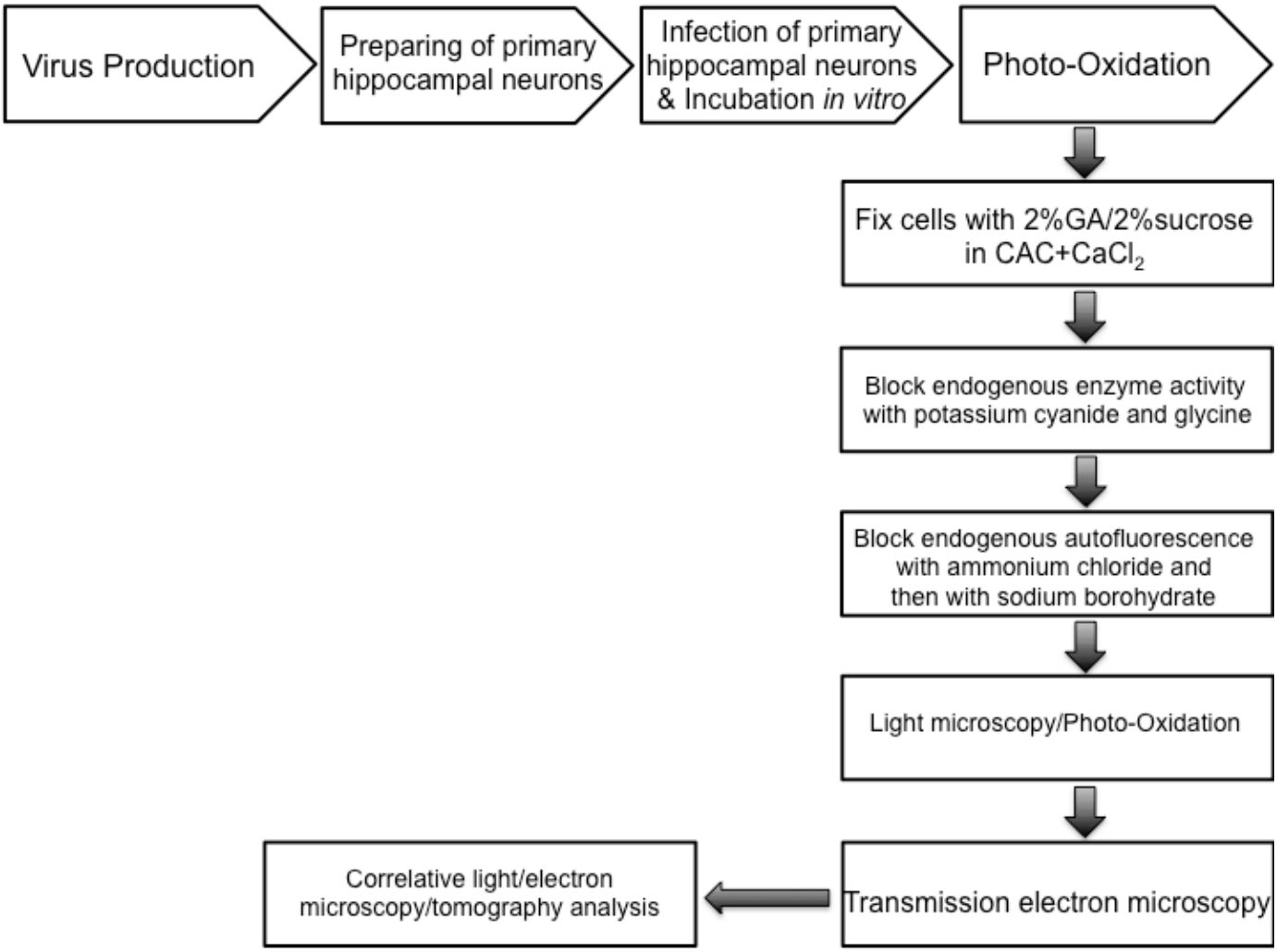

Figure 3.4 Unified workflow for Correlative Light and Electron Microscopy of neuronal cell cultures. This workflow was developed, optimized and applied routinely for correlative light and electron microscopy of neurons using photo-oxidation through GFPs.

The hippocampal neurons were 15 days in vitro (DIV) before starting the chemical fixation step. The cells were infected with AAV on the 6th day and then incubated for additional 9 days. The optimization of the chemical fixation protocol resulted in a substantially improved morphological preservation of cultured neurons, as visualized by electron microscopy (Figure 3.5A), comparable to high-pressure freeze fixation preparations. Additionally, this improvement allowed for the detection of specific DAB staining in the cisternal lumina of somatic Golgi (Figure 3.5B) as markers correlated to

fluorescence signals.

For high-pressure freeze fixation experiments, hippocampal neurons were also 15 DIV before they were fixed (Figure 3.5C). At higher magnifications, well preserved Golgi structures composed of several cisternae were identified (Figure 3.5D).

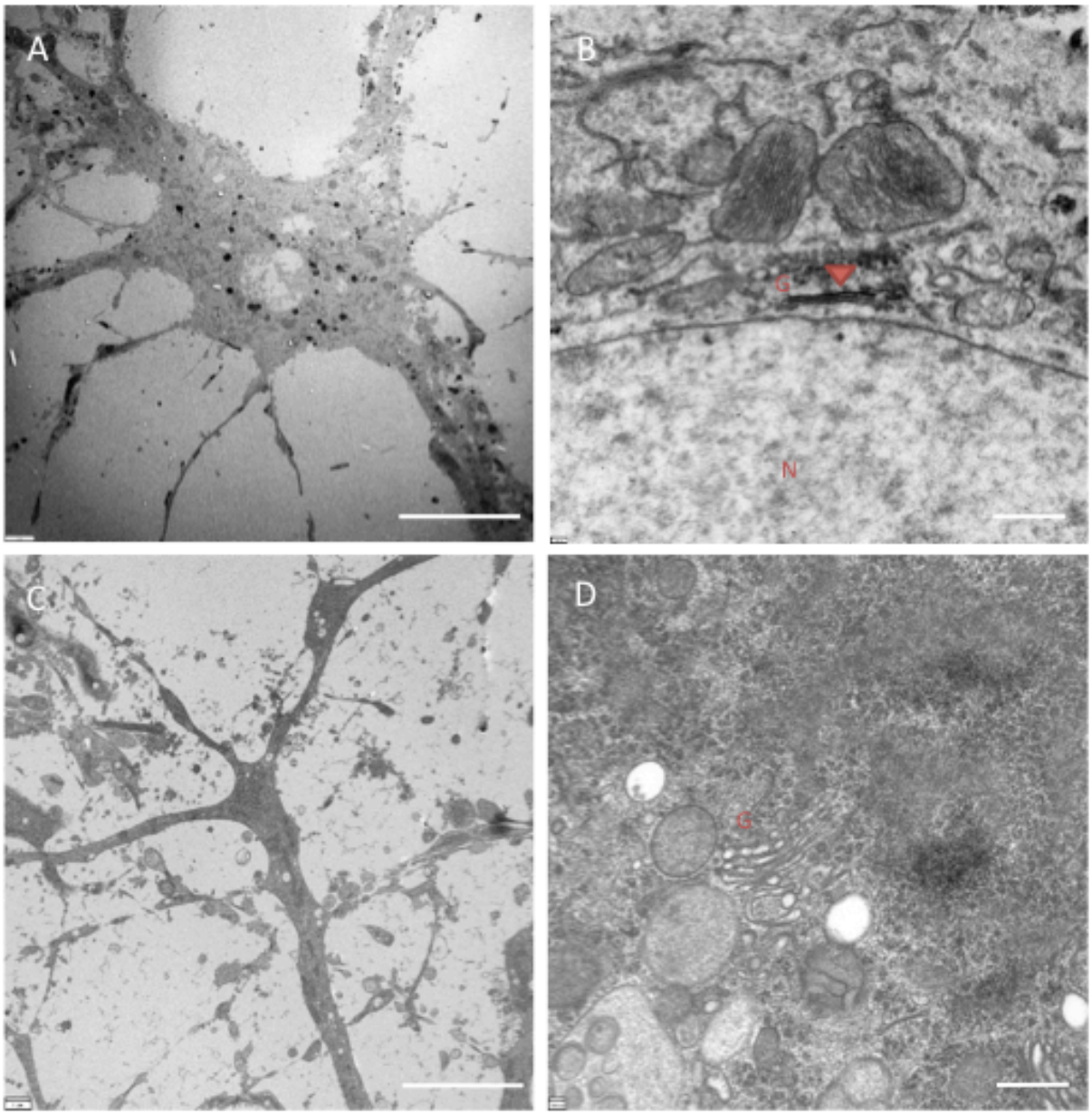

Figure 3.5 Optimization of photo-oxidation and fixation conditions for cultured hippocampal neurons. (A) TEM of hippocampal neurons after chemical fixation. **(B)** Specific DAB staining in cisternal lumina of somatic Golgi through photo-oxidation of infected hippocampal neurons with AAV-GalNAcT2-mTurquoise2 using an optimized chemical fixation protocol. **(red arrowheads)** Golgi cisternae contain specific DAB precipitate. **(C)** TEM of hippocampal neurons fixed by high-pressure freezing. **(D)** Somatic Golgi apparatus fixed by high-pressure freezing and subsequent freeze substitution. **G =** Golgi apparatus, **N =** Nucleus. **N**=16 samples. Scale bars: 8 µm (A), 400 nm (B), 4 µm (C), 800 nm (D).

3.2.3 Ultrastructural analysis of Golgi stacks in neuronal soma and dendrites

To study the morphology of Golgi outposts (GOs) in dendrites and juxtanuclear Golgi complex in soma, I adapted and optimized preparative procedures for correlative light and electron microscopy. This combines fluorescence microscopy of *in vivo* dynamics with the superior resolution of electron microscopy, and therefore allows to analyse if GOs in the dendrites show comparable ultrastructure to those of somatic Golgi.

To address that, I performed the photo-oxidation experiments in neurons using the mTurquoise2 fluorescent protein variant. The experiments were carried out with two different GalNAcT2 fusion proteins, AAV1/2-GalNAcT2-mTurquoise2 and AAV1/2-GalNAcT2-APEX-mTurquoise2. This experiment was continuously imaged in light microscopy mode to illustrate the time course of the photo-oxidation reaction. I imaged the initial Golgi-like fluorescence of GalNAcT2-mTurquoise2 (Figure 3.6A) overlaid with a bright field channel (Figure 3.6B) to follow the time course of the reaction. After 1 min, a cytosolic background DAB staining appeared, which increased over time. The reaction was stopped after 2 min when mTurquoise2 was bleached completely (Figure 3.6C). To better correlate thereafter the embedded sample and trim the correct cell, I over-bleached some adjacent cells close to cell of interest (Figure 3.6D) that later could be used as reference points. Then, I subjected the sample to Epon embedding, cut ultrathin sections (60–70 nm) and examined them by TEM.

Finally, specific DAB staining could be detected in several cisternae of somatic Golgi complex resembling a gradient-like distribution throughout the Golgi stack (Figure 3.6E). At higher magnification, DAB precipitate appears restricted to the luminal side of the membrane in areas of slightly dilated cisternae (Figure 3.6F and Figure 3.6G). This is consistent with the presence of mTurquoise2 Fluorescent Protein on the luminal, carboxy_terminal part of GalNAcT2 residing in cisternal membranes. This was observed in 24 samples taken from 24 cultures.

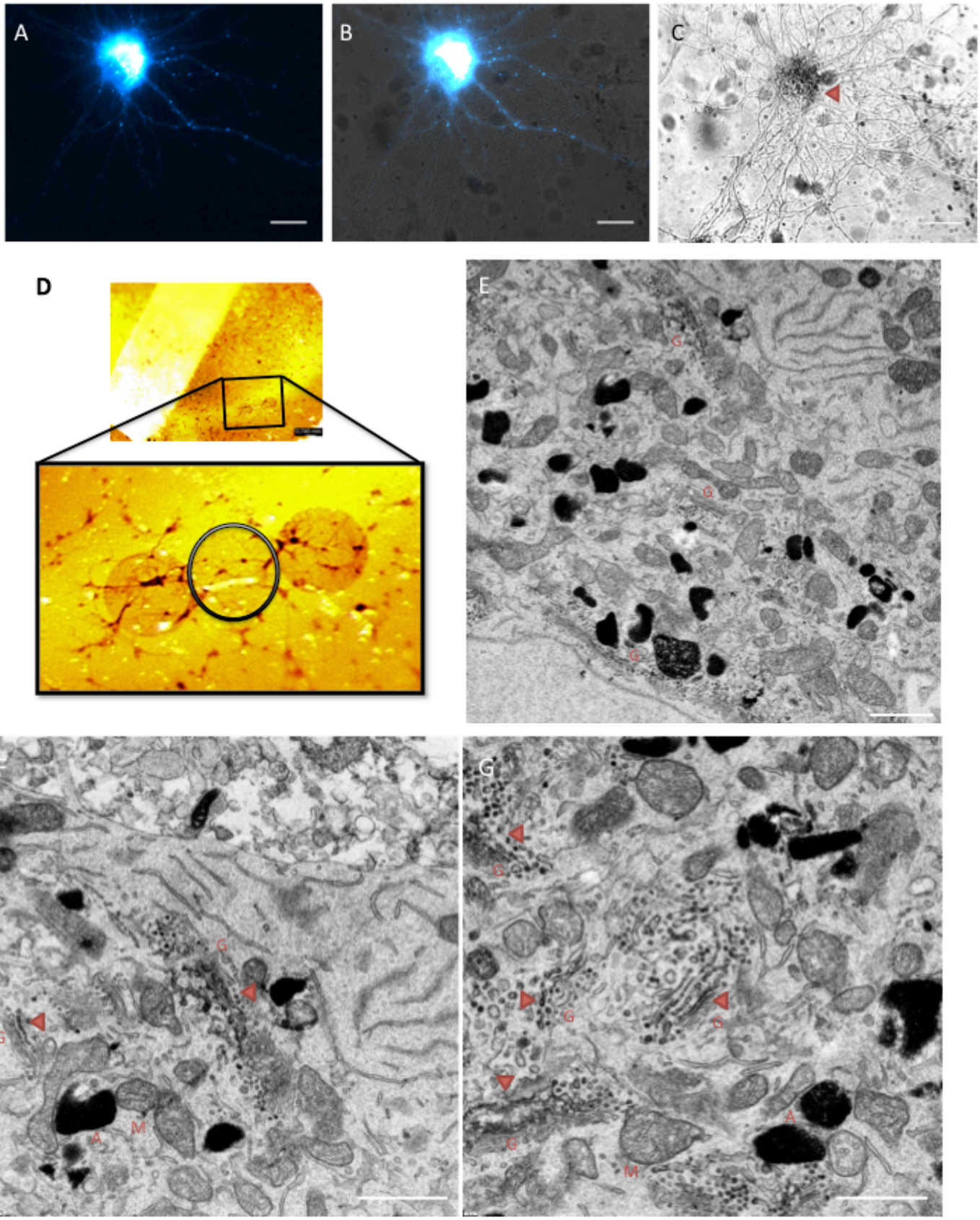
A
B
C
D
E
G
F
G
A
M
G
G
G
G
A
M

Figure 3.6 The bleaching process and correlative light and electron microscopy of the same hippocampal cell. **(A)** Wide-field fluorescence microscopy of a single image of hippocampal neurons infected with AAV-GalNAcT2-mTurquoise2. **(B)** Blue fluorescence combined with the bright field channel. **(C)** mTurquoise2 bleaching process in presence of DAB while background staining appears. **(D)** The bleached cell of interest from C between two over-bleached cells as markers. **(E)** TEM micrograph of the cell of interest in D showing DAB staining in cisternal lumina of somatic Golgi apparatus in neurons. **(F)** and **(G)** Higher magnification from E. **G =** Golgi apparatus, **M =** Mitochondria, **(black circle)** cell of interest, **(red arrowheads)** Golgi cisternae containing specific DAB precipitate. **N**=24. Scale bars: 10 µm (A-C), 740 μm (D), 800 nm (E), 100 nm (F-G).

Applying the photo-oxidation method in hippocampal neurons allowed for the demonstration of Golgi outposts in the dendrite, which were detected from 80 up to 120 µm distant from soma (Figure 3.7B and Figure 3.7C). This was observed in 2 samples taken from 3 cultures.

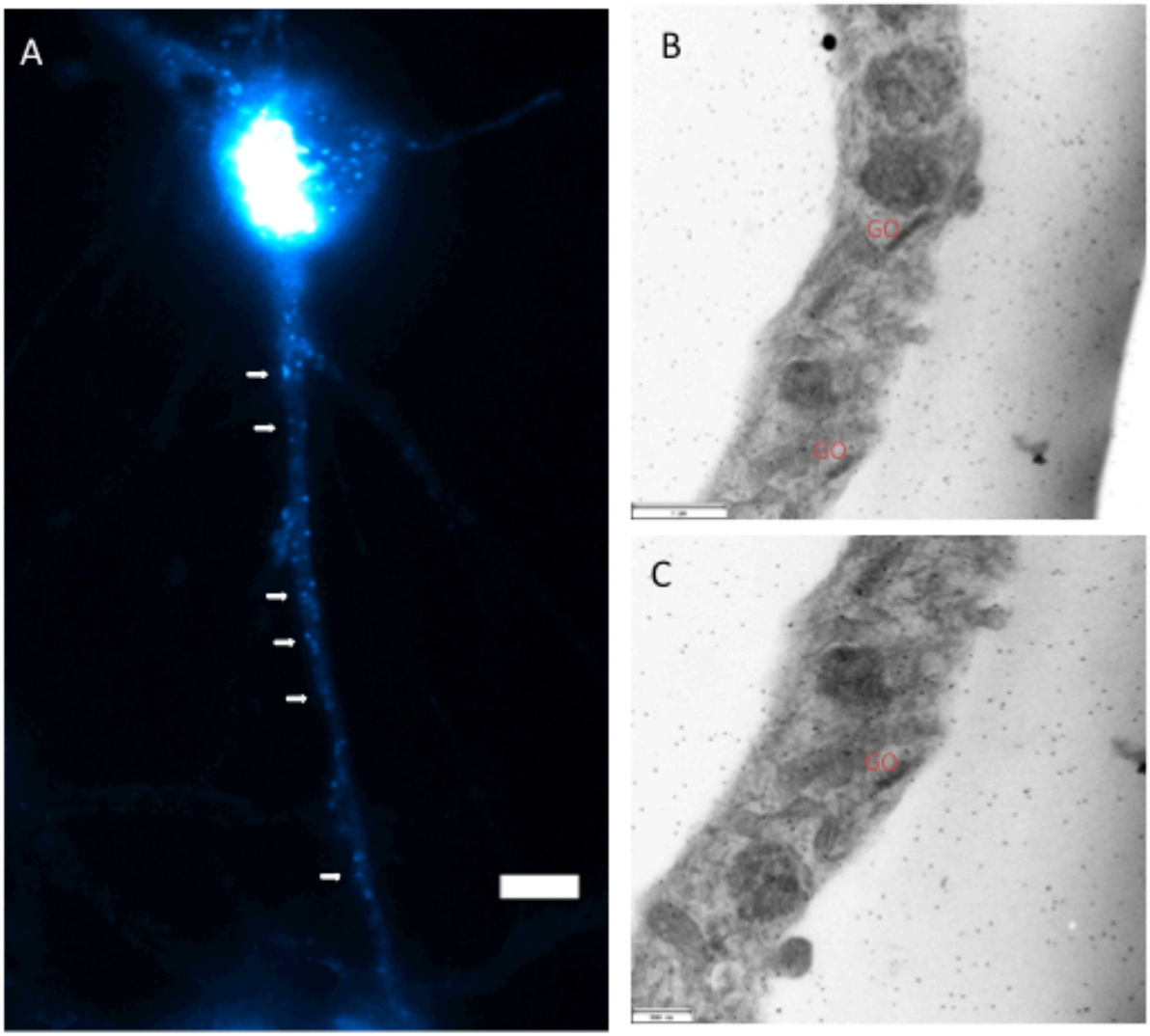

Figure 3.7 Photo-oxidation through mTurquoise2 polymerizes DAB to an electron-dense precipitate in dendritic Golgi outposts. (A) Wide-field fluorescence microscopy of a single image of hippocampal neurons infected with AAV-GalNAcT2-mTurquoise2. Bright spots in dendrite resemble putative GOs. **(B)** and **(C)** TEM micrographs of DAB staining in cisternal lumina of dendritic Golgi in neuron cells. **GO =** Golgi outposts. Scale bars: 10 μm (A), 100 nm (B-C).

3.2.4 Photo-Oxidation using the APEX system

In order to further examine the morphology of Golgi complex, I additionally utilized the APEX system. APEX is a genetically encoded EM tag, which is enzymatically active in all cellular compartments without requiring light. It catalyzes via the H_2O_2-dependent generation of reactive oxygen species the subsequent polymerization of DAB to a localized precipitate which gives contrast for EM after post-fixation with OsO_4. Therefore, the APEX tag was integrated into the GalNAcT2-mTurquoise2 plasmid to yield construct pAM-GalNAcT2-APEX-mTurquoise2. This is predicted to generate a specific DAB precipitate without bleaching, yet the fusion protein can be located in the FLM.

I imaged the initial fluorescence of GalNAcT2-APEX-mTurquoise2 at Golgi apparatus during the pre-incubation phase immersed in DAB buffer without H_2O_2 (Figure 3.8A), and overlaid the fluorescence channel with the bright field channel (Figure 3.8B). After 1 h of pre-incubation with DAB buffer, the samples were incubated with fresh DAB and H_2O_2 to catalyze DAB's oxidative polymerization generating a precipitate that is cross-linked and locally deposited (Figure 3.8C). This allowed for the demonstration of Golgi outposts in the dendrite, which were detected up to 80 µm distant from soma, by genetically encoded Golgi-resident protein tags (Figure 3.8D). This was observed in 16 samples taken from 16 cultures.

Thus, these results show that generation of DAB precipitate using APEX is feasible, however the generated DAB precipitate using APEX was clearly less pronounced, compared to DAB precipitation generated through fluorophore bleaching.

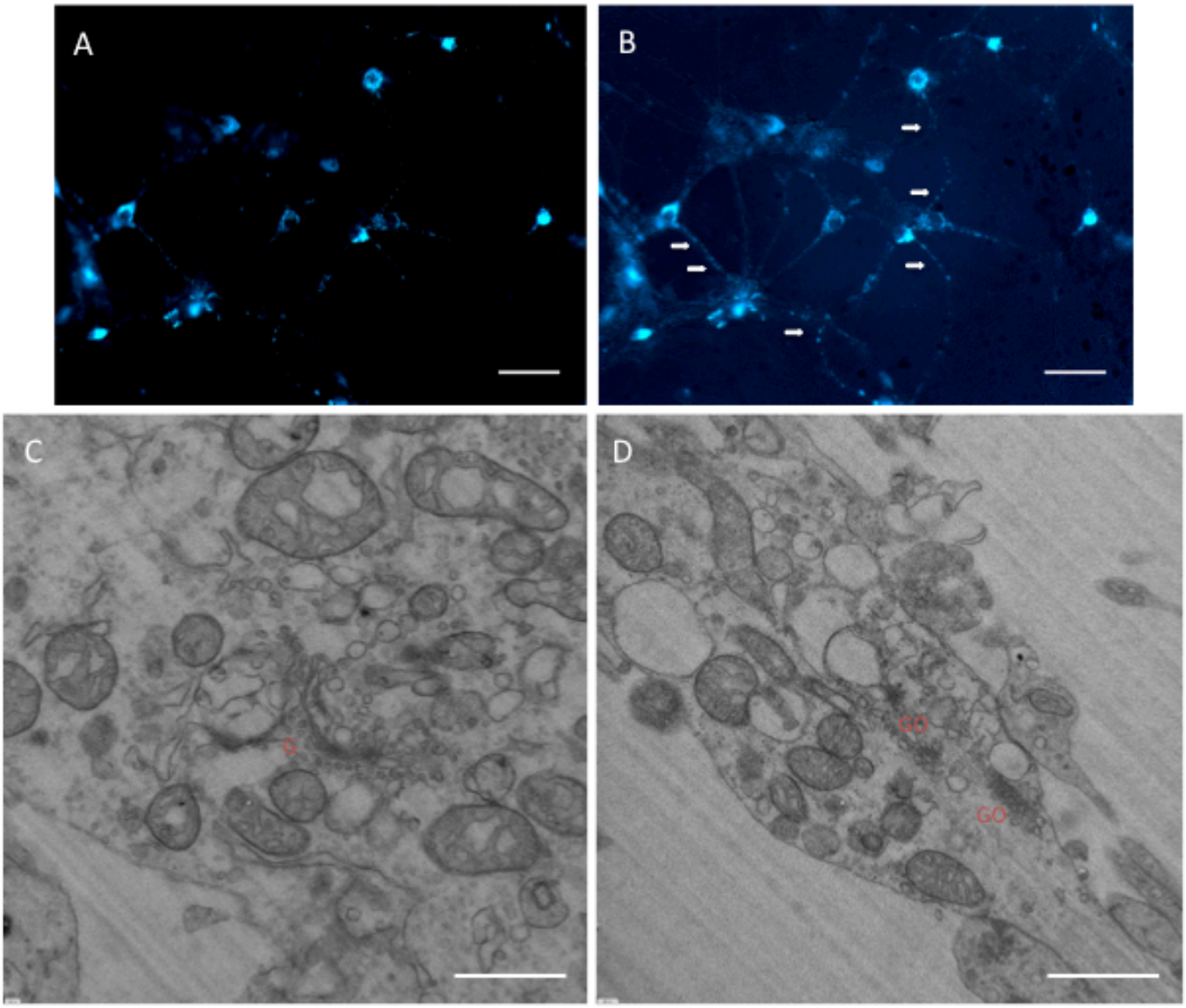

Figure 3.8 Golgi outposts and somatic Golgi demonstrated by DAB precipitation generated by enzymatic reaction (APEX) in hippocampal cell cultures. (A) Wide-field fluorescence microscopy of a single image of hippocampal neurons shows the expression of AAV-GalNAcT2-APEX-mTurquoise2 in blue channel. (B) Overlay of fluorescence and bright field channel shows high infection rate of the neuron cultures. White arrows denote GalNAcT2-APEX-mTurquoise2 expression in Golgi outposts. (C) TEM showing DAB staining generated by enzymatic activity of APEX in cisternal lumina of **somatic** Golgi in neurons. (D) TEM showing DAB staining in cisternal lumina of **dendritic** Golgi outposts of neurons. **G =** Golgi apparatus, **GOs =** Golgi outposts. **N**=16. Scale bars: 25 μm (A-B), 400 nm (C), 800 nm (D).

3.2.5 Negative controls for photo-oxidation experiments

To demonstrate the specificity of DAB staining during photo-oxidation, several negative control experiments were performed. For example, cells infected with AAV1/2-GalNAcT2-mTurquoise2 were bleached in a buffer without DAB. Some electron-dense spots most likely resembling osmophilic autophagic vacuoles were detected (Figure 3.9A), but could be separated easily from specific signals, which were absent in negative-control experiments. In such samples, cisternal lumina of Golgi stacks showed no DAB precipitation after illumination (Figure 3.9B). Further, cells lacking any mTurquoise2 expression did not show any DAB precipitation at Golgi complex after incubation and bleaching using DAB buffer (Figure 3.9C and Figure 3.9D). This was observed in 8 samples taken from 8 cultures.

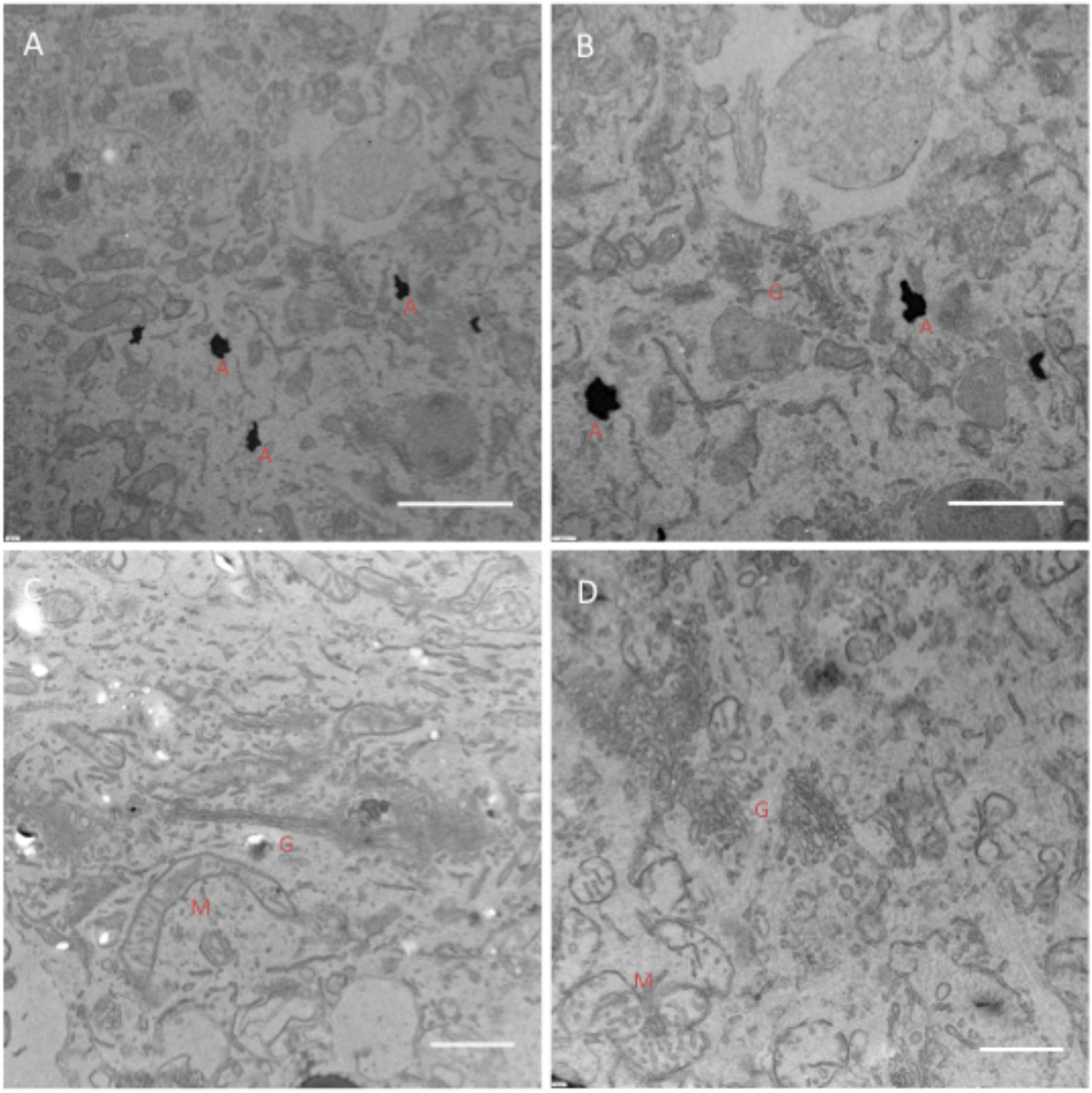

Figure 3.9 Negative control experiments of photo-oxidation reaction in neurons using AAV1/2-GalNAcT2-mTurquoise2. (A) TEM shows osmophilic autophagic vacuoles after bleaching without DAB in neurons infected with AAV-GalNAcT2-mTurquoise2. **(B)** TEM of neurons infected with AAV-GalNAcT2-mTurquoise2 bleached without DAB shows no specific DAB staining in cisternal lumina of somatic Golgi. **(C) and (D)** TEM of neurons without infection of AAV-GalNAcT2-mTurquoise2 shows no DAB staining in cisternal lumina of somatic Golgi. **G =** Golgi apparatus, **M =** Mitochondria, **A =** Osmophilic autophagic vacuoles. **N**= 8. Scale bars: 800 nm (A) and (B), 400 nm (C) and (D).

3.2.6 Ultrastructure of Golgi outposts and somatic Golgi analyzed by transmission electron microscopy and electron tomography

To study the ultrastructure of Golgi outposts and somatic Golgi apparatus in neuronal cell cultures and to examine possible differences of their morphology, electron tomography was used for detailed three-dimensional analysis.

Through the specific labeling generated by the DAB photo-oxidation reaction, several Golgi outposts in three different cells could be identified (Figure 3.10). Epon sections cut to approx. 250 nm containing stained Golgi stacks have been subjected to 3D analysis by electron tomography. This allowed us to analyze the ultrastructure of Golgi outposts in dendrites in three dimensions (3D) and to differentiate their morphology from somatic Golgi apparatus. Therefore, several somatic Golgi apparatus showing specific DAB photo-oxidation reactions were also analyzed in 3D by electron tomography for comparison (Figure 3.11). Tilt series were imaged using high-angle EM specimen holder. The tilted images were computationally aligned to a stack by using the gold particles as fiducals. In Figure 3.10, some 15 nm gold particles are marked by arrows. The tomograms were generated using the R-weighted projection algorithm and were evaluated operating the IMOD software package (Kremer et al., 1996).

From these tomograms containing Golgi apparatus from different areas of neurons, it was readily identifiable that Golgi outposts are smaller than the somatic Golgi apparatus consistently showing a smaller number of cisternae. Moreover, the number of vesicles associated with GOs appears to be less compared with somatic Golgi. Additionally, while Golgi polarity in soma is not unidirectional, it was recognizable that the Golgi outposts have strictly unidirectional polarity.

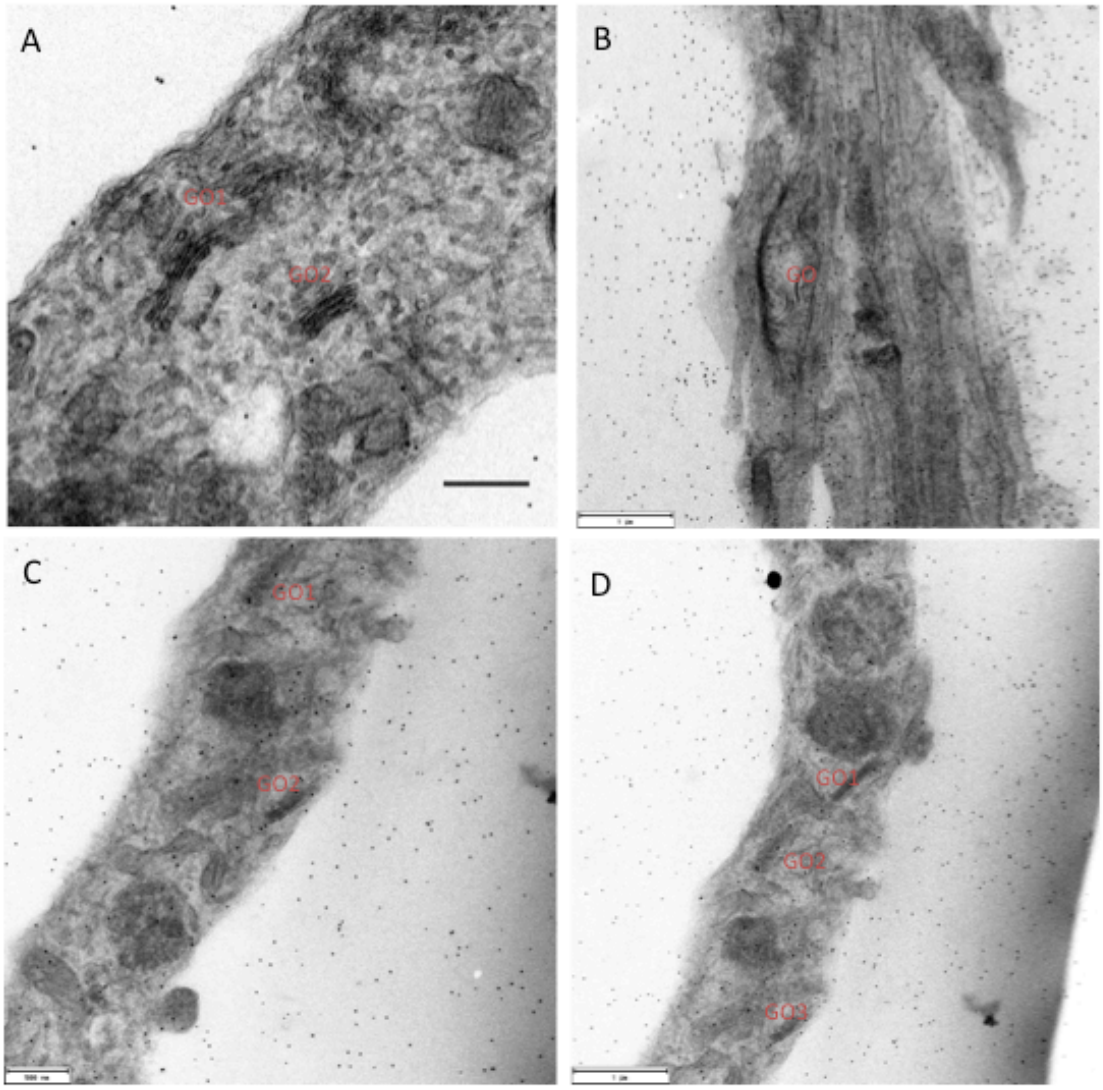

Figure 3.10 Golgi outposts in dendrites of hippocampal neurons labeled through DAB photo-oxidation of GalNAcT2-mTurquoise2. (A-D) Representative images from tilt series showing different Golgi outposts in dendrites of hippocampal neurons**.** Section thickness 250 nm of serial sections**. GO =** Golgi outposts, (red arrows) 15 nm gold particles as fiducial markers for electron tomographic 3D recontruction. The images are representative of 2 independent experiments in 3 different cells. Scale bars: 200 nm (A), 1 µm (B), 500 nm (C), 1 µm (D).

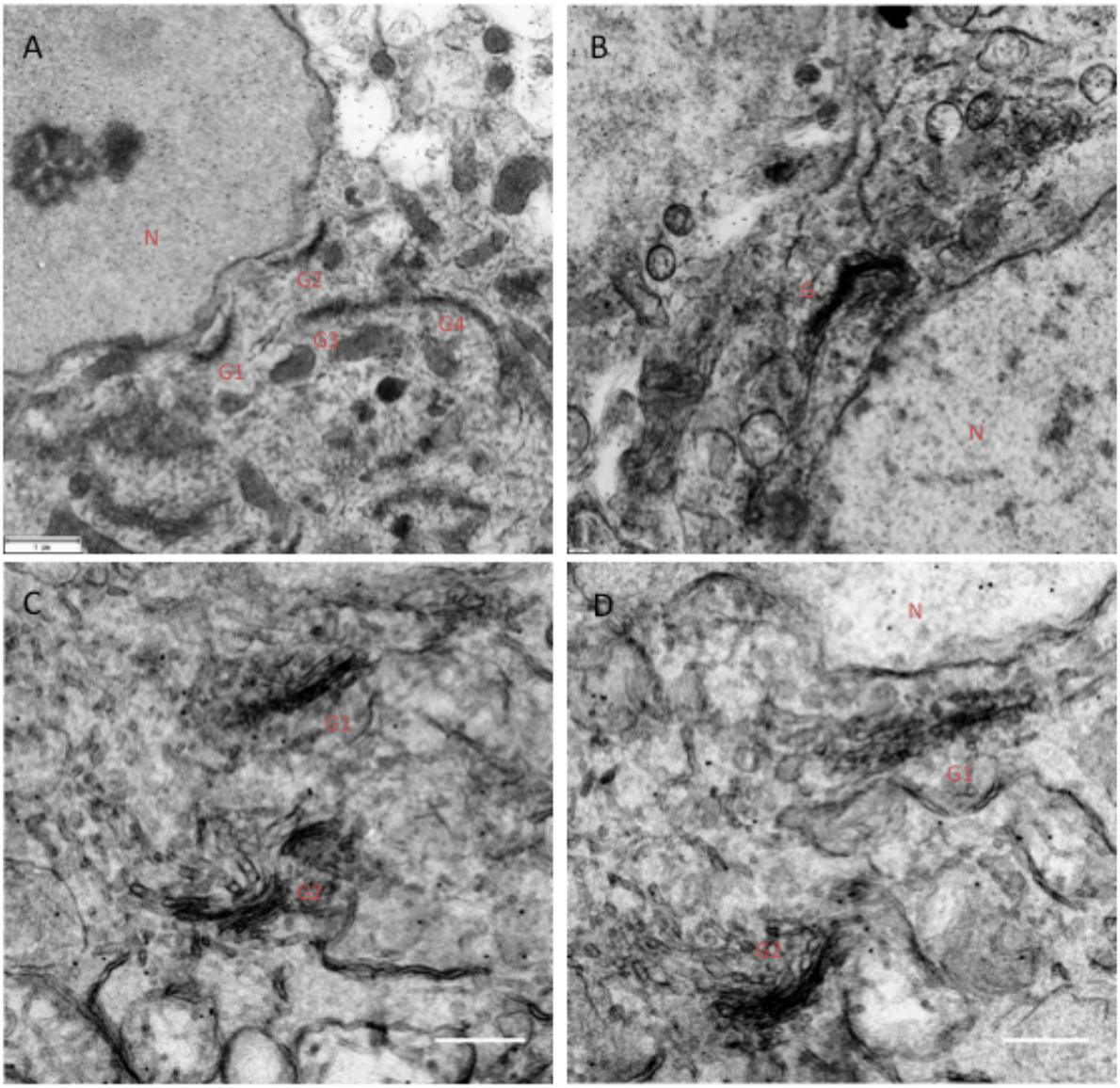

Figure 3.11 Tomographic slice image of somatic Golgi apparatus in hippocampal neurons labeled by DAB photo-oxidation of GalNAcT2-mTurquoise2. (A-D) Tomographic slice image of somatic Golgi apparatus in hippocampal neurons. Section thickness 250 nm of serial sections. **G =** Golgi apparatus, (red arrows) 15 nm gold particles as fiducial markers for electron tomography. The images are representative of 2 independent experiments in 3 different cells. Scale bars: 1 µm (A), 800 nm (B-D).

3.2.7 Three-dimensional analysis of Golgi outposts and somatic Golgi apparatus tomograms

The electron tomograms of several Golgi outposts and somatic Golgi apparatus, which were identified through specific DAB precipitation, were segmented using a Matlab software package developed by Dr. Hongwei Zheng (See 2.6.3 in Materials and Methods) (Figure 3.12 and Figure 3.13).

Analyzing the 2D maximum intensity projections shows that the number of vesicles and number and size of cisternae in Golgi outposts appear to be different from those in somatic Golgi apparatus. Although GO2 and GO1 in Figure 3.10A are located at the same distance from the cell body (up to 80 µm), the size of GO2 (Figure 3.12A) is clearly smaller and contains less cisternae and vesicles than GO1 (Figure 3.12B). Nevertheless, both GO1 and GO2 are different in size, in number of cisternae and number of vesicles compared to typical somatic Golgi apparatus as represented in Figure 3.13. Another comparison is shown in Figure 3.12C. The GO1 in Figure 3.10D is up to 100 µm from soma and contains smaller and minor cisternae and smaller number of vesicles in contrast to somatic Golgi apparatus in Figure 3.13. The Golgi outpost in Figure 3.12D (GO from Figure 3.10B) was the furthest away from the cell body, which it was up to 120 µm from soma. It shows noticeably difference to somatic Golgi apparatus. It has single cisternae and almost no vesicles. This type of GO would be not recognizable without the DAB staining through the photo-oxidation of GalNAcT2-mTurquoise2.

In summary, the DAB labeling through the photo-oxidation of GalNAcT2-mTurquoise2 has enabled the detection of several Golgi outposts. The detected Golgi outposts demonstrated in this study show differences in size and number of cisternae and also in number of vesicles compared to typical somatic Golgi apparatus.

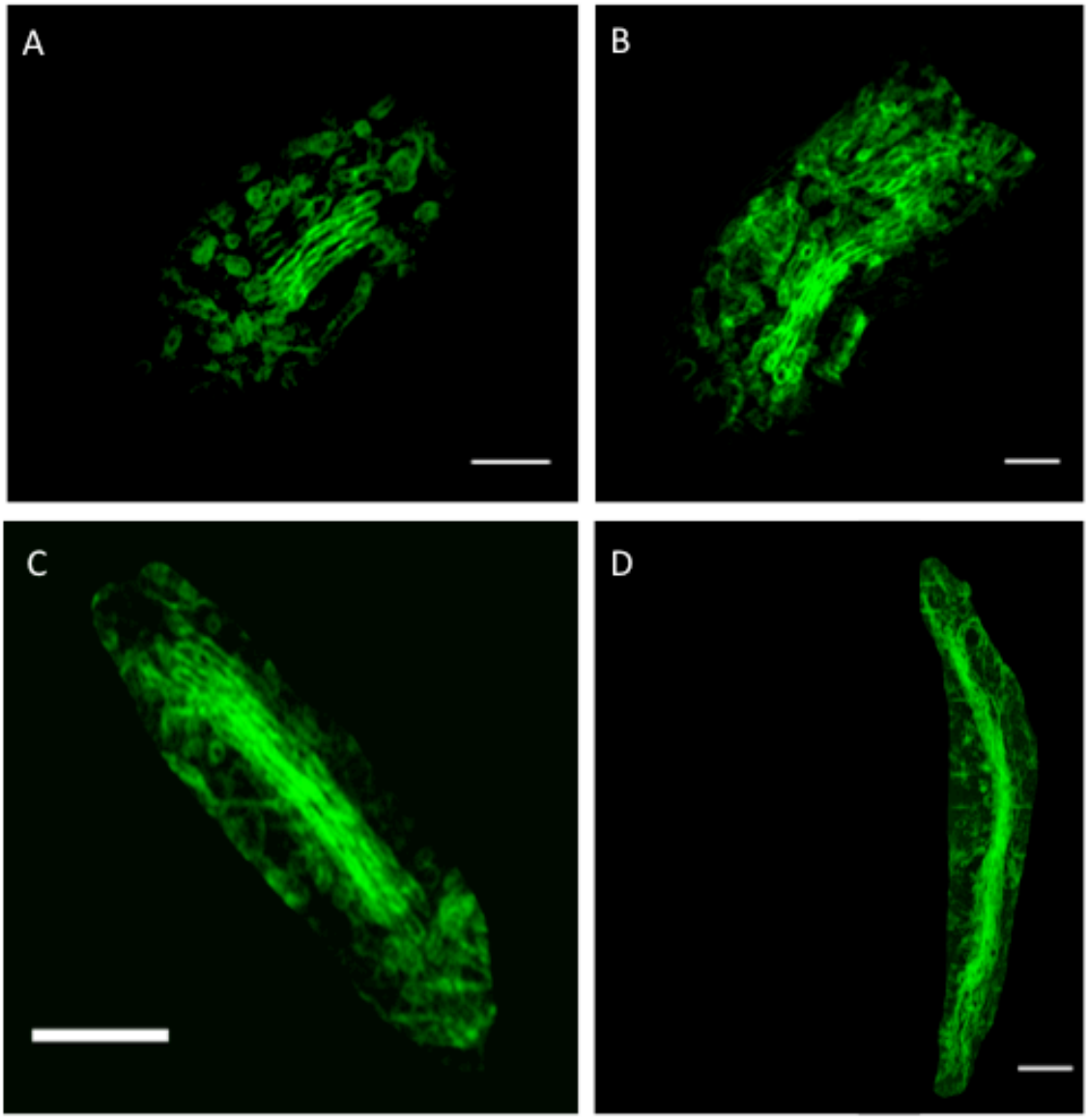

Figure 3.12 2D maximum intensity projections of 3D stacks from segmented dendritic Golgi outposts of cultured hippocampal neurons. (A-D) show four different segmented Golgi outpost models as extracted from electron tomograms with membranes shown in green. A = GO2 from Figure 3.10A, B = GO1 from Figure 3.10A, C = GO1 from Figure 3.10D, D = GO from Figure 3.10B. Scale bars: 200 nm (A-D).

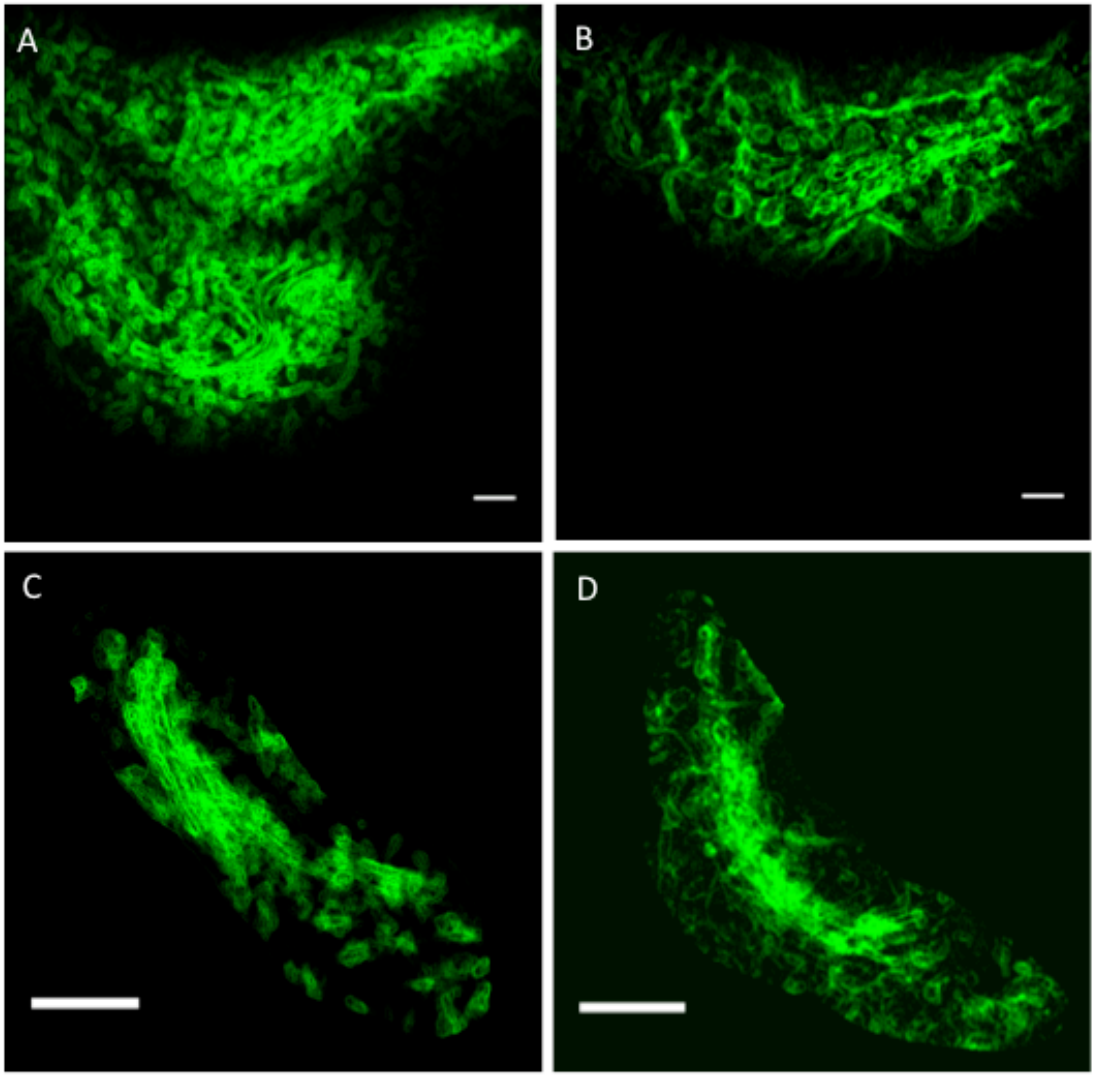

Figure 3.13 2D maximum intensity projections of 3D stacks from segmented somatic Golgi apparatus of cultured hippocampal neurons. (A-D) show six different segmented somatic Golgi apparatus models extracted from electron tomograms with membranes shown in green. A = G from Figure 3.11C, B = G2 from Figure 3.11D, C = GO2 from Figure 3.11A, D = G1 from Figure 3.11D. Scale bars: 200 nm (A-D).

3.3 Morphology and ultrastructure of Golgi apparatus in mammalian neuronal tissue studied by correlative microscopy

3.3.1 Application of correlative light and electron microscopy in neuronal tissue

After successfully demonstrating the ultrastructure of somatic Golgi apparatus and of dendritic Golgi outposts in *vitro* by improving the photo-oxidation procedure for correlative light and electron microscopy in neuronal cell cultures, the next challenge of this study was the application of this correlative method in neuronal tissue. The well-established mammalian neuronal tissue model of mouse brain was chosen to examine the morphology of Golgi complex using viral stereotaxically injected neuronal tissue. Therefore, I first established a functional workflow for the correlative light and electron microscopy method of mouse brain through photo-oxidation (Figure 3.14). (See Materials and Methods for a detailed protocol).

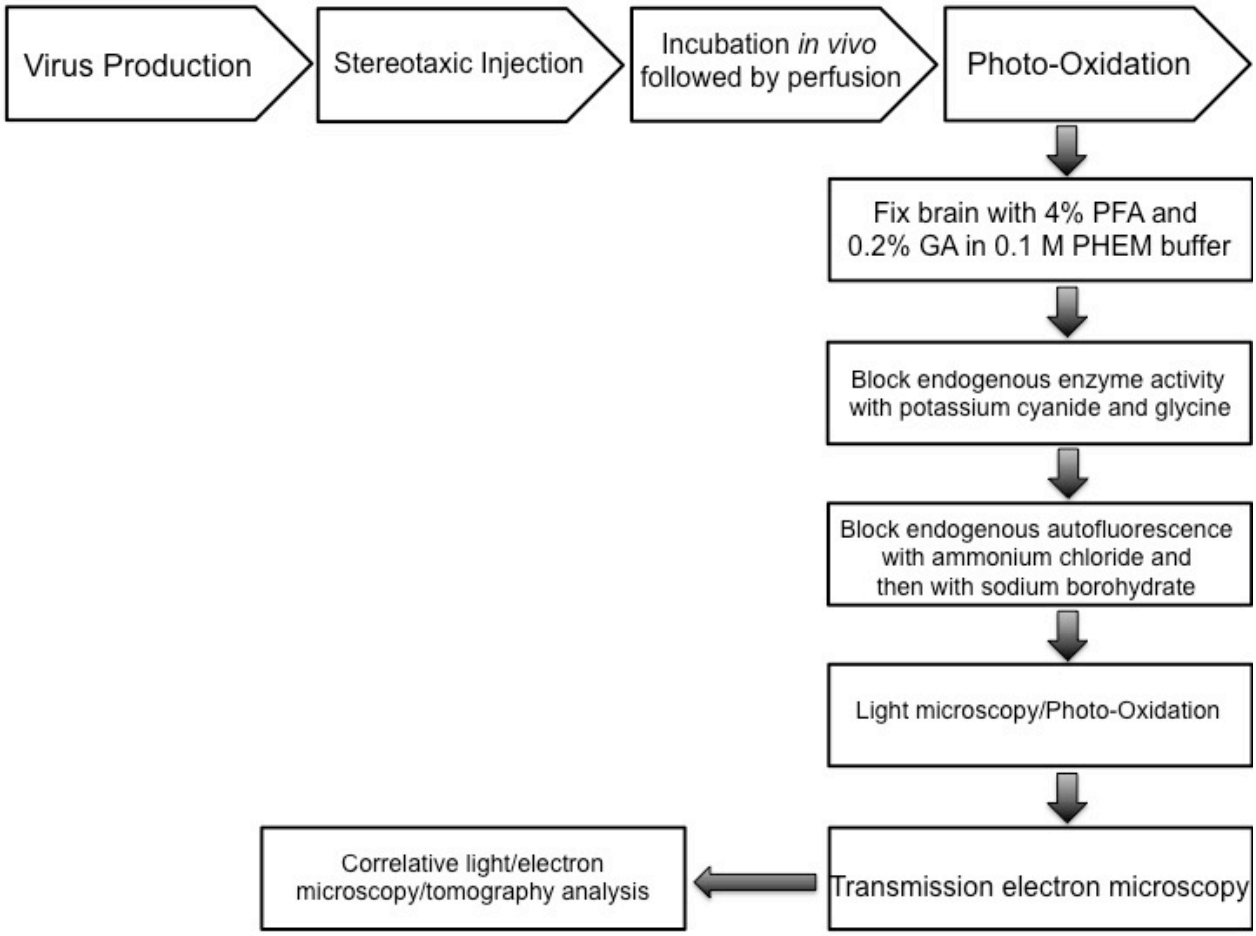

Figure 3.14 Unified workflow for Correlative Light and Electron Microscopy of mammalian neuronal tissue. This workflow was developed, optimized and used for correlative light and electron microscopy, which combines fluorescence microscopy with the superior resolution of electron microscopes through photo-oxidation.

To analyze ultrastructure of Golgi complex, both in the soma and in dendrites of neuronal tissue, I injected 9 wild type mice with AAV1/2-GalNAcT2-mTurquoise2 and 3 wild type mice with AAV1/2-GalNAcT2-APEX-mTurquoise2 in two different brain regions for subsequent photo-oxidation procedures. Eight mice were injected in visual cortex and 4 mice were injected in hippocampus, both regions in the left hemisphere. After 6 to 8 weeks of the stereotaxic injections, both contructs were successfully expressed in the chosen injected areas (Figure 3.15A, Figure 3.16A and Figure 3.17A).

First, I imaged the initial Golgi-like fluorescence of GalNAcT2-APEX-mTurquoise2 or GalNAcT2-mTurquoise2 in perfusion-fixed mouse brain sections and overlaid this with a bright field image. For the photo-oxidation procedure, the sections were incubated in freshly prepared DAB solution and illuminated (see Methods). After 2 min, a cytosolic background staining of DAB precipitate appeared, which increased over time, and I stopped the reaction after 3 min and 30 sec when mTurquoise2 fluorescence was bleached completely. Afterwards, samples were prepared for trimming and ultrathin Epon sections (60–70 nm) were cut and examined by TEM. To trim the correct bleached cells, I also used the over-bleaching technique of adjacent cells close to the cells of interest. At higher magnification TEM, specific DAB staining in several cisternae of somatic Golgi complexes could be detected in cisternal lumina supports the identification of juxtanuclear Golgi apparatus in neuronal soma through the expression of AAV-GalNAcT2-mTurquoise2 in the left visual cortex (Figure 3.15B and Figure 3.15C). This was observed in 6 samples taken from 2 mice.

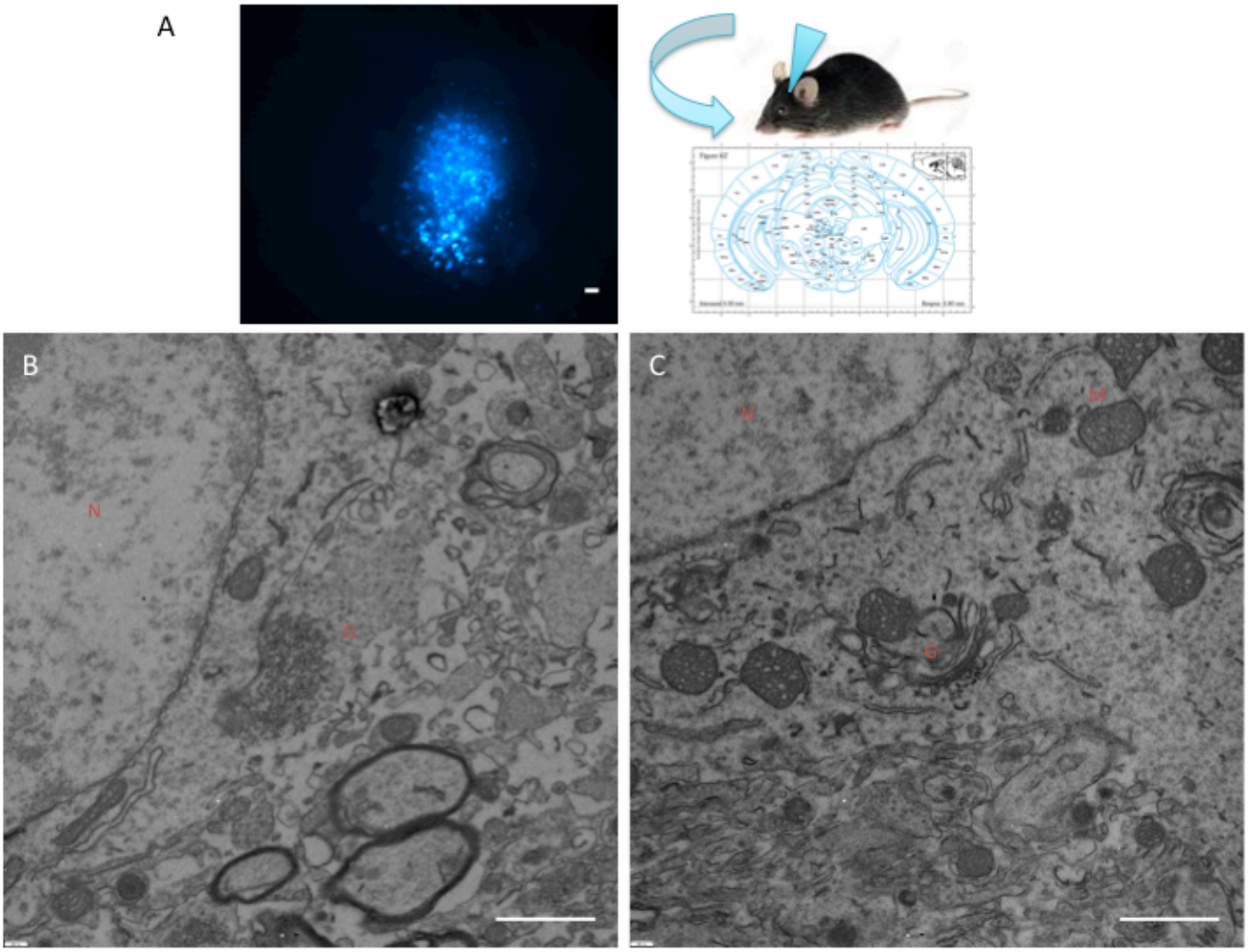

Figure 3.15 Expression of AAV-GalNAcT2-mTurquoise2 as correlative marker in neuronal tissues. (A) Schematic representation of injection site in visual cortex of a wild type mouse **(right)**, confocal single image of mTurquoise2 in the left visual cortex of a coronal section of fixed mouse brain injected with AAV-GalNAcT2-mTurquoise2 **(left)**. **(B)** and **(C)** Electron microscopy shows superior ultrastructure preservation of neurons after photo-oxidation procedure. DAB staining in cisternal lumina supports the identification of juxtanuclear Golgi apparatus in neuronal soma. **G =** Golgi apparatus, **M =** Mitochondria. **N**= 6. Scale bars: 100 µm (A-left), 800 nm (B) and (C).

Moreover, specific DAB staining in several cisternae of somatic Golgi complexes could be detected (Figure 3.16 C) and also of Golgi outpost (Figure 3.16B), which hints at a gradient-like distribution across the stack. This is consistent with the presence of mTurquoise2 Fluorescent Protein on the luminal, carboxy-terminal part of GalNAcT2 expressed in the left hippocampus. This was observed in 4 samples taken from 2 mice.

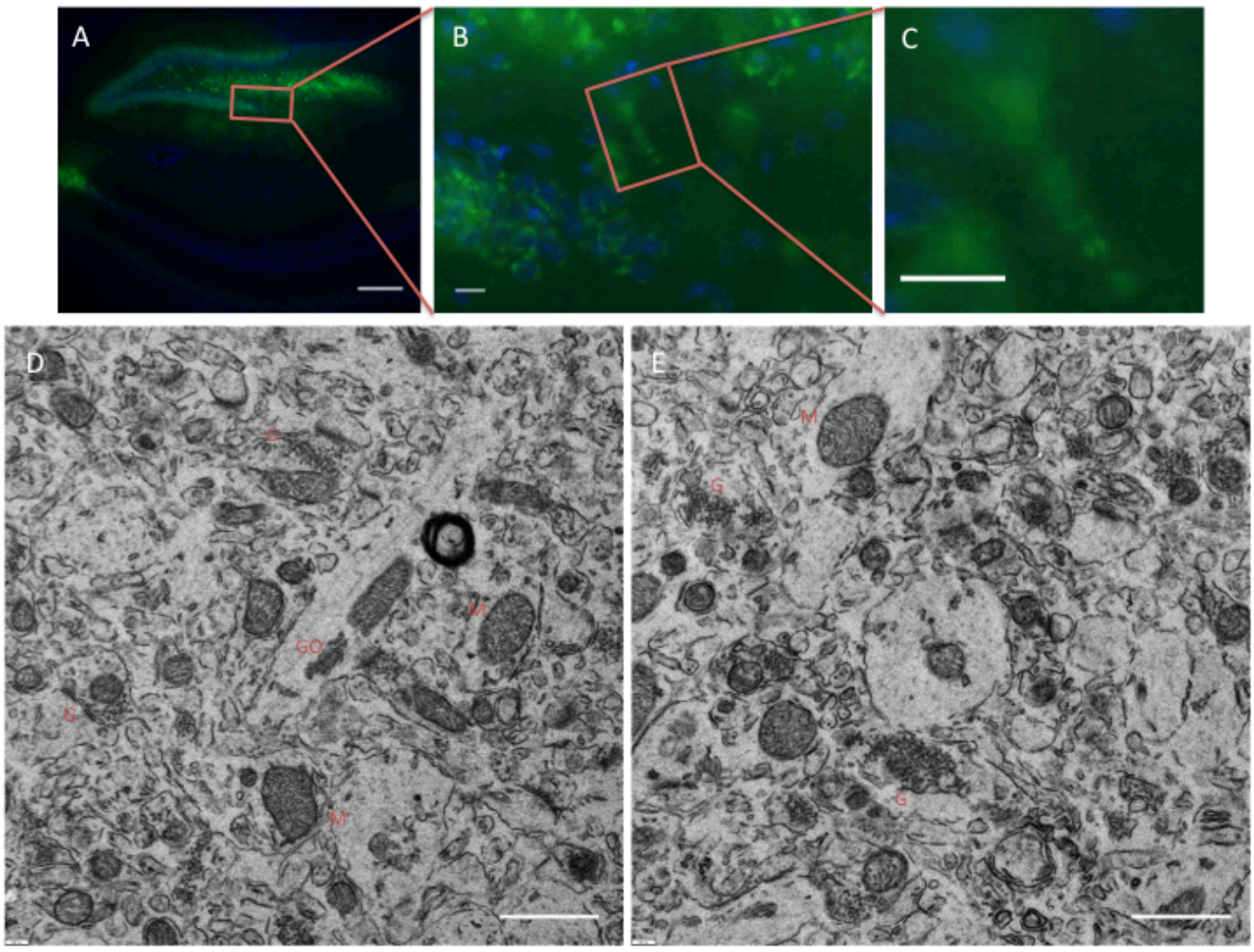

Figure 3.16 Correlative microscopy of AAV-GalNAcT2-mTurquoise2 in mouse hippocampus. (A) Confocal single image of a coronal section of fixed mouse brain injected with AAV-GalNAcT2-mTurquoise2 in the left hippocampus. **(B)** Higher magnification from A. **(C)** Higher magnification from B. **(D)** Specific DAB staining in cisternal lumina supports identification of a Golgi outpost in neuronal dendrite. **(E)** Somatic Golgi apparatus in hippocampal neurons close to B. **G =** Golgi apparatus, **GO =** Golgi outpost**, M =** Mitochondria. **N**= 4. Scale bars: 200 µm (A), 100 µm (B), 50 µm (C), 800 nm (D) and (E).

Generally, the DAB precipitation is driven by reactive oxygen species derived from bleaching processes – as in the photo-oxidation reaction – or enzymatically through H_2O_2, as in the APEX system. In this experiment, using the GalNAcT2-APEX-mTurquoise2 double construct, both cytochemical schemes have been combined: the fluorophor bleaching process was supported by application of H_2O_2 resulting in a stronger but still very specific DAB precipitation (original observation: K. van Eickels, MPI Dortmund, unpublished results).

Using this type of correlative microscopy, DAB staining could be identified in cisternal lumina of juxtanuclear Golgi apparatus in neuronal soma through the expression of AAV-GalNAcT2-APEX-mTurquoise2 in the left visual cortex (Figure 3.17D and Figure 3.17E). This was observed in 6 samples taken from 2 mice.

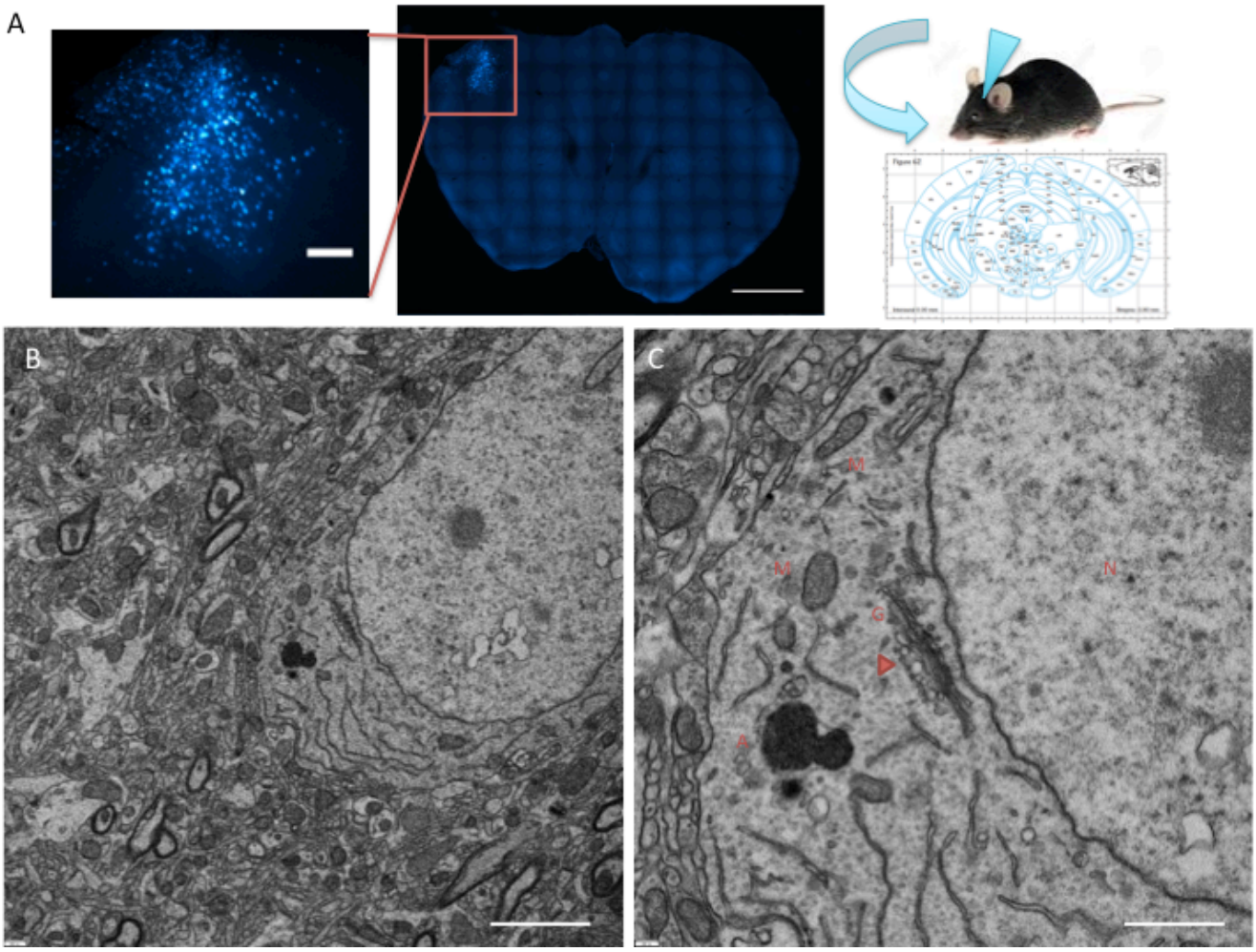

Figure 3.17 Correlative microscopy of GalNAcT2-APEX-mTurquoise2 expression in mouse visual cortex. (A) Schematic representation of AAV-GalNAcT2-APEX-mTurquoise2 injection site in visual cortex of a wild type mouse. **(B)** Confocal single image of a coronal section of an injected and fixed brain expressing AAV-GalNAcT2-APEX-mTurquoise2. **(C)** Higher magnification of visual cortex showing strong expression of mTurquoise2. **(D)** TEM showing correlated DAB staining in cisternal lumina of somal Golgi apparatus in neurons. **(E)** A higher magnification from D. **G =** Golgi apparatus, **M =** Mitochondria, **A =** Osmophilic autophagic vacuoles, **(red arrowheads)** Golgi cisternae contain specific DAB precipitate. **N**= 6. Scale bars: 500 µm (B), 200 µm (C), 2000 nm (D), 800 nm (E).

3.3.2 Neuronal tissue negative control experiments

To examine the specificity of DAB staining generated by photo-oxidation in neuronal tissue, several negative control experiments were performed. For example, brain sections injected with AAV-GalNAcT2-mTurquoise2 were incubated in DAB buffer without bleaching or injected sections were bleached in a buffer without DAB. Comparable to hippocampal neuron cultures, osmophilic autophagic vacuoles were detected in neuronal tissues (Figure 3.18A and Figure 3.18B), but could be separated from specific DAB signals. In all control samples, no DAB precipitation could be detected in cisternal lumina of Golgi stacks after illumination (Figure 3.20A and Figure 2.20B). Moreover, brain sections injected with AAV-GalNAcT2-APEX-mTurquoise2 were bleached in a buffer with DAB and without H_2O_2. Although the generation of DAB using APEX is H_2O_2-dependent without requiring light, DAB signal could be detected in cisternal lumina of Golgi stacks after illumination with hints at a gradient-like distribution across the stack. Additionally, osmophilic autophagic vacuoles were also detected and could be separated from specific DAB signals (Figure 3.18C and Figure 3.18D. This was observed in 4 samples taken from 4 mice.

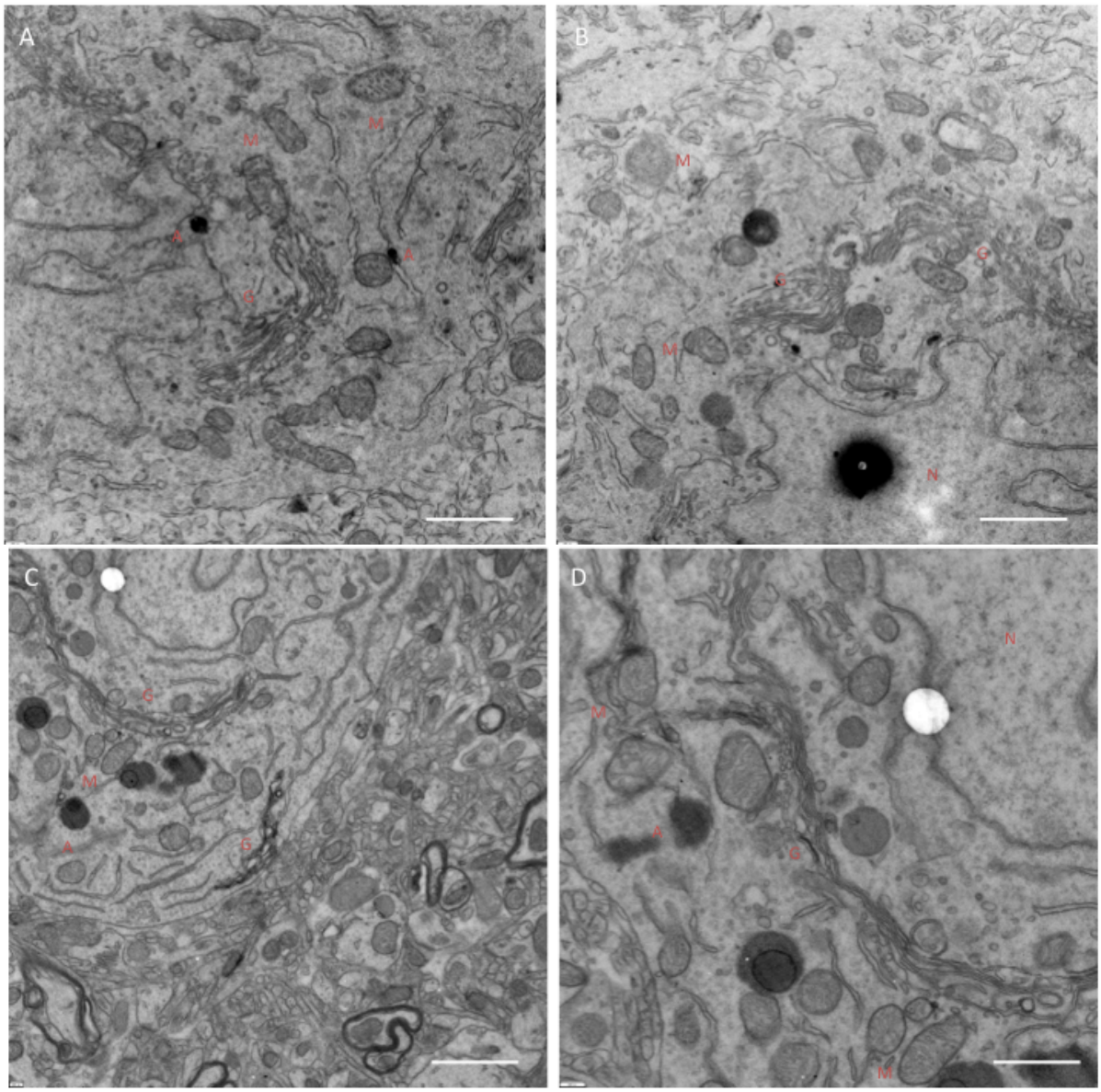

Figure 3.18 Negative control experiments of photo-oxidation reaction in neuronal tissues using AAV-GalNAcT2-mTurquoise2. (A) and (B) Careful inspection of neuronal tissue injected with AAV-GalNAcT2-mTurquoise2 shows no DAB staining after bleaching without DAB and no specific DAB staining in cisternal lumina of somatic Golgi apparatus. **(C) and (D)** Neuronal tissue injected with AAV-GalNAcT2-APEX-mTurquoise2 shows DAB staining after bleaching with DAB and without H_2O_2 in cisternal lumina of somatic Golgi apparatus. Osmophilic autophagic vacuoles are present but easily to discern from DAB signals. **G =** Golgi apparatus, **M =** Mitochondria, **A =** Osmophilic autophagic vacuoles. **N**= 4. Scale bars: 200 nm (A-D).

3.4 Correlative Light and Electron Microscopy (CLEM) of neuronal cell cultures using high-pressure freeze fixation and freeze substitution

To analyze the ultrastructure of Golgi complex in neurons using an alternative fixation method, I applied high-pressure freezing. Infected cultured hippocampal neurons expressing AAV-GalNAcT2-mTurquoise2 were subjected to high-pressure freeze fixation, followed by a freeze substitution.

A technical challenge of this fixation technique to be combined with a correlative light and electron microscopy (CLEM) approach was that neuronal cells showed delayed or no growing on the top of sapphire discs. Therefore, I established an improved protocol for preparing sapphire discs for hippocampal cell cultures. Sapphire discs were double coated with Poly-DL-ornithine hydrobromide (Figure 3.19A-C). In particular, the sapphire discs were covered with Poly-DL-ornithine hydrobromide first before and secondly after the carbon coating step (See Materials and Methods for a detailed protocol).

Hippocampal cells were cultured on coated sapphire discs 15 DIV, 6 days before AAV infection and 9 days afterwards, permanently incubated at 37°C. Directly before fixation using high-pressure freezing the Golgi-like fluorescence of GalNAcT2-mTurquoise2 in neuronal cells was imaged by fluorescence microscopy (Figure 3.19D) and overlaid with the according bright field image (Figure 3.19E) to find the region of interest on the finder-grid during subsequent correlation (Figure 3.19F).

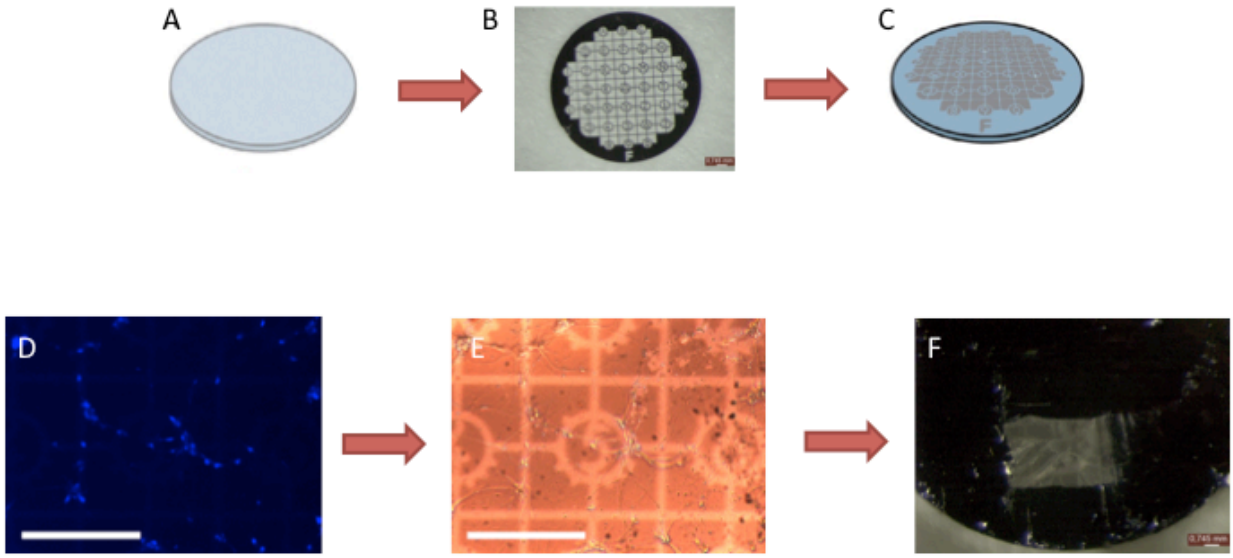

Figure 3.19 Correlative light and electron microscopy (CLEM) of neurons using high-pressure freeze fixation and freeze substitution of hippocampal cell cultures. **(A-C)** Schematic representation showing the preparation of sapphire discs for hippocampal cell cultures. The sapphire discs were treated with Poly-DL-ornithine hydrobromide double coating, and carbon coating using a finder-grid as marker for correlation. **(D)** Wide-field FM of hippocampal neuron cells expressing AAV-GalNAcT2-mTurquoise2. **(E)** Fluorescence is combined with the bright field channel showing the finder-grid and the cell of interest, **(F)** Epon-block with marked region of interest. Scale bars: 10 µm (D and E), 0,745 mm (F).

An example of correlative light and electron microscopy of neurons fixed by high-pressure freeze fixation, followed by freeze substitution is shown in Figure 3.20. For image-based correlation, the fluorescence image of hippocampal neurons expressing GalNAcT2-mTurquoise2 was overlaid with an electron microscopic image of the same infected cell. This was observed in 6 samples taken from 6 cultures.

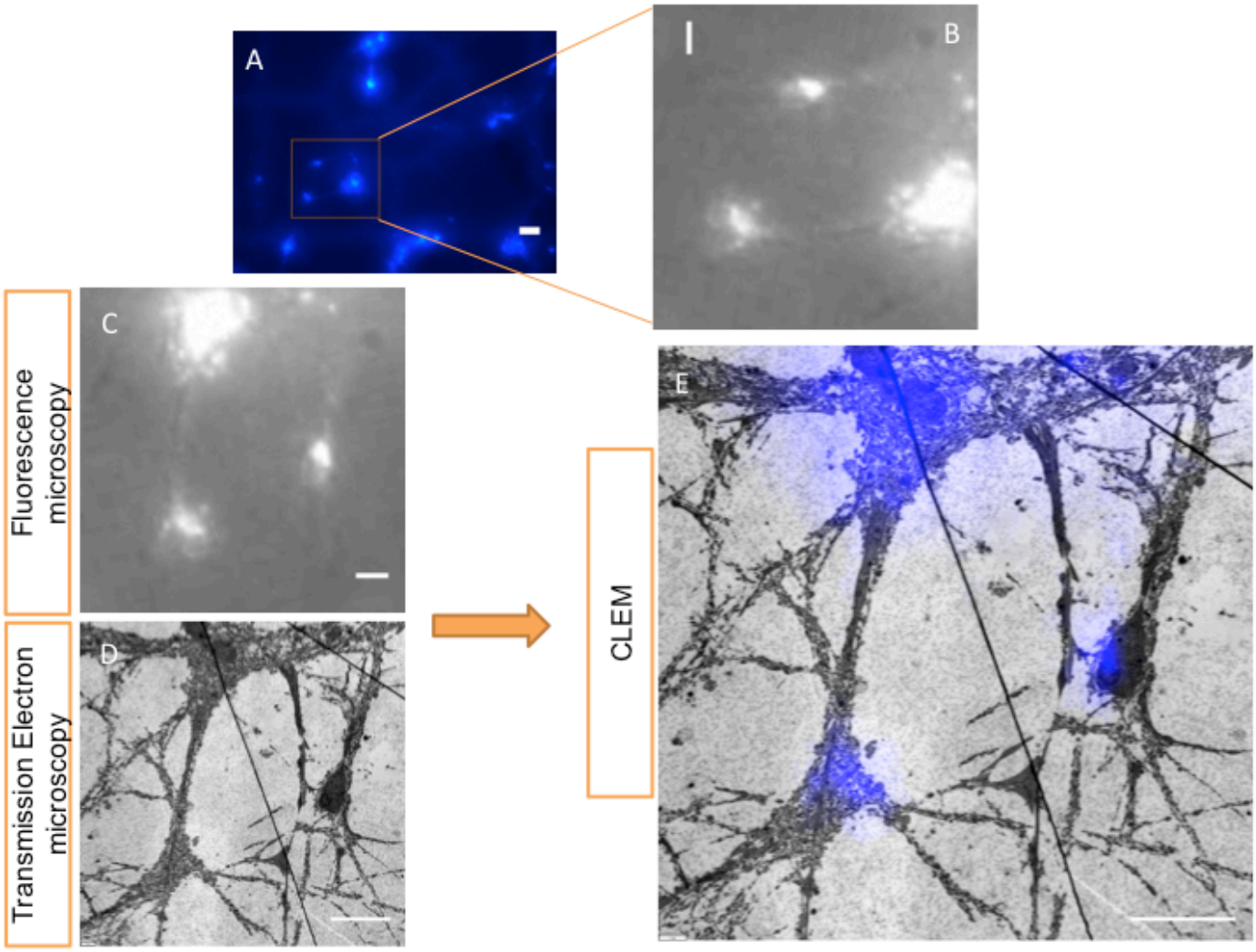

Figure 3.20 CLEM of hippocampal cell cultures expressing AAV-GalNAcT2-mTurquoise2 using high-pressure freeze fixation and freeze substitution. (A) Wide-field FM of hippocampal neuron cells expressing AAV-GalNAcT2-mTurquoise2. **(B)** Higher magnification from A showing the cell of interest. **(C)** FM showing the same cell of interest turned clockwise by 90°. **(D)** TEM showing the cell of interest. **(E)** CLEM of hippocampal neuron cell infected with AAV-GalNacT2-mTurquoise 2. N= 6. Scale bars: 10 µm (A), 5 µm (B and C), 4 µm (D and E).

At higher electron microscopic magnification of neurons fixed by high-pressure freezing and freeze substitution, the excellent morphological preservation allowed for detection of intracellular organelles including Golgi apparatus and structures of secretory pathway (Figure 3.21A). Dendrites and synapses also showed excellent ultrastructural preservation (Figure 3.21B). Unfortunately, the direct correlation of Golgi apparatus ultrastructure to their specific fluorescence signals imaged beforehand

by light microscopy failed due to lower correlation precision of image-based correlation methods. Also, specific Golgi outposts could not be detected due to this limitation.

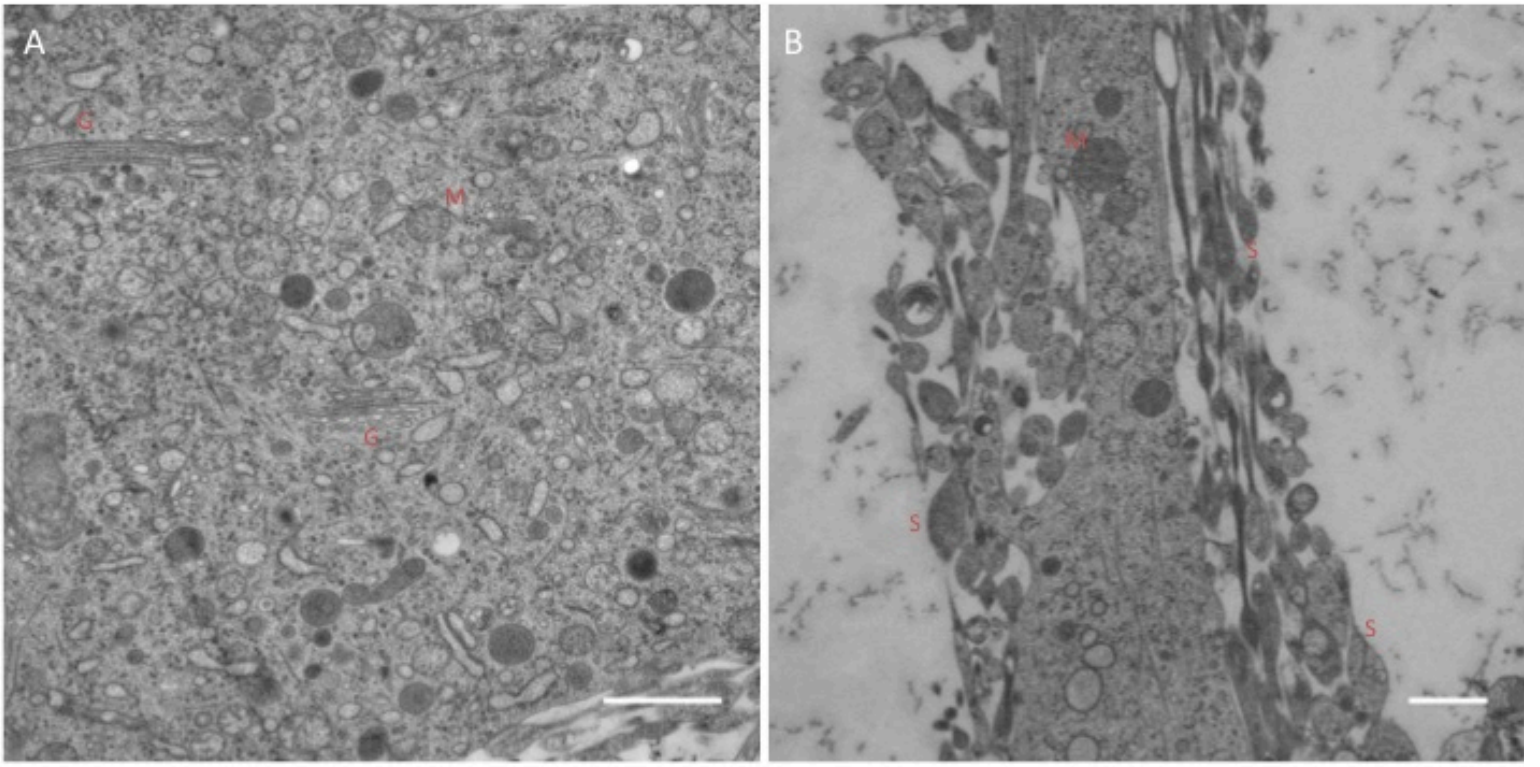

Figure 3.21 TEM of hippocampal cell cultures expressing AAV-GalNAcT2-mTurquoise2. **(A)** TEM showing excellent preservation of Golgi apparatus ultrastructure after high-pressure freeze fixation and freeze substitution. **(B)** Morphology of dendrite and synapses after high-pressure freeze fixation and freeze substitution. **(G)** Golgi apparatus, **(S)** Synapse. Scale bars: 500 nm (A), 1 µm (B).

3.5 Detection of Golgi outposts in dendrites via immunofluorescence staining

To confirm whether Golgi outpost and somatic Golgi complex fluorescence signals are specific in the neuronal cell cultures infected with AAV-GalNAcT2-mTurquoise 2, immunofluorescence experiments with various antibodies were performed.

First, 15 DIV cultured hippocampal neurons expressing GalNAcT2-mTurquoise2 (Figure 3.22A) were stained for the dendritic marker, MAP2 (Figure 3.22B) to confirm the localization of AAV-GalNAcT2-mTurquoise2 in dendrites.

The next step was the confirmation of AAV-GalNAcT2-mTurquoise2 localization specifically at Golgi apparatus, both in somatic Golgi and in Golgi outposts, but not in other organelles as for example lysosomes. Therefore, DIV 15 cultured hippocampal neurons expressing GalNAcT2-mTurquoise2 (Figure 3.22D) were stained with antibodies against Lamp2 as lysosomes marker (Figure 3.22E). The fluorescence signal of GalNAcT2-mTurquoise 2 could be clearly separated from lysosomal signals (Figure 3.22F).

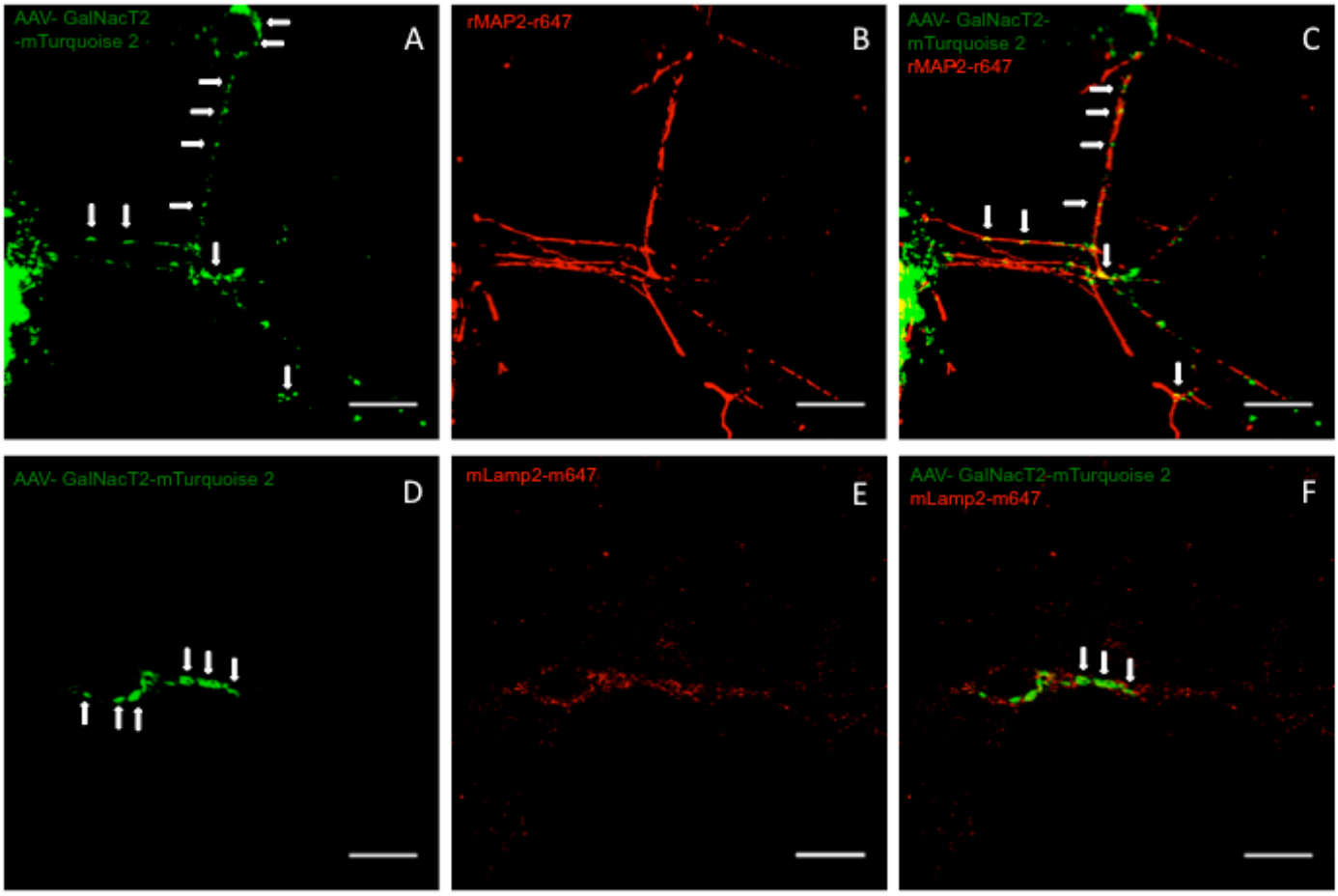

Fig. 3.22 Immunofluorescence co-staining of cultured hippocampal neurons expressing GalNAcT2-mTurquoise2 to confirm specificity of fluorescence signals at somatic Golgi and Golgi outposts. **(A)** Confocal image showing somatic Golgi apparatus and Golgi outposts in 15 DIV hippocampal neurons expressing GalNAcT2-mTurquoise2 (green). **(B)** Confocal image showing 15 DIV hippocampal neurons stained for MAP2 (red) as dendrite marker. **(C)** Overlay image showing the localization of somatic Golgi apparatus and Golgi outposts in dendrites of a neuron expressing GalNAcT2-mTurquoise2 (green) and stained for MAP2 (red). **(D)** Confocal image showing somatic Golgi apparatus and Golgi outposts in 15 DIV hippocampal neurons expressing GalNAcT2-mTurquoise2 (green). **(E)** Confocal image showing lysosomes of 15 DIV hippocampal neurons stained for Lamp2 (red). **(F)** Overlay image showing the localization of somatic Golgi apparatus and Golgi outposts (green) and lysosomes stained for Lamp2 (red), the different fluorescence signals of Golgi markers could be clearly separated from lysosomes. A, B, C: z-collapse of a confocal stack, D, E, F: single confocal images. Images are presented in pseudo-colors. (white arrows) AAV-GalNAcT2-mTurquoise2 expression in somatic Golgi apparatus and Golgi outposts. Scale bars: 10 µm (A-F). The images are representative of 12 independent experiments.

Additionally it was essential to verify the identity of Golgi outposts in dendrites using antibodies against endogenous Golgi apparatus proteins, such as TGN38. Therefore, 15 DIV cultured hippocampal neurons were stained for TGN38 (Figure 3.23A andC, green channel) and images were merged with MAP2 (Figure 3.23B and D, red channel).

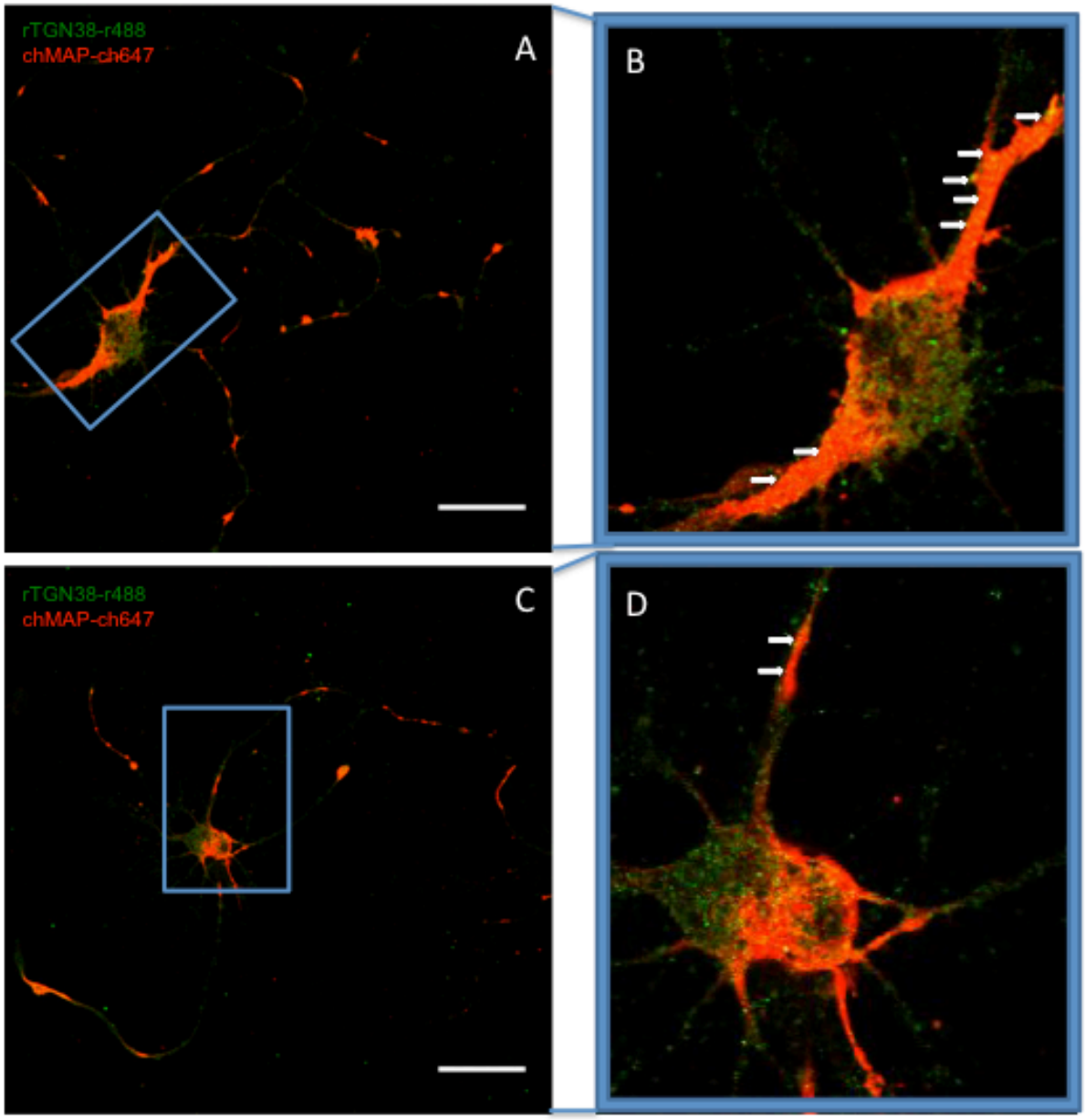

Fig. 3.23 Detection of Golgi outpost in cultured hippocampal neurons using TGN38 immunofluorescence staining. (A, C) Confocal image displaying the morphology of a 15 DIV hippocampal neuron stained for MAP2 (red) and TGN38 (green). **(B)** A higher-magnification image of the insert displayed in (A); the arrows point to fluorescent dots representing Golgi outposts in dendrites **(D)** A higher-magnification image of the insert displayed in (C); the arrows point at Golgi outposts further away from soma. A, B, C, D: z-collapse of a confocal stack. The images are displayed in pseudo-colors. Scale bars: 10 μm (A and C), 5 μm (B and D). The images are representative of 8 independent experiments.

4. Discussion

In the present study I examined the ultrastructure of somatic Golgi apparatus and Golgi outposts in neuronal cell culture and neuronal tissue using correlative light and electron microscopy. Various studies have reported the roles of Golgi outposts and their functions in dendrites. However, the morphology of Golgi outposts is still poorly understood. To facilitate the investigation of Golgi outpost ultrastructure in 3D, I established a correlative microscopy method in neuronal cell cultures and in neuronal tissue. The preferred light and electron microscopic correlation method is based on photo-oxidation through GFP-labeled Golgi enzymes and allows for direct ultrastructure visualization and analysis of Golgi apparatus, both in neuronal soma and in dendrites. Electron tomography and 3D analysis showed that the polarity, size and number of Golgi outpost cisternae differ morphologically from primary Golgi complex in the soma of the neuron.

4.1 Applying the correlative light and electron Microscopy of GFPs through photo-oxidation in HeLa cells

The correlation of light and electron microscopy is a powerful technique, which combines the fluorescence signals with the high resolution of the electron microscope. The correlative microscopy of GFPs through the photo-oxidation method allows for direct ultra-structural visualization of fluorophores upon illumination (Grabenbauer et al., 2005). The generation of oxygen radicals during the GFP bleaching process photo-oxidize DAB into a precipitate with high electron density. It is possible then to visualize the DAB precipitate both by EM of thin sections and by electron tomography for 3D analysis (Grabenbauer, 2012).

Based on practical experiences of photo-oxidation preparation (Grabenbauer et al., 2005), I first applied this method using stably transfected HeLa cells expressing Golgi-tagged ECFP fusion proteins (Figure 3.1 and Figure 3.2). The specificity of the DAB signal through the photo-oxidation of GalNAcT2-ECFP in HeLa cells, was successfully accomplished in this study, resembling earlier results in Grabenbauer et al., 2005.

On one side, the photo-oxidation method using HeLa cells as establishied model system was essential to set up this challenging method in the given laboratory environment, e.g. choosing the right fluorescence microscope and its settings, or determining the exact time span needed for the bleaching process to generate sufficient and specific DAB precipitation. On the other side, using the photo-oxidation technique as a labeling method to correlate the fluorescence signals with electron microscopic resolution was the key element in this study to be able to analyze the ultrastructure of somatic Golgi and dendritic Golgi outposts. Pure coordinate-localization based correlations for example of morphologically superior high-pressure frozen material failed to detect specific Golgi outposts. The GFP-based DAB signal was necessary to detect and identify such rare organelles at electron microscopy level, in particular Golgi outposts in dendrites of neurons.

In contrast to immuno-EM as more commonly used EM labeling method, photo-oxidation through GFPs enables a higher localization precision. First, the selected protein is tagged genetically before the fixation, and second, all small subsequent components, such as OsO_4, DAB or O_2, easily penetrate into fixed samples, in contrast to antibodies. Moreover, some drawbacks of immuno-labelling are absent in photo-oxidation procedures, such as low labeling efficiency of antibodies, the absence of compatible antibodies, or non-specific background binding of various antibodies (Horstmann et al., 2013). Most importantly, a 3D analysis, which is necessary for complex membrane systems like Golgi apparatus or Golgi outposts, is more likely to be feasible using photo-oxidation than immuno-labeling methods, where the markers of post-embedding labeling are mainly restricted to the surface of the section.

Nevertheless, applying correlative light and electron microscopy through photo-oxidation is demanding and also time consuming. It needs fine handling and experience in specialized instrumentation and numerous controls experiments, which have to be processed in parallel (Gaietta et al., 2006; Grabenbauer, 2012; Kopek et al., 2012, Horstmann at al., 2013). Furthermore, the generation of the DAB precipitate in an amount sufficient for detection may depend on the expression density of the protein of interest, thereby limiting the scope of this approach to highly clustered proteins expressed at a high level. These could be reasons why nowadays the method is not very frequently applied (Grabenbauer, 2012).

4.2 Golgi complex visualization in neuronal cell culture with correlative light and electron microscopy through the photo-oxidation method

Regarding Golgi outposts and their functions in dendrites, there have been recent reports in various studies (Hanus and Schuman; 2013, Kelliher et al., 2018; Merianda et al., 2009). However, accurate knowledge about Golgi outpost ultrastructure was lacking. Being relatively rare organelles in cultured cells or in tissue, correlative microscopy is the method of choice to study Golgi outpost morphology in neurons. The advantage of using marker-based correlative microscopy through photo-oxidation as labeling method is the possibility of direct correlation of the initial fluorescence signals in Golgi apparatus to the final DAB precipitates, which can be analysed subsequently in 2D as well as 3D electron microscopy and electron tomography. This allows for the specific detection of Golgi-like structures in dendrites and for examining the differences in ultrastructure between somatic Golgi apparatus and Golgi outposts.

Although EGFP has not the highest quantum yield (QY), which means, it produces lower amounts of reactive oxygen-mediated DAB precipitates than some other organic fluorophores (Jimenez-Banzo et al., 2008; Shu et al., 2011), previous studies showed that EGFP can be successfully used to generate specific DAB precipitates, if a high level of oxygen environment is assured during the photo-oxidation process (Grabenbauer et al., 2005; Horstmann et al., 2013). However, a fluorescent protein with a higher quantum yield should increase DAB precipitation. We utilized ECFP in HeLa cells, resulting in an increased generation of specific DAB. Goedhart and colleagues in 2012 have examined different fluorescent proteins regarding their quantum yield levels. In this seminal paper, it was confirmed that mTuorquoise2 has a higher quantum yield compared to ECFP or EGFP. This means, it delivers an enhanced amount of oxygen radicals during the bleaching process, which is essential for the polymerization of DAB. Considering these findings, mTuorquoise2 was used in this study as the green fluorescent protein mutant of choice to apply the photo-oxidation method in neurons.

In summary, the photo-oxidation method enables the correlation of fluorescence signals as detected by fluorescence microscopy to the final DAB precipitate analysed by electron microscopy and electron tomography. Nevertheless, many variables of the

photo-oxidation protocol need to be adjusted, depending on which type of sample it is being applied on, to ensure a specific correlation of the fluorescence signals and the generated DAB precipitates. Therefore, establishing the photo-oxidation labeling method in neurons was an essential requirement in this study.

4.2.1 Establishment of the photo-oxidation reactions in neuronal cell cultures

An important step in establishing the photo-oxidation method for neuronal cell cultures was to improve the labeling sensitivity as well as ultrastructural preservation. For this purpose, I first optimized the chemical fixation of hippocampal cell cultures. There are different factors influencing the chemical fixation efficiencies of a fixative, including osmolarity, pH, time and temperature of fixation, and the final fixative concentration. I examined each factor to see how sensitive the general structures of the hippocampal neurons among these various conditions reacted. I found one very important aspect by chemical fixation, which strongly influences the ultrastructural quality of cultured hippocampal neurons, namely the pH value. During the fixation process, the contents of the lysosome are released and the pH of the cells becomes acidic (Chang-Hyun Park et al., 2016). The average pH of most animal cells is 7.4 (Chang-Hyun Park et al., 2016). Therefore, it is important to adjust the fixative to ~ pH 7.4. To keep this optimum pH value constant during the entire fixation process, I used a sodium cacodylate buffer supplemented with calcium chloride instead of the usual PBS buffer (Figure 3.3). Furthermore, to reduce the glutaraldehyde-induced auto-fluorescence, I used chemical blocking solutions, such as glycine, ammonium chloride, and sodium borohydrate (Grabenbauer et al., 2005; Baschong et al., 2001; Harata et al., 2001).

Next, the establishment of a functional protocol and unified workflow for correlative light and electron microscopy through the photo-oxidation technique (Figure 3.4) improved the specificity of DAB staining in cisternal lumina of Golgi apparatus (Figure 3.7).

There were several factors that needed to be considered during the adjustment of the photo-oxidation protocol for hippocampal cell cultures. Most important were the quality and age of the hippocampal cell cultures (William J. Brown (ed.), 2016). The

probability for detection and visualization of Golgi outposts was highest in long and highly branched dendrites (Horton et al., 2003; Horton et al., 2005; Pierce et al., 2001). These were found predominantly in neuronal cell cultures with at least 10 DIV (William J. Brown (ed.), 2016). Therefore, hippocampal neurons used in this study were 15 days *in vitro* (DIV) before starting the chemical fixation step. The cells were infected with AAV on the 6th day and then incubated for additional 9 days.

Another important aspect in the development of correlative microscopy techniques in neurons was to achieve a higher correlation between the bleached cell of interest and trimming this particular cell for further electron microscopic analysis. Hence, I over-bleached some adjacent cells close to cell of interest as indirect markers (Figure 3.6).

In summary, establishing a sensitive protocol for correlative light and electron microscopy through photo-oxidation allowed me to examine neuronal cell cultures, to gain deeper insights at ultrastructure of Golgi outposts, and finally begin to answer essential questions about the differences between somatic Golgi apparatus and Golgi outposts.

4.2.2 Golgi outposts and somatic Golgi visualization with transmission electron microscopy and electron tomography

Since the increasing discussion in recent years about the presence and function of Golgi outposts, the first detection of Golgi-like structure in dendrites has been shown using an immuno-gold labeling approach for TGN38 in adult rat dendritic spines by Pierce and colleagues in 2001 (Pierce et al., 2001). In this seminal paper, it was suggested that a satellite membrane system near synapses could only be needed under specific conditions, such as synapse modification in response to synaptic activity and it could provide rapid and spatially localized delivery of proteins to specific synapses. However, the ultrastructural visualization of Golgi outposts has been demonstrated once, in particular through an immuno-gold labeling for GM130 in adult rat hippocampus by C. Horton and colleagues in 2005 (Figure 4.1A) (Horton et al., 2005).

Since then, Golgi outposts have been detected mainly by fluorescence microscopy of neuronal cell cultures, and higher resolution or ultrastructure examination is lacking (Hanus and Ehlers et al.; 2016; Hanus and Schuman; 2013; Horton et al., 2005).

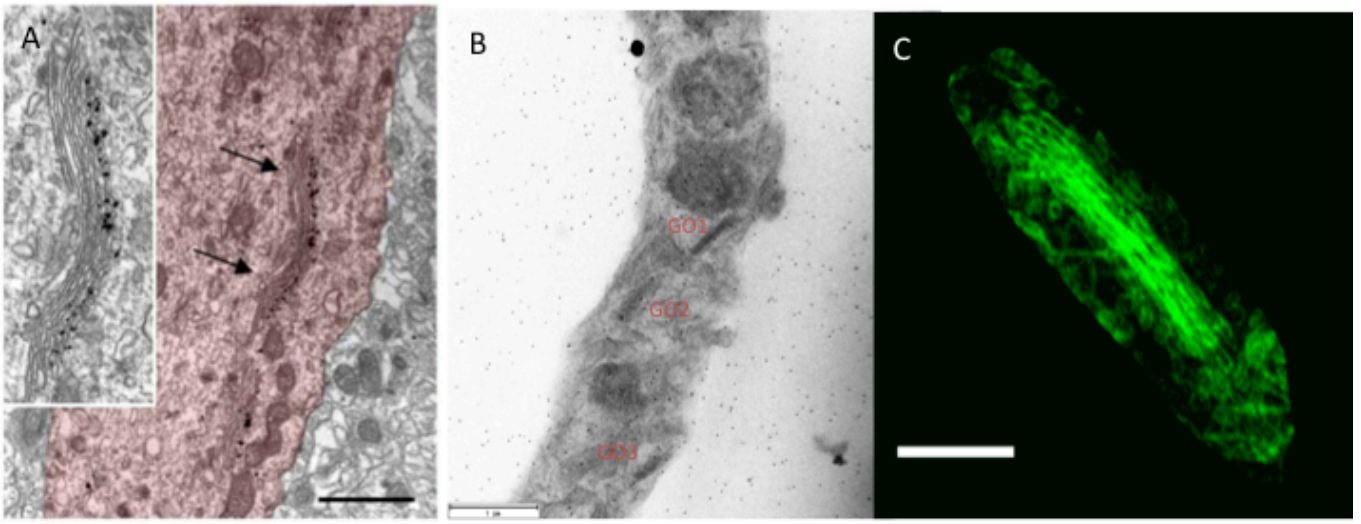

Figure 4.1 Ultrastructure of Golgi outposts in neurons. (A) Electron micrograph of Golgi outpost in adult rat hippocampus using immuno-gold labeling for GM130**. (B)** Electron micrograph of Golgi outposts in dendrite of hippocampal neurons labeled by DAB photo-oxidation through GalNAcT2-mTurquoise2**. (C)** 2D maximum intensity projection image of segmented Golgi outpost model extracted from GO1 in B with membranes shown in green color Scale bar: 0.5 µm (A) Figures are adopted from Horton et al., 2005. 1 µm (B), 200 nm (C).

Through the specific DAB staining of GFP-tagged Golgi-resident enzymes, I was able to detect and demonstrate Golgi outposts and somatic Golgi apparatus in conventional two-dimensional transmission electron microscopy (Figure 3.10 and Figure 3.11) as well as in three-dimensions using electron tomography (Figure 3.12 and Figure 3.13). This allowed me to analyze in detail the structural differences between Golgi outposts and somatic Golgi apparatus. The three-dimensional segmentation of these models showed that the number and size of cisternae in Golgi outposts are different from those in somatic Golgi apparatus. In addition, it was recognizable that Golgi outposts have strictly unidirectional polarity, while the somatic Golgi apparatus polarity appears interchangeable along the stacks.

Moreover, the initial ultrastructure description of a Golgi outpost (Horton et al., 2005) was restricted to apical dendrites, although in further studies using fluorescence microscopy and live-cell imaging, Golgi outposts have been shown in apical and in distal dendrites (Quassollo et al., 2015; Chung et al., 2017). The sizes of Golgi outposts in the initial electron micrographs using GM130 immuno-gold labeling were relatively large and comparable to the extent of somatic Golgi apparatus (Figure 4.1A,), while all Golgi outposts shown in this study appear to be smaller (Figure 3.10). Furthermore, the published Golgi outposts in pyramidal neuron apical dendrites by Horton et al., 2005 contains several cisternae (Figure 4.1A), while the Golgi outposts analyzed in this study, which were found up to 100 µm distance from soma appear to have fewer cisternae (Figure 4.1B and Figure 4.1C). Given the large diameters of the dendrites in the article of Horton et al., 2005, the positions of these particular Golgi stacks might be relatively close to the soma. However, here I present obvious differences in size between genuine Golgi outposts and somatic Golgi apparatus. A possible explanation for this could be the localization of Golgi outposts in dendrites with respect to their distance from the cell body. Golgi outposts located close to the soma show no difference in size compared to somatic Golgi apparatus. Direct membrane connections to the somatic Golgi apparatus might still exist. A *bona fide* Golgi outpost is supposed to have not such direct membrane contacts. All Golgi outposts shown in this study were detected from 80 up to 120 µm distant from soma. These genuine Golgi outposts residing more distally in dendrites appear smaller than Golgi apparatus in soma.

4.3 Golgi complex visualization in neuronal tissue using correlative light and electron microscopy

After the successful ultrastructural visualization of Golgi outposts and somatic Golgi complex in neuronal cell cultures establishing photo-oxidation of mTuorquoise2 in neurons, the consequential goal was to use this technical achievement for detailed analysis of Golgi complex ultrastructure in neuronal tissue, in particular to analyze the morphology of Golgi outposts in mammalian brain. Therefore, the adaptation of a functional protocol and workflow for correlative microscopy through photo-oxidation for mouse brain as model system was required (Figure 3.14). This optimized approach allowed me to generate and analyze specific DAB staining in several cisternae of somatic Golgi complexes (Figure 3.15 B and C), (Figure 3.16 B and C) and (Figure 3.17 C), as well as in Golgi outposts (Figure 3.17 B). However, the intensity of DAB precipitation in neuronal tissue was lower compared to DAB signals in neuronal cell cultures. This indicates the need for further optimization of photo-oxidation protocols for neuronal tissue.

Immuno-gold labeling for GM130 was initially used to show Golgi outposts *in situ* (Horton et al., 2005). It displayed the existence of Golgi stacks in the apical dendrite of a pyramidal neuron and the electron micrographs of GM130 immuno-gold labeling marked Golgi outposts at the proximal apical dendrite. Further and consequential higher resolution analyses of Golgi outposts *in vivo* or in fixed neuronal tissue are still lacking.

In summary, applying the photo-oxidation method in neuronal cell cultures and neuronal tissue enabled the detection of somatic Golgi apparatus and Golgi outposts in dendrites. Golgi like-structure in dendrites would not be recognizable without the DAB staining due their unknown structure.

4.4 Golgi outposts and somatic Golgi visualization in neuronal cell cultures and neuronal tissues using the APEX system

The objective of using APEX as EM tag protein is to generate enzymatically a specific DAB precipitate without a bleaching process. This means, there should be no limit to DAB polymerization, since APEX is enzymatically active through H_2O_2 in all cellular compartments without requiring light. Indeed, I was able to detect Golgi outposts and somatic Golgi apparatus labeled by DAB precipitation without bleaching (Figure 3.8). However, the DAB precipitate generated using APEX was clearly less pronounced, compared to DAB precipitation generated through fluorophore bleaching.

Consequently, I attempted to generate stronger DAB precipitation by combining the H_2O_2-driven enzymatic reaction of APEX enhanced by the photo-oxidation reaction using bleaching processes in neuronal dendrites (original observation on HeLa cells: K. van Eickels, MPI Dortmund, unpublished results). Areas showing H_2O_2 reaction only, and areas where this reaction was supported by an additional bleaching processes were clearly distinguishable. DAB precipitation was enhanced by the additional bleaching process (Figure 4.2 A). However, specific DAB precipitation in putative Golgi outpost structures could not be detected. Moreover, DAB signal seems also present in ER-like structures of dendrites (Figure 4.2 B), where the relatively large APEX-GFP-tagged protein might be trapped by chaperones due to potential folding problems.

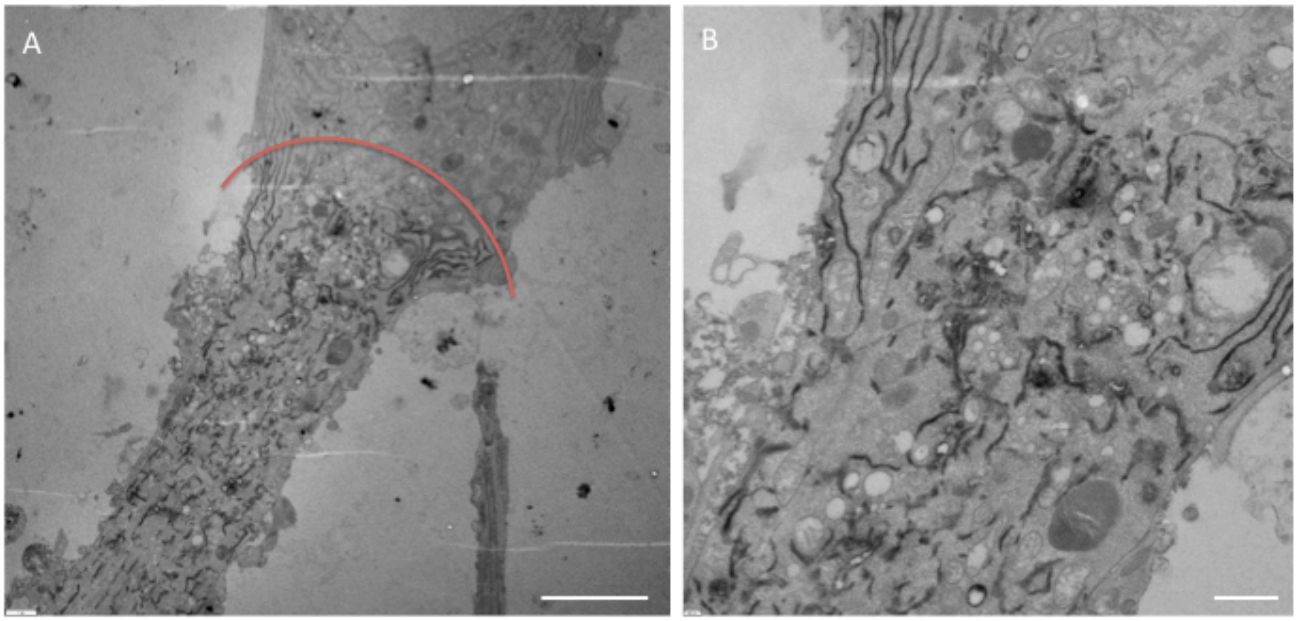

Figure 4.2 DAB precipitation in hippocampal cell cultures generated by enzymatic reaction (APEX), supported by a bleaching process. (A) TEM showing DAB staining in neurons generated by enzymatic activity of APEX, partly supported by a bleaching process. (B) Higher magnification from A. (red line) the border between the bleached and not bleached area. **N**=16. Scale bars: 8 µm (A), 400 nm (B).

However, the reaction of this combination in brain tissue was surprisingly different. The generated DAB precipitation was slightly stronger using the H_2O_2 and bleaching combination than using tH_2O_2 only. Moreover, the DAB precipitate was specifically visible in cisternal lumina of Golgi apparatus (Figure 3.15), while ER-like structures or mitochondria were not stained.

In summary, APEX could be used as a genetically encoded reporter of fusion proteins for EM without requiring light or a bleaching step (Martell et al., 2012). However, fusion to a fluorescent protein is necessary for the correlation of light microscopy and EM. Therefore, APEX was fused to mTuorquoise2 enabling the detection of Golgi like structures in soma and in dendrites by light/fluorescence microscopy, and to correlate subsequently with EM. The combination of the reaction between H_2O_2 and the bleaching process to generate stronger DAB precipitate appears to be not specific in neuronal cell cultures, while the DAB signal was slightly stronger using this combination in neuronal tissue.

4.5 Golgi complex visualization in neuronal cell culture with CLEM using high-pressure freeze fixation and freeze substitution

The superior morphological quality of high-pressure freeze fixation and freeze substitution is most evident on highly dynamic organelles and membrane systems of the secretory pathway (Dahl and Staehelin, 1989; McDonald, 1999; McDonald et al., 2007). Therefore, I utilized an alternative correlative light and electron microscopy technique using high-pressure freezing, followed by freeze substitution, to examine Golgi outposts in dendrites and somatic Golgi complex in hippocampal cell cultures.

To correlate the light and electron microscopy (CLEM) approach in neuronal cell culture, I used a special finder-grid on top of a sapphire disc. This allowed me to visualize the cell of interest by electron microscopy, which was imaged beforehand by light microscopy ((Figure 3.19). However, the technical challenge of this particular CLEM method was that attachment and growing of cultured neurons on top of sapphire discs seemed utterly difficult. To my knowledge, there is no study available that has shown a technique of growing neuronal cell cultures on top of sapphire discs for high-pressure freezing and freeze substitution. Therefore, the development of a protocol for preparing sapphire discs suitable for hippocampal cell cultures was an essential step in this type of CLEM, which was successfully solved in this present study. Consequently, I could combine light and electron microscopy of specific neurons, which were fixed by high-pressure freeze fixation, followed by freeze substitution (Figure 3.20).

However, the attempt to detect specific Golgi outposts in dendrites through this type of CLEM failed. Although the grid pattern aids as a localization and correlation tool (Brown et al., 2009; Guizetti et al., 2010; Jimenez et al., 2010; Spiegelhalter et al., 2010), the combination of live cell imaging and vitrification is still challenging due to the precision required during individual steps. Potentially, with further adjustments in the method, this might be possible to accomplish.

4.6 Summary

In this study, I was able to analyze the ultrastructure of Golgi outposts in dendrites by photo-oxidation and electron tomography. This enables to better understand the morphology of this crucial organelle. Although the regulation and generation of Golgi outposts in dendrites is still an unsolved issue and many open questions about its function remain open, the morphology and ultrastructural details of this organelle became clearer through the results of this study. The number and size of cisternae in Golgi outposts appear to differ from those of somatic Golgi apparatus. Additionally, the number of vesicles associated with GOs implies to be less compared with somatic Golgi apparatus. Moreover, Golgi outposts have strictly unidirectional polarity, while the somatic Golgi apparatus polarity is not unidirectional. These findings allows for further investigations into the structure of this important organelle and to better understand its function.

The establishment and optimization of photo-oxidation as labeling method for correlative light and electron microscopy in neuronal cell cultures and neuronal tissue was key to enable this approach. I succeeded to develop a novel and functional protocol and unified workflow to study neurons by correlative microscopy, both in neuronal cell cultures and in fixed neuronal tissue. Thereby, rare organelles such as Golgi outposts in apical and in distal dendrites were localized and their ultrastructure was morphologically analyzed in 3D. Putative Golgi-like structure in dendrites, particularly more distally in dendrites, would not be recognizable without a specific DAB staining. My findings suggest that the differential structure of Golgi outposts is depends on their localization in dendrites with respect to their distance from the cell soma. Golgi outposts in a distance of up to 120 µm distally from neuron soma appear to have fewer cisternae per stack compared to Golgi outposts proximal to the soma or juxtanuclear Golgi apparatus. Moreover, in proximal Golgi outposts direct membrane connections to somatic Golgi apparatus might still exist, while a *bona fide* Golgi outpost is supposed to have not such direct membrane contacts.

Future studies, based on these results, can further improve our knowledge of the functionality of this vital organelle in neurons.

5. Literature

Ariotti N., Hall T. E., Rae J., Ferguson C., McMahon K.-A., Martel N., et al. . (2015). Modular detection of GFP-labeled proteins for rapid screening by electron microscopy in cells and organisms. Dev. Cell 35, 513–525. 10.1016/j.devcel.2015.10.016.

Baschong, W., Suetterlin, R., & Laeng, R. H. (2001). Control of autofluorescence of archival formaldehyde- fixed, paraffin-embedded tissue in confocal laser scanning microscopy (CLSM). The Journal of Histo- chemistry and Cytochemistry, 49, 1565–1572.

Biel, S.S., K. Kawaschinski, K.P. Wittern, U. Hintze, and R. Wepf. (2003). From tissue to cellular ultrastructure: closing the gap between micro- and nanostructural imaging. J Microsc 212: 91-9.

Borst JG, Soria van Hoeve J. (2012). The calyx of held synapse: from model synapse to auditory relay. Annu Rev Physiol 74: 199–224.

Branco, T., Marra, V., & Staras, K. (2010). Examining size-strength relationships at hippocampal synapses using an ultrastructural measurement of synaptic release probability. Journal of Structural Biology, 172, 203–210.

Brian Storrie, Jamie White, Sabine Röttger, Ernst H.K. Stelzer, Tatsuo Suganuma, Tommy Nilsson. (1998). Recycling of Golgi-resident Glycosyltransferases through the ER Reveals a Novel Pathway and Provides an Explanation for Nocodazole-induced Golgi Scattering. The Journal of Cell Biology, 143 (6) 1505-1521.

Bumbarger, D. J., M. Riebesell, C. Rodelsperger and R. J. Sommer. (2013). "System-wide rewiring underlies behavioral differences in predatory and bacterial-feeding nematodes." Cell 152(1-2): 109-119.

Chang-Hyun Park, Hyun-Wook Kim, Im Joo Rhyu, Chang-Sub Uhm. (2016). How to Get Well-Preserved Samples for Transmission Electron Microscopy. Applied Microscopy (Korean Society of Microscopy). 46(4):188-192.

Chung C. G., Kwon M. J., Jeon K. H., Han M. H., Park J. H., Cha I. J., et al. (2017). Golgi outpost synthesis impaired by toxic polyglutamine proteins contributes to dendritic pathology in neurons. Cell Rep. 20 356–369. 10.1016/j.celrep.2017.06.059.

Dacks JB, Doolittle WF. (2001). Reconstructing/deconstructing the earliest eukaryotes: How comparative genomics can help. Cell 107: 419–425.

Dahl R, Staehelin LA. (1989). High-pressure freezing for the preservation of biological structure: theory and practice. J Electron Microsc Tech;13:165–74.

Dalton, A. J. and M. D. Felix (1954). "Cytologic and cytochemical characteristics of the Golgi substance of epithelial cells of the epididymis in situ, in homogenates and after isolation." Am J Anat 94(2): 171-207.

Deerinck, T. J., Martone, M. E., Lev-Ram, V., Green, D. P., Tsien, R. Y., Spector, D. L., et al. (1994). Fluores- cence photooxidation with eosin: a method for high resolution immunolocalization and in situ hybridiza- tion detection for light and electron microscopy. The Journal of Cell Biology, 126, 901–910.

Deerinck, T. J., Martone, M. E., Lev-Ram, V., Green, D. P., Tsien, R. Y., Spector, D. L., et al. (1994). Fluores- cence photooxidation with eosin: a method for high resolution immunolocalization and in situ hybridiza- tion detection for light and electron microscopy. The Journal of Cell Biology, 126, 901–910.

Denker, A., Bethani, I., Krohnert, K., Korber, C., Horstmann, H., Wilhelm, B. G., et al. (2011). A small pool of vesicles maintains synaptic activity in vivo. Proceedings of the National Academy of Sciences of the United States of America, 108, 17177–17182.

Denker, A., Bethani, I., Krohnert, K., Korber, C., Horstmann, H., Wilhelm, B. G., et al. (2011). A small pool of vesicles maintains synaptic activity in vivo. Proceedings of the National Academy of Sciences of the United States of America, 108, 17177–17182.

Deo, S. K. und Daunert, S. (2000). "Green fluorescent protein mutant as label in homogeneous assays for biomolecules." Analytical Biochemistry 289: 52-59.

Durdu, S., M. Iskar, C. Revenu, N. Schieber, A. Kunze, P. Bork, Y. Schwab and D. Gilmour (2014). "Luminal signalling links cell communication to tissue architecture during organogenesis." Nature 515(7525): 120-124.

Farquhar, M. G. and G. E. Palade. (1981). "The Golgi apparatus (complex)-(1954-1981)-from artifact to center stage." J Cell Biol 91(3 Pt 2): 77s-103s.

Gaietta GM, Giepmans BN, Deerinck TJ, Smith WB, Ngan L, et al. (2006). Golgi twins in late mitosis revealed by genetically encoded tags for live cell imaging and correlated electron microscopy. Proc Natl Acad Sci U S A 103: 17777–17782.

Giepmans, B.N., T.J. Deerinck, B.L. Smarr, Y.Z. Jones, and M.H. Ellisman. (2005). Correlated light and electron microscopic imaging of multiple endogenous proteins using Quantum dots. Nat Methods 2: 743-9.

Gill D.J., Clausen H., Bard F. Location, location, location: New insights into O-GalNAc protein glycosylation. (2011). Trends Cell Biol. 21:149–158.

Glick BS, Luini A. (2011). Models for Golgi traffic: a critical assessment. Cold Spring Harbor Perspectives in Biology. 3:a005215. doi: 10.1101/cshperspect.a005215.

Goedhart, J., von Stetten, D., Noirclerc-Savoye, M., Lelimousin, M., Joosen, L., Hink, M. A., … Royant, A. (2012). Structure-guided evolution of cyan fluorescent proteins towards a quantum yield of 93%. Nature communications, 3, 751.

Grabenbauer M, Geerts WJ, Fernadez-Rodriguez J, Hoenger A, Koster AJ, Nilsson T. (2005). Correlative microscopy and electron tomography of GFP through photooxidation'. Nat Methods (11):857-62.

Grabenbauer M. Correlative light and electron microscopy of GFP. (2012). Methods Cell Biol. 111:117–138.

Grant G. (2007). How the 1906 Nobel Prize in Physiology or Medicine was shared between Golgi and Cajal. Brain Res Rev. 55 (2): 490–498.

Griffiths, G. (2000). "Gut thoughts on the Golgi complex." Traffic 1(9): 738-745.

Hanus C, Ehlers MD. Secretory outposts for the local processing of membrane cargo in neuronal dendrites. Traffic. (2008). 9:1437–1445.

Harata, N., Ryan, T. A., Smith, S. J., Buchanan, J., & Tsien, R. W. (2001). Visualizing recycling synaptic vesicles in hippocampal neurons by FM 1-43 photoconversion. Proceedings of the National Academy of Sciences of the United States of America, 98, 12748–12753.

Harata, N., Ryan, T. A., Smith, S. J., Buchanan, J., & Tsien, R. W. (2001). Visualizing recycling synaptic vesicles in hippocampal neurons by FM 1-43 photoconversion. Proceedings of the National Academy of Sciences of the United States of America, 98, 12748–12753.

Harata, N., Ryan, T. A., Smith, S. J., Buchanan, J., & Tsien, R. W. (2001). Visualizing recycling synaptic vesicles in hippocampal neurons by FM 1-43 photoconversion. Proceedings of the National Academy of Sciences of the United States of America, 98, 12748–12753.

Harter, C., and C. Reinhard. (2000). The secretory pathway from history to the state of the art. Subcell Biochem. 34:1-38.

Hempelmann A., Spilker C., tom Dieck S., Altrock W. D., Zuschratter W., Garner C. C., Gundelfinger E. D. (2003). Functional regions of the presynaptic cytomatrix protein bassoon. Significance for synaptic targeting and cytomatrix anchoring. Mol. Cell. Neurosci. 23, 279–291

Henderson D, Weber K. (1979). Three-dimensional organization of microfilaments and microtubules in the cytoskeleton. Immunoperoxidase labelling and stereo-electron microscopy of detergent-extracted cells. Exp Cell Res, 124:301–316.

Henkel AW, Lübke J, Betz WJ. (1996). FM1-43 dye ultrastructural localization in and release from frog motor nerve terminals. Proceedings of the National Academy of Sciences of the United States of America, 93(5):1918-23.

Henrissat B, Surolia A, Stanley P. (2017). A Genomic View of Glycobiology. In: Essentials of Glycobiology. Cold Spring Harbor NY: Cold Spring Harbor Laboratory Press.

Hirst, J., and M.S. Robinson. (1998). Clathrin and adaptors. Biochim Biophys Acta. 1404:173-93.

Hoopmann, P., Rizzoli, S. O., & Betz, W. J. (2012). FM dye photoconversion for visualizing synaptic vesicles by electron microscopy. Cold Spring Harbor Protocols, 84–86.

Hoopmann, P., Rizzoli, S. O., & Betz, W. J. (2012). FM dye photoconversion for visualizing synaptic vesicles by electron microscopy. Cold Spring Harbor Protocols, 84–86. Markers for correlated light and electron microscopy. Methods in Cell Biology, 79, 575–591.

Hopkins C, Gibson A, Stinchcombe J, Futter C. (2000). Chimeric molecules employing horseradish peroxidase as reporter enzyme for protein localization in the electron microscope. Methods Enzymol 327:35–45.

Horstmann, H., Körber, C., Sätzler, K., Aydin, D., and Kuner, T. (2012). Serial Section Scanning Electron Microscopy (S(3)EM) on Silicon Wafers for Ultra-Structural Volume Imaging of Cells and Tissues. PLoS ONE 7, e35172.

Horstmann H, Vasileva M, Kuner T (2013) Photooxidation-Guided Ultrastructural Identification and Analysis of Cells in Neuronal Tissue Labeled with Green Fluorescent Protein. PLoS ONE 8(5): e64764.

Horton AC, Ehlers MD. (2003). Dual modes of endoplasmic reticulum-to-Golgi transport in dendrites revealed by live-cell imaging. J Neurosci ;23: 6188–6199.

Horton AC, Racz B, Monson EE, Lin AL, Weinberg RJ, Ehlers MD. (2005). Polarized secretory trafficking directs cargo for asymmetric dendrite growth and morphogenesis. Neuron;48:757–771.

Huang, S., & Wang, Y. (2017). Golgi structure formation, function, and post-translational modifications in mammalian cells. F1000Research, 6, 2050.

Inouye S, Tsuji FI. (1994). Aequorea green fluorescent protein: Expression of the gene and fluorescent characteristics of the recombinant protein. FEBS Lett. 341: 277-280.

Jimenez-Banzo A, Nonell S, Hofkens J, Flors C. (2008). Singlet oxygen photosensitization by EGFP and its chromophore HBDI. Biophys J 94: 168– 172.

Joesch M, Mankus D, Yamagata M, Shahbazi A, Schalek R, Suissa-Peleg A, Meister M, Lichtman JW, Scheirer WJ, Sanes JR. (2016). Reconstruction of genetically identified neurons imaged by serial-section electron microscopy. Elife 5:e15015.

Kopek BG, Shtengel G, Xu CS, Clayton DA, Hess HF (2012) Correlative 3D superresolution fluorescence and electron microscopy reveal the relationship of mitochondrial nucleoids to membranes. Proc Natl Acad Sci U S A 109: 6136– 6141.

Kirchhausen, T. (2000). Three ways to make a vesicle. Nat Rev Mol Cell Biol. 1:187-98.

Klugmann, M., Symes, C.W., Leichtlein, C.B., Klaussner, B.K., Dunning, J., Fong, D., Young, D., and During, M.J. (2005). AAV-mediated hippocampal expression of short and long Homer 1 proteins differentially affect cognition and seizure activity in adult rats. Mol Cell Neurosci 28, 347-360.

Koster, A.J., and J. Klumperman. (2003). Electron microscopy in cell biology: integrating structure and function. Nat Rev Mol Cell Biol Suppl: SS6-10.

Kremer, J. R., Mastronarde, D. N. and McIntosh, J. R. (1996). Computer visualization of three-dimensional image data using IMOD. J Struct Biol 116, 71-76.

Kukulski, W., M. Schorb, M. Kaksonen and J. A. G. Briggs. (2012). "Plasma Membrane Reshaping during Endocytosis Is Revealed by Time-Resolved Electron Tomography." Cell 150(3): 508-520.

Lam S. S., Martell J. D., Kamer K. J., Deerinck T. J., Ellisman M. H., Mootha V. K., et al. (2015). Directed evolution of APEX2 for electron microscopy and proximity labeling. Nat. Methods 12 51–54. 10.1038/nmeth.3179.

Lindsey, J. D. and M. H. Ellisman. (1985). "The Neuronal Endomembrane System .2. The Multiple Forms of the Golgi-Apparatus Cis Element." Journal of Neuroscience 5(12): 3124- 3134.

Lowe, M., and T.E. Kreis. (1998). Regulation of membrane traffic in animal cells by COPI. Biochim Biophys Acta. 1404:53-66.

M. Grabenbauer, W.J.C. Geerts, J. Fernadez-Rodriguez, A. Hoenger, A.J. Koster, T. Nilsson. (2005). Nat. Methods, 2, pp. 857-862.

Mandelman D, Schwarz FP, Li H, Poulos TL. (1998). The role of quaternary interactions on the stability and activity of ascorbate peroxidase. Protein Science 7,2089–2098.

Maranto AR. (1982). Neuronal mapping: a photooxidation reaction makes Lucifer yellow useful for electron microscopy. Science 217:953–955.

Maranto, A. R. (1982). Neuronal mapping: a photooxidation reaction makes Lucifer yellow useful for elec- tron microscopy. Science, 217, 953–955.

Marsh, B. J. (2005). "Lessons from tomographic studies of the mammalian Golgi." Biochim Biophys Acta 1744(3): 273-292.

Martell, J. D., Deerinck, T. J., Lam, S. S., Ellisman, M. H., & Ting, A. Y. (2017). Electron microscopy using the genetically encoded APEX2 tag in cultured mammalian cells. Nature protocols, 12(9), 1792–1816.

Martell, J. D., Deerinck, T. J., Lam, S. S., Ellisman, M. H., & Ting, A. Y. (2017). Electron microscopy using the genetically encoded APEX2 tag in cultured mammalian cells. Nature protocols, 12(9), 1792–1816.

Mastronarde, D. (2005). Automated electron microscope tomography using robust prediction of specimen movements. Journal of Structural Biology 152, 36–51.

McDonald KL, Morphew M, Verkade P, Müller-Reichert T. (2007). Recent advances in high pressure freezing: equipment and specimen loading methods. In: Kuo J, editor. Methods in molecular biology, vol. 369: electron microscopy: methods and protocols. 2nd edition Totowa, NJ: Humana Press Inc. p. 143–73.

McDonald KL. (1999). High pressure freezing for preservation of high resolution fine structure and antigenicity for immunolabeling. In: Hajikbagheri MAN, editor. Electron microscopy methods and protocols. 1st edition Totowa, NJ: Humana Press;. p. 77–97.

Meisslitzer-Ruppitsch C, Vetterlein M, Stangl H, Maier S, Neumuller J, et al. (2008) Electron microscopic visualization of fluorescent signals in cellular compartments and organelles by means of DAB-photoconversion. Histochem Cell Biol 130: 407–419.

Mironov, A.A., R.S. Polishchuk, and A. Luini. (2000). Visualizing membrane traffic in vivo by combined video fluorescence and 3D electron microscopy. Trends Cell Biol 10: 349-53.

Moor H, Riehle U. (1968). Snap-freezing under high pressure: a new fixation technique for freezeetching. Proc. 4th European Reg. Conf. Elect. Microsc. 2: 33-34.

Müller M, Graeve L . (2014). Proteine – Transport, Modifikation und Faltung. In: P C Heinrich, M Müller & L Graeve, Hrsg. Löffler/ Petrides Biochemie und Pathobiochemie. 9 Hrsg. Berlin Heidelberg: Springer Verlag, pp. 615-628.

Nickel, W., and F.T. Wieland. (1998). Biosynthetic protein transport through the early secretory pathway. Histochem Cell Biol. 109:477-86.

Nikonenko, I., Boda, B., Alberi, S., & Muller, D. (2005). Application of photoconversion technique for correlated confocal and ultrastructural studies in organotypic slice cultures. Microscopy Research and Technique, 68, 90–96.

Orci, L., B.S. Glick, and J.E. Rothman. (1986). A new type of coated vesicular carrier that appears not to contain clathrin: its possible role in protein transport within the Golgi stack. Cell. 46:171-84.

Ou, H. D., Phan, S., Deerinck, T. J., Thor, A., Ellisman, M. H., & O'Shea, C. C. (2017). ChromEMT: Visualizing 3D chromatin structure and compaction in interphase and mitotic cells. Science (New York, N.Y.), 357(6349), eaag0025.

Päbo S, Weber F, Nilsson T, Schaffner W, Peterson PA. (1986). Structural and functional dissection of an MHC class I antigen-binding adenovirus glycoprotein. EMBO J. 1986 Aug;5(8):1921–1927.

Pagano, R. E., Martin, O. C., Kang, H. C., & Haugland, R. P. (1991). A novel fluorescent ceramide analogue for studying membrane traffic in animal cells: accumulation at the Golgi apparatus results in altered spec- tral properties of the sphingolipid precursor. The Journal of Cell Biology, 113, 1267–1279.

Pagano, R. E., Martin, O. C., Kang, H. C., & Haugland, R. P. (1991). A novel fluorescent ceramide analogue for studying membrane traffic in animal cells: accumulation at the Golgi apparatus results in altered spec- tral properties of the sphingolipid precursor. The Journal of Cell Biology, 113, 1267–1279.

Pagano, R. E., Sepanski, M. A., & Martin, O. C. (1989). Molecular trapping of a fluorescent ceramide ana- logue at the Golgi apparatus of fixed cells: interaction with endogenous lipids provides a trans-Golgi marker for both light and electron microscopy. The Journal of Cell Biology, 109, 2067–2079.

Patterson WR and Poulos TL. (1995). Crystal structure of recombinant pea cytosolic ascorbate peroxidase. Biochemistry 34, 4331–4341.

Pearse, B.M., and M.S. Robinson. (1990). Clathrin, adaptors, and sorting. Annu Rev Cell Biol. 6:151-71.

Plattner H, Zingsheim HP. (1987). Elektronenmikroskopische Methodik in der Zell- und Molekularbiologie. Gustav Fischer.

Pokrovskaya, I. D., Willett, R., Smith, R. D., Morelle, W., Kudlyk, T., & Lupashin, V. V. (2011). Conserved oligomeric Golgi complex specifically regulates the maintenance of Golgi glycosylation machinery. Glycobiology, 21(12), 1554–1569.

Prasher DC, Eckenrode VK, Ward WW, Prendergast FG, Cormier MJ. (1992). Primary structure of the Aequorea victoria green fluorescent protein. Gene 111: 229-233.

Quassollo G., Wojnacki J., Salas D. A., Gastaldi L., Marzolo M. P., Conde C., et al. (2015). A RhoA signaling pathway regulates dendritic Golgi outpost formation. Curr. Biol. 25 971–982.

Quassollo, G., Wojnacki, J., Salas, D.A., Gastaldi, L., Marzolo, M.P., Conde, C., Bisbal, M., Couve, A., and Ca´ ceres, A. (2015). A RhoA signaling pathway regulates dendritic Golgi outpost formation. Curr. Biol. 25, 971–982.

Quinn, P., G. Griffiths and G. Warren. (1983). "Dissection of the Golgi complex. II. Density separation of specific Golgi functions in virally infected cells treated with monensin." J Cell Biol 96(3): 851-856.

Rabouille C, Misteli T, Watson R, Warren G. (1995). Reassembly of Golgi stacks from mitotic Golgi fragments in a cell-free system. J Cell Biol. 129:605–618.

Rambourg A., Clermont Y. (1997). Three-dimensional structure of the Golgi apparatus in mammalian cells. In: Berger E.G., Roth J. (eds) The Golgi Apparatus. Molecular and Cell Biology Updates. Birkhäuser, Basel.

Rambourg, A., Y. Clermont and A. Marraud. (1974). "Three-dimensional structure of the osmium-impregnated Golgi apparatus as seen in the high voltage electron microscope." Am J Anat 140(1): 27-45.

Romoser, V. A., Hinkle, P. M. und Persechini, A. (1997). "Detection in living cells of Ca2+- dependent changes in the fluorescence emission of an indicator composed of two

green fluorescent protein variants linked by a calmodulin-binding sequence." The Journal of Biological Chemistry 272: 13270-13274.

Royston, C. und Sorkin, A. (1998). "Endocytosis of functional epidermal growth factor receptor-green fluorescent protein chimera." The Journal of Biological Chemistry: 35000- 35007.

Saraste J, Marie M. Intermediate compartment (IC): from pre-Golgi vacuoles to a semi-autonomous membrane system. (2018). Cell Biol. 150(5):407-430. doi: 10.1007/s00418-018-1717-2.

Schuman EM, Dynes JL, Steward O. 2006. Synaptic regulation of translation of dendritic mRNAs. J. Neurosci. 26, 7143–7146.

Sewell RA, Halpern JH, Pope HG. (2006). Response of cluster headache to psilocybin and LSD. Neurology 66:1920–1922.

Shimomura O, Hohnson FH, Saiga Y. (1962). Extraction, purification and properties of aequorin, a bioluminescent protein form the luminous hydromedusan, Aequorea. J. Cell Comp. Physiol. 59: 223-227.

Shimoni E, Müller M: On Optimizing high-pressure freezing. (1998). from heat transfer theory to a new microbiopsy device. J. Microsc. 192(3): 236-247.

Shu X, Lev-Ram V, Deerinck TJ, Qi Y, Ramko EB, Davidson MW, Jin Y, Ellisman MH, Tsien RY. (2011). A genetically encoded tag for correlated light and electron microscopy of intact cells, tissues, and organisms. PLoS Biol. 9(4):e1001041. doi: 10.1371/journal.pbio.1001041. Epub 2011 Apr 5. PubMed PMID: 21483721; PubMed Central PMCID: PMC3071375.

Spiegelhalter, C., J. F. Laporte and Y. Schwab. (2014). "Correlative light and electron microscopy: from live cell dynamic to 3D ultrastructure." Methods Mol Biol 1117: 485-501.

Steinbrecht RA, Müller M. (1987). Freeze substitution and freeze drying. In Steinbrecht R. A., Zierold K(eds): Cryotechniques in Biological Electron Microscopy. Springer Verlag: 149-172.

Storrie, B. et al. (1998). Recycling of Golgi-resident glycosyltransferases through the ER reveals a novel pathway and provides an explanation for nocodazole- induced Golgi scattering. J. Cell Biol. 143, 1505–1521.

Studer D, Michel M, Müller M. (1989). High pressure freezing comes of age. Scanning Microsc. Suppl. 3: 253-268, discuss. 268-269.

Studer D, Michel M, Wohlwendt M, Hunziker EB, Buschmann MD. (1995). Vitrification of articular cartilage by high-pressure freezing. J. Microsc. 179: 321-332.

Sundaramoorthy V, Sultana JM, Atkin JD. (2015). Golgi fragmentation in amyotrophic lateral sclerosis, an overview of possible triggers and consequences. Front Neurosci ;9:400.

Svitkina, T.M., and G.G. Borisy. (1998). Correlative light and electron microscopy of the cytoskeleton of cultured cells. Methods Enzymol 298: 570-92.

Ten Hagen KG, Tran DT, Gerken TA, Stein DS, Zhang Z. (2003). Functional characterization and expression analysis of members of the UDP-GalNAc:polypeptide N-acetylgalactosaminyltransferase family from Drosophila melanogaster. Journal of Biological Chemistry. 278:35039–35048.

Tian E, Ten Hagen KG. (2009). Recent insights into the biological roles of mucin-type O-glycosylation. Glycoconjugate Journal. 26:325–334.

Trucco A, Polishchuk RS, Martella O, Di Pentima A, Fusella A, Di Giandomenico D, San Pietro E, Beznoussenko GV, Polishchuk EV, Baldassarre M, Buccione R, Geerts WJ, Koster AJ, Burger KN, Mironov AA, Luini A. (2004). Secretory traffic triggers the formation of tubular continuities across Golgi sub-compartments. Nature Cell Biology. 6:1071–1081.

U. Ziese A. H. Janssen J.-L. Murk W. J. C. Geerts T. Van der Krift A.J. Verkleij A.J. Koster. (2002). Automated high-throughput electron tomography by pre-calibration of image shifts. J. Microsc 205, 187-200.

Valentijn J.A.; van Driel L.F.; Jansen K.A.; Valentijn K.M.; Koster A.J. (2010). Towards a 3D View of Cellular Architecture: Correlative Light Microscopy and Electron Tomography. Book chapter in: Reiner Salzer. Biomedical Imaging: Principles and Applications. Wiley.

Valenzuela JI, Perez F. (2015). Diversifying the secretory routes in neurons. Frontiers in neuroscience. 2015;9:358.

Valenzuela JI, Perez F. (2015). Diversifying the secretory routes in neurons. Frontiers in neuroscience. 9:358.

Valenzuela, J. I., & Perez, F. (2015). Diversifying the secretory routes in neurons. Frontiers in neuroscience, 9, 358. doi:10.3389/fnins.2015.00358.

van Driel LF, Knoops K, Koster AJ, Valentijin JA. (2008). Fluorescent labeling of resin-embedded sections for correlative electron microscopy using tomography-based contrast enhancement. J Struct Biol. 161:372–383. doi: 10.1016/j.jsb.2007.09.021.

van Rijnsoever, C., V. Oorschot and J. Klumperman. (2008). "Correlative light-electron microscopy (CLEM) combining live-cell imaging and immunolabeling of ultrathin cryosections." Nat Methods 5(11): 973-980.

Varki A, Gagneux P. (2017). Biological Functions of Glycans. In: Essentials of Glycobiology. 3 Hrsg. Cold Spring Harbor (NY): Cold Spring Harbor Laboratory Press.

von Bartheld, C. S., Cunningham, D. E., & Rubel, E. W. (1990). Neuronal tracing with DiI: decalcification, cryosectioning, and photoconversion for light and electron microscopic analysis. The Journal of Histo-chemistry and Cytochemistry, 38, 725–733.

von Bartheld, C. S., Cunningham, D. E., & Rubel, E. W. (1990). Neuronal tracing with DiI: decalcification, cryosectioning, and photoconversion for light and electron microscopic analysis. The Journal of Histo-chemistry and Cytochemistry, 38, 725–733.

Walther P, Ziegler A. (2002). Freeze substitution of high-pressure frozen samples: the visibility of biological membranes is improved when the substitution medium contains water. J. Microsc. 208: 3-10.

Wieland, F., and C. Harter. (1999). Mechanisms of vesicle formation: insights from the COP system. Curr Opin Cell Biol. 11:440-6.

William J. Brown (ed.), The Golgi Complex: Methods and Protocols, Methods in Molecular Biology, vol. 1496, DOI 10.1007/978-1-4939-6463-5_3, © Springer Science+Business Media New York 2016

Yang, T. T., Kain, S. R., Kitts, P., Kondepudi, A., Yang, M. M., and Youvan, D. C. (1996). Dual color microscopic imagery of cells expressing the green fluorescent protein and a red-shifted variant. Gene 173, 19–23.

Ye, B., Zhang, Y., Song, W., Younger, S.H., Jan, L.Y., and Jan, Y.N. (2007). Growing dendrites and axons differ in their reliance on the secretory pathway. Cell 130, 717–729.

Zheng, Y., Wildonger, J., Ye, B., Zhang, Y., Kita, A., Younger, S.H., Zimmerman, S., Jan, L.Y., and Jan, Y.N. (2008). Dynein is required for polarized dendritic transport and uniform microtubule orientation in axons. Nat. Cell Biol. 10, 1172–1180.

6. Appendix

Abbreviations

rAAV	recombinant Adeno-associated virus
CGN	cis-Golgi network
TGN	trans-Golgi network
GlcNAc	N-acetyl-D-glucosamine
GalNAc	N-acetylgalactosamine
GalNAc-T2	N-acetylgalactosaminyltransferase 2
ER	Endoplasmic reticulum
COP	coat protein
IC	intermediate compartment
EM	electron microscopy
TEM	transmission electron microscopy
SEM	scanning Electron microscopy
3D	Three Dimensional
2D	Two Dimensional
GOs	Golgi outposts
CLEM	Correlative light and electron microscopy
LM	Light microscopy
DAB	3,3'-diaminobenzidine
APEX	Pea ascorbate peroxidase
H_2O_2	Hydrogen peroxide
OsO_4	Osmium tetroxide
AFS	Automatic freeze substitution
H	hour

min	Minute
mM	Millimolar
ms	Millisecond
PBS	Phosphate Buffered Saline
PFA	Paraformaldehyde
µm	Micrometer
RT	Room temperature

List of figures